Interrogation of System State of Lead-Free Electronics Subjected to Mixed Sequential Steady-State and Cyclic Thermal Environments

by

Rahul Chandramohan Vaidya

A thesis submitted to the Graduate Faculty of
Auburn University
in partial fulfillment of the
requirements for the Degree of
Master of Science

Auburn, Alabama
December 13, 2010

Keywords: PHM, Solder Joint Reliability, Life Prediction
Prognostics, Electronic Packaging

Approved by

Pradeep Lall, Chair, Thomas Walter Professor of Mechanical Engineering
Jeffrey C Suhling, Quina Distinguished Professor of Mechanical Engineering
Roy W Knight, Assistant Professor of Mechanical Engineering

Abstract

Electronic assemblies deployed in harsh field environments may be exposed to single and multiple thermal environments during their service life. In real world setting it is often required to know during the service life of the system what is the amount of life consumed well before the actual failure occurs to schedule maintenance well in advance. The thermal conditions can change according to the change in the usage profile or also during redeployment from one field environment to another. For example in case of defense applications, military equipments come back from a particular field environment and are redeployed in different field environments after certain time intervals. Or in case of space missions the electronic systems embedded in the space equipments have to undergo different operational temperatures depending on the field conditions. It is important to note that different field environments have different magnitudes of damage incursions on electronic systems. Also electronic systems are often stored for a very long time before they are deployed in the intended environment. It is extremely important to quantify the expended life during storage especially for electronic systems used in mission critical applications. Although ambient temperature storage does not lead to any macro indicators of failure like cracks or de-lamination but it is well known that aging has an adverse effect on the life of electronics. Modern day electronic systems perform well when exposed to such multiple harsh environments and often times may not fail before their designed service life however the latent damage incurred at each stage can

not be neglected and has to be taken in to account to avoid catastrophic failures and system down time in the field. Quantification of thermal environments during use-life is often not feasible because of the data-capture and storage requirements, and the overhead on core-system functionality. Thus there is a growing need to develop and demonstrate technologies that can monitor and predict the remaining useful life (RUL) of electronics in single thermal environments and also assess operational readiness of the electronic system during redeployment. Proposed prognostic models are based on physics-of-failure based damage-proxies of second level solder interconnects found in today's commercially available high I/O packaging architectures. Test vehicles have been carefully selected for the development and implementation of the models so that they are relevant to the current packaging trends. Prognostic framework involves the use of condition monitoring devices for gathering data on damage pre-cursors at periodic intervals. The presented Prognostic Health Management (PHM) framework lies in the pre-failure space without any knowledge of prior stress histories i.e. in the absence of macro-indicators like cracks or de-lamination. In this thesis, test cases have been presented to demonstrate the viability of the approach for assessment of prior damage, operational readiness, cyclic life reduction due to long-term storage and residual life for electronics.

Acknowledgments

I would like to express my deep gratitude to my research advisor Dr. Pradeep Lall for giving me the opportunity to work under his guidance and mentorship at NSF Center for Advanced Vehicle and Extreme Environment Electronics (CAVE^3) as a Graduate Research Assistant at Auburn University. I would also like to thank my other committee members Dr. Jeffrey Suhling and Dr. Roy Knight for their support and guidance while completing this thesis.

I would like to thank my parents Mr. C.T Vaidya and Mrs. Shailaja C Vaidya and my elder brother Rohan for having faith in me and providing endearing love, encouragement and moral support. I would also like to thank all my friends and colleagues for their priceless friendship and camaraderie all throughout my graduate studies.

Table of Contents

Abstract ii

Acknowledgments iv

List of Figures viii

List of Tables xii

1 Introduction 1

1.1 Electronic Packaging Overview 1

1.2 Reliability Concerns 2

1.3 Prognostic Health Management Systems 6

1.4 Thesis Layout 8

2 Literature Review 10

2.1 Solder Joint Reliability 10

2.1.1 Reliability of BGA Packages 11

2.1.2 Lead-Free (Pb-Free) Solders 12

2.2 Life Prediction Models 14

2.2.1 Physics-of-Failure (POF) Models 15

2.2.2 Finite Element Analysis (FEA) Models 16

2.3 Diagnostic Models 18

2.4 Applications of Prognostic Health Management Systems 21

2.4.1 General PHM Applications 21

2.4.2 PHM for Electronics 24

3 Prognostic Model for Life Prediction of Electronics Subjected to Steady-State Thermal Environment 28

3.1 Introduction 28

3.2 Test Vehicle 28

3.3 Inter-Metallic Compound (IMC) Growth as Leading Indicator of Failure...31

3.3.1 Formation of Different Inter-Metallic Compounds 32

3.3.2 Inter-Metallic Compound (IMC) Measurement and Analysis.............33

3.4 Problem Definition and Prognostication Methodology 34

3.5 Levenberg-Marquardt Algorithm (LMA) 37

3.6 Case Study: Prognostication of Life Consumed due to Steady-State Aging 41

3.6.1 Inter-Metallic Compound (IMC) Growth Measurement and Analysis 41

3.6.2 Life Prediction using PHM Model..44

3.6.3 Model Validation 49

3.7 Conclusion 52

4 Prognostic Model for the Quantification of Reduction in Cyclic Life Due to Long-Term Dormant Storage 53

4.1 Introduction 53

4.2 Test Vehicle 54

4.2.1 Custom PCB Design 56

4.2.2 Test Conditions 61

4.3 Leading Indicators of Failure 62

4.3.1 Phase-Growth as the Leading Indicator of Failure 63

4.3.2 Phase-Growth Measurement 66

4.4 Concept of Sequential Thermal Aging and Thermal Cycling 67

4.5 Concept of Damage Equivalency Based Mapping 69

4.6 Case Study: Prognostication of Life of Electronics Subjected to Sequential Stresses 70

4.6.1 Damage Equivalency Relationship between Thermal Aging and Thermal Cycling 71

4.6.2 Prognostication of Life under Overlapping Stresses 83

4.7 Prognostic Performance Metrics 95

4.8 Conclusion 102

5 Summary and Future Work 107

Bibliography 111

List of Figures

Figure 1: Electronic Packaging Trends [Evans 2008, ELEC 6740] 2

Figure 2: Typical Ball Grid Array (BGA) Electronic Package Architecture.......................3

Figure 3: CABGA 100 Package Front and Back View 29

Figure 4: Test Vehicle..30

Figure 5: Inter-metallic Compound (IMC) at Solder Ball, Copper Pad Interface 31

Figure 6: Problem Definition 35

Figure 7: Flowchart for Life Estimation of Electronics Subjected to Single Isothermal Aging Environment..36

Figure 8: Schematic of a Multidimensional Solution Space...38

Figure 9: Schematic highlighting drawbacks of Steepest Descent Method.......................39

Figure 10: SEM Back-scattered images of IMC Growth versus Thermal Aging for Sn1Ag0.5Cu (SAC 105) (Magnification 1000x) 42

Figure 11: SEM Back-scattered images of IMC Growth versus Thermal Aging for Sn3Ag0.5Cu (SAC 305) (Magnification 1000x) 43

Figure 12: IMC Growth, at various levels of time for CABGA 100 with Sn1Ag0.5Cu alloy (SAC 105) 44

Figure 13: IMC Growth, at various levels of time for CABGA 100 with Sn3Ag0.5Cu alloy (SAC 305) 44

Figure 14: Prognostication Approach 45

Figure 15: Global Minima for IMC based History Calculation for 100 I/O CABGA, Sn1Ag0.5Cu Solder Alloy Interconnects 47

Figure 16: Global Minima for IMC based History Calculation for 100 I/O CABGA, Sn3Ag0.5Cu Solder Alloy Interconnects 47

Figure 17: Global Minima for IMC based History Calculation for 100 I/O CABGA, Sn1Ag0.5Cu Solder Alloy Interconnects 48

Figure 18: Global Minima for IMC based History Calculation for 100 I/O CABGA, Sn3Ag0.5Cu Solder Alloy Interconnects 48

Figure 19: Computation of IMC Thickness (based on prognosticated y0 and k) vs. IMC from experimental values for 98.5Sn1.0Ag0.5Cu alloy 51

Figure 20: Computation of IMC Thickness (based on prognosticated y0 and k) vs. IMC from experimental values for 96.5Sn3.0Ag0.5Cu alloy 51

Figure 21: PBGA 676 Front and Back Side 55

Figure 22: PBGA 676 Component Side Daisy Chain Courtesy: Practical Components ...57

Figure 23: 4 Daisy Chain Schematic 57

Figure 24: ExpressPCB Snapshot for PBGA 676 Daisy Chain Pattern 58

Figure 25: Component Side Daisy Chain (BLACK) and Board Side Daisy Chain (GRAY) Overlaid to Show 4 Daisy Chain Patterns 58

Figure 26: Actual PCB with PBGA 676 Footprint Accommodating 4 Daisy Chain Patterns 59

Figure 27: Reflow Profile for SAC 305 Solder 60

Figure 28: Test Vehicle 60

Figure 29: Thermal Cycling Profile 62

Figure 30: IMC Growth as the Leading Indicator of Failure 63

Figure 31: Ag3Sn Grains in 95.5Sn4.0Ag0.5Cu solder microstructure 64

Figure 32: SEM Image for Phase-Growth Analysis 66

Figure 33: Phase Size Measurement using NI-IMAQ 67

Figure 34: Concept of Sequential Thermal Aging and Thermal Cycling 68

Figure 35: Mapping Reduction in Life Due to Dormant Storage. 68

Figure 36: Accrued Damage Due to Thermal Aging and Thermal Cycling respectively. 69

Figure 37: Concept of Damage Equivalency and Mapping of Life Consumed Due to Storage. 70

Figure 38: SEM backscattered images of Phase growth versus number of cycles (Thermal cycling -55°C to 125°C, 96.5Sn3.0Ag0.5Cu solder, 676 I/O PBGA, magnification 750x) 74

Figure 39: SEM backscattered images of IMC growth versus number of cycles (Thermal cycling -55°C to 125°C, 96.5Sn3.0Ag0.5Cu solder, 676 I/O PBGA, magnification 1000x) 75

Figure 40: Plot of Normalized Phase growth versus No. of Cycles for 96.5Sn3.0Ag0.5Cu solder, 676 PBGA, subjected to thermal cycling from -55°C to 125°C 75

Figure 41: Plot of Normalized IMC growth versus No. of Cycles for 96.5Sn3.0Ag0.5Cu solder, 676 PBGA, subjected to thermal cycling from -55°C to 125°C 76

Figure 42: SEM backscattered images of Phase growth at different aging time intervals (Thermal aging at 125°C, 96.5Sn3.0Ag0.5Cu solder, 676 I/O PBGA, magnification 750x) 77

Figure 43: SEM backscattered images of Intermetallic Thickness at different aging time intervals (Thermal aging at 125°C, 96.5Sn3.0Ag0.5Cu solder, 676 I/O PBGA, magnification 1000x) 77

Figure 44: Plot of Phase growth versus Aging Time for 96.5Sn3.0Ag0.5Cu solder, 676 PBGA, subjected to thermal aging at 125°C 78

Figure 45: Plot of IMC growth versus Aging Time for 96.5Sn3.0Ag0.5Cu solder, 676 PBGA, subjected to thermal aging at 125°C 78

Figure 46: Combined plot Normalized Phase growth versus thermal aging time and thermal cycling..80

Figure 47: Combined plot Normalized IMC growth versus thermal aging time and thermal cycling 81

Figure 48: Combine plot of No of Cycles (N) versus Time in hrs, due to damage mapping from Phase growth and IMC thickness...82

Figure 49: Prognostication of Life Consumed Due to Aging in number of hours. 84

Figure 50: Prognostication of Life in Overlapping Environment.....................................84

Figure 51: Schematic for Prognostication of Storage Time (for 48 hours Experimental Exposure) 88

Figure 52: 3D plot of error versus aging time in hours for 676 PBGA 96.5Sn3.0Ag0.5Cu solder interconnects for experimental exposure of 48 hours in isothermal aging at 125°C. 89

Figure 53: Schematic for Prognostication of Total Life in Sequential Stress Environment (for 48 hours+100 Cycles Experimental Exposure) 90

Figure 54: 3D plot of error versus number of cycles for 676 PBGA 96.5Sn3.0Ag0.5Cu solder interconnects for experimental exposure of 48 hours in isothermal aging at 125°C followed by 100 cycles in -55°C to 125°C. 91

Figure 55: Schematic for Prognostication of Storage Time (for 192 hours Experimental Exposure) 92

Figure 56: 3D plot of error versus aging time in hours for 676 PBGA 96.5Sn3.0Ag0.5Cu solder interconnects for experimental exposure of 192 hours in isothermal aging at 125°C. 92

Figure 57: Schematic for Prognostication of Total Life in Sequential Stress Environment (for 192 hours+100 Cycles Experimental Exposure) 93

Figure 58: 3D plot of error versus number of cycles for 676 PBGA 96.5Sn3.0Ag0.5Cu solder interconnects for experimental exposure of 192 hours in isothermal aging at 125°C followed by 100 cycles in -55°C to 125°C. 93

Figure 59: α-λ curve for Prognostication using normalized phase-growth as the leading indicator of failure..99

Figure 60: α-λ curve for Prognostication using normalized IMC growth as the leading indicator of failure..100

List of Tables

Table 1: Thermal and Mechanical Attributes of Various Materials in BGA Package........3

Table 2: Package Attributes (All Dimensions are in mm)...43

Table 3: Comparison of computed values of t, y0 and k from prognostication model and experimental result...49

Table 4: Package Architecture Details..55

Table 5: Condition Monitoring Cells..61

Table 6: Damage Mapping from Leading Indicators of Failure.......................................83

Table 7: Error Estimation in Prognostication of Thermal Aging (Storage).......................94

Table 8: Error Estimation in Reduction in Cyclic Life Due to Thermal Aging (Storage).94

Table 9: Error Estimation in Prognostication of Overlapping Damage.............................95

Table 10: Prognostic Metric Comparison..102

CHAPTER 1

INTRODUCTION

1.1 Electronic Packaging Overview

Electronic packaging is an inter-disciplinary field of study which deals with methods of construction and integration of diverse electronic circuits on a chip broadly referred to as IC's (Integrated Circuits) or Packages. A single IC Package can fit multiple electronic circuits or devices thereby drastically reducing the size of a system as a whole. Nanotechnology has brought the microelectronic revolution over the last couple of decades. Wide scale research and development is carried out in this area in employing advanced techniques to further shrink the size of the individual packages to achieve higher component density per area. However it is extremely important to take into account the design considerations while scaling down the size like the mechanical or structural damage caused due to shock and exposure to extreme environments or the electrical constraints like electromagnetic interference, undesirable shorting of tracks and heat dissipation requirements.

The Packaging techniques can broadly be classified into two main types' viz. Through-hole technology and Surface Mount technology. Through hole technology of mounting electronic components was in use from 1950's – 1970's and is no longer employed for the manufacturing of commercial electronic products because although the through-hole mounting provides strong mechanical bonds and are more reliable and

robust, the shrinkage of the component size is restricted which makes the overall electronic assembly bulky. In order to find the solution to the size constraints in through hole technology industry came up with the new mounting technology called surface mount technology which was invented in 1970's and still finds its application in today's electronic manufacturing. Components became much smaller and component placement on both sides of a board became far more common with surface-mounting than through-hole mounting, allowing much higher circuit densities. It has evolved greatly in all these years with the current version requiring complete rethinking of design and production, along with new infrastructure to develop and sustain it. Figure 1 shows the schematic depicting evolution of electronic packaging over the years.

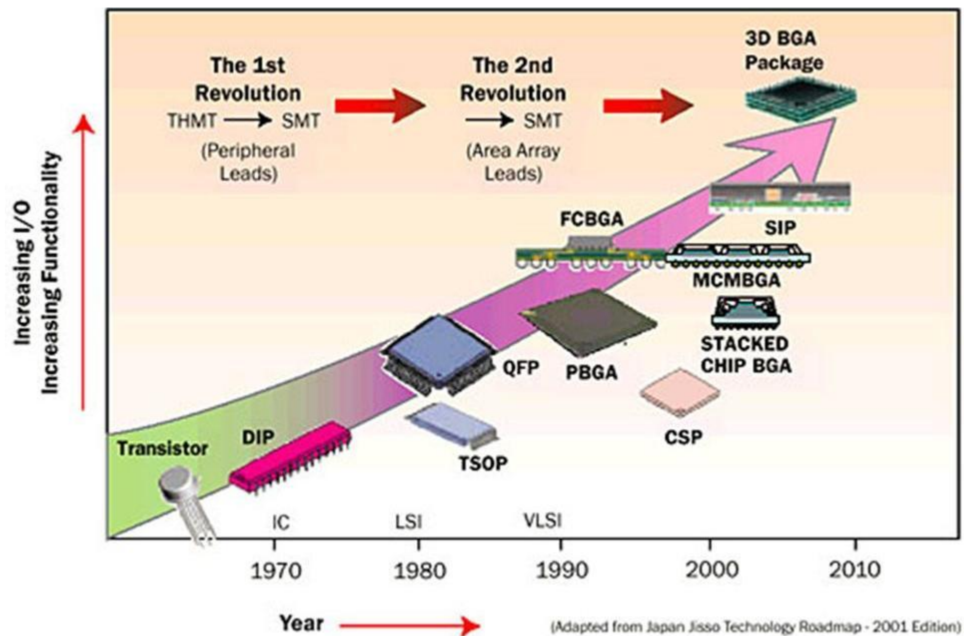

Figure 1: Electronic Packaging Trends [Evans 2008, ELEC 6740]

1.2 Reliability Concerns

Microelectronic device integration has progressed to the point where complete systems-on-a-chip (SoC), Multi-chip Module (MCM) and 3D Stacking are being realized

these days. It is inevitable to ensure product reliability to fully exploit the device shrinkage accomplished with the advent of Very Large Scale Integration (VLSI) and nanotechnology. Typically an electronic package consists of various materials (Figure 2) having different mechanical and thermal properties as shown in Table 1. The individual behavior and the interaction with other materials at different operating or field conditions raise mechanical, structural and electrical reliability issues in a package.

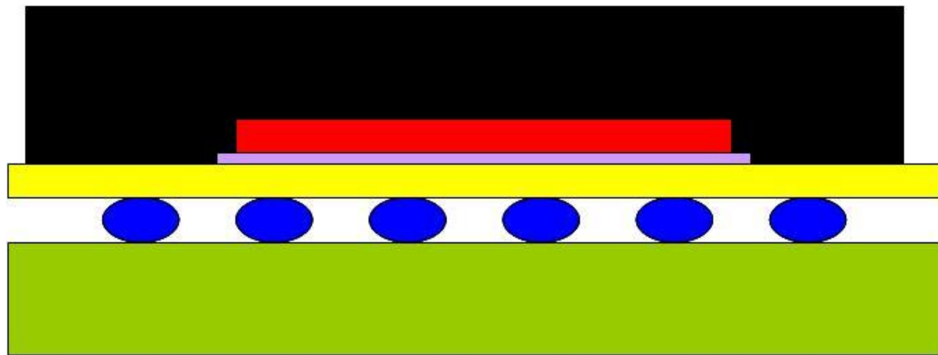

Figure 2: Typical Ball Grid Array (BGA) Electronic Package Architecture

Table 1: Thermal and Mechanical Attributes of Various Materials in BGA Package

Color	**Material**	**Elastic Modulus (E) (GPA)**	**Coefficient of Thermal Expansion (CTE) (10^{-6} 1/K)**
Black	Mold Compound	23.5	15
Red	Silicon Die	162.7	2.5
Lavender	Adhesive	6.8	52
Yellow	BT Substrate	18	12.4
Blue	Solder Balls	30.5	24.5
Green	Printed Circuit Board	17	14.5

Electronic assemblies undergo numerous unavoidable stresses and strains during their service life. The stresses are induced due to the different operational conditions. For example the electronic circuitry inside a commercial laptop undergoes power and or

thermal cycling even during normal usage which induces thermal-structural stresses on electronic packages embedded inside. It is not unlikely that a portable electronic product like a cellular phone is accidently drop from a certain height. This typically is a high strain rate phenomenon which stresses various materials at different rates in a package and eventually after repeated drops the cellular phone stops working due to mechanical or electrical failures. Electronics used in automobiles have to undergo harsh thermal cycling environments (-55C to 125C) and demands high reliability for ideal functioning.

Stresses are induced on an electronic system when it is exposed to one or more combinations of operating conditions like thermal cycling, isothermal aging, thermal shock, drop, shock, vibration, hazardous chemical exposure etc. It is important to identify the failure modes associated with different field conditions for ensuring long term reliability of the products. Some of the commonly encountered failures are solder joint fatigue, die fracture, chip delamination, silicon cratering, underfill cracking, pop-corn effect, corrosion etc. Some of these failures are attributed to as material and or processing defects like pop-corn failure which occurs during high temperature reflow due to the moisture absorbed by the package during storage. The presented work lies in the area of solder joint reliability under low cycle thermal fatigue and hence this has been discussed in great detail in the subsequent section.

Electronic package design and development is a concurrent approach which takes into account many material and process variables. Solder is one of the crucial variables which has to be taken into account for reliable electronic performance. Solders used in surface mount technology not only have to serve the purpose of electrical connection but also has to ensure robust mechanical connection. Solder joint cracking is the most

dominant failure mode in microelectronics. The coefficient of thermal expansion (CTE) of electronic package and the printed circuit board (PCB) are different as a result of which they expand and contract at different rates during power and thermal cycling. This CTE mismatch induced disparity in rates of expansion causes shear stress in the solder joints which leads to fracture in extreme cases and has been a major reliability concern. [Ye 2006, Abdulhamid 2008] have also reported on electro-migration and thermo-migration in high temperature power electronic modules and its detrimental effect on solder joint reliability. Various techniques are used to reduce stress on the solder joints to improve solder joint reliability. Some of the techniques include developing substrates with matching CTEs thereby minimizing CTE differences in the substrate and package being mounted, developing substrates with compliant top layers that can absorb some stress and using underfill that provide stability to the solder joints during shearing thereby maintaining integrity of the joints.

With the advent of Restriction of Hazardous Substances (RoHS) compliance and lead-free restrictions, electronics industry is looking into lead-free solders that can replace the universally accepted and widely used tin-lead solder. Research and development efforts are focused on the study of potential alloys that provide physical, mechanical, thermal and electrical properties similar to those of eutectic tin-lead solder. It has not been a smooth transition to switch from leaded to lead-free solders as the conventional eutectic Sn/Pb solder has been in use for almost half a century and all its properties pertaining to electronics assemblies is readily available. The biggest obstacle in switching to lead-free solders is the lack of material characterization data available for these solders for varied applications. Also the mechanical behavior of lead-free solder

alloys is radically different from eutectic tin-lead which only compounds the sustainability and reliability issues of lead-free electronics. As a result electronic systems are not used to the desired degree in terms of life, especially in mission critical applications, in order to reduce the probability of failure in the field. Current tools and techniques can not perform reliability assessment of the system due to lack of sufficient information about the on going damage and its progression. The major problem in the industry today is the need to extend the useful life of such critical systems. Also the electronic components used in commercial applications like automotive safety systems are used to a lesser degree than desirable to avoid prospective malfunction in the long run. This is because the reliability associated with such safety equipments can not be compromised at any given point which forces the use of dependable components in such critical applications. Health monitoring of electronics is very relevant to such high reliability applications and there is a growing need to develop techniques that can evaluate the reliability of the system and provide information about the health of the system. The work presented in this thesis is based on health management of electronics using solder joint reliability and its associated damage proxies under thermo-mechanical loading.

1.3 Prognostic Health Management Systems

Health Management (HM) refers to the broad concept of assessing the on-going, in-service performance of a system using variety of measurement techniques. Prognostics can be thought of as a predictive diagnostics which includes determining the remaining life of the operational component. Prognostic Health Management (PHM) is the methodology of interrogation of state of a system based on computation of certain

damage proxies to predict the Remaining Useful Life (RUL) of the system. The core function of any PHM model is to detect fault in the system and compute residual life at any given time. Typically fault detection involves interrogation of system state for physics-of-failure (POF) based damage proxies that provide information about the ongoing damage and impending failure. These damage proxies are classified as the leading indicators of failure and are used in PHM model development which directly or indirectly relates to the overall life of the system.

Health monitoring of electronics has always gained utmost importance from the research community as it provides information about the current state of health of a system, identify faults and their behavior and assess accumulated damage thereby providing estimates of remaining life of the product [Lopez 2007]. Application of prognostic and health management (PHM) in electronics is still relatively at a nascent stage compared to its applications in other domains like aerospace, medicine, finance and weather [Saxena 2008].

There is a growing need to develop techniques for reliability prediction of electronics that are exposed to sequential or overlapping multiple thermal environments. State-of-Art prognostic health management models are proposed in this thesis which helps in reliability assessment of electronics deployed in single and complex multiple thermal environments. The strength of the techniques lies in its ability to predict reliability of the electronic system without worrying about the previous usage profiles or materials used in the electronic component except for the solder joint. The models provide the decision framework for operational readiness of systems during redeployment and also account for reduction in cyclic life due to long-term dormant storage. The

prognostic models have been developed based on micro-structural evolution of second level solder interconnects.

1.4 Thesis Layout

Chapter 2 encompasses literature survey on solder joint reliability and various life prediction models used in electronics. Since the presented work is for high I/O electronic packages, significant amount of literature has been reviewed pertaining to Ball Grid Array (BGA) packages. Reliability enhancement techniques for BGAs have also been discussed in detail. Transition from eutectic tin-lead solders to lead-free solders and its effect on solder joint reliability and overall package reliability has also been discussed in great detail. Life prediction models have been systematically classified into physics-of-failure (POF) based models and finite element analysis (FEA) models for lucid understanding of the reader. To set the stage for Prognostic Health Management (PHM) systems, an overview of diagnostic models has also been presented in this chapter. Lastly vast literature on PHM systems and its application in various engineering domains has been discussed followed by its motivation and scope in electronics.

Chapter 3 presents the prognostic model for life estimation of electronics subjected to steady-state aging. It involves in-depth discussion about test vehicle coverage, physics-of-failure based leading indicator of failure and implementation of novel non-linear least square (NLLSQ) method called Levenberg-Marquardt (LM) algorithm. Multiple case-studies have been presented wherein the life of the electronic system has been computed using the proposed prognostic model followed by model validation.

Chapter 4 expands the realm of application of PHM systems for electronics from single environment to multiple thermo-mechanical environments. It provides the overview of multiple thermal environment scenarios and its complex nature of operation and why conventional life prediction models fail to predict life accurately. Specifically it addresses the issue of long-term dormant storage of electronics and its detrimental effect on the reliability. State-of-art prognostic model has been proposed in this chapter which quantifies the reduction in life due to storage. Multiple case-studies have been presented to investigate the effect of storage on cyclic life. Finally, Chapter 5 includes the conclusion of the presented prognostic health management models and briefly discusses the scope for future work.

CHAPTER 2

LITERATURE REVIEW

2.1 Solder Joint Reliability

In electronics the integrity of solder joints remains the backbone for ensuring quality of the product. A perfect joint is a joint showing complete wetting of solder to pad and this is a universal requirement that applies to surface mount as well as through-hole components. As suggested by [Woodgate 1987] the only acceptable joint is the perfect joint. In the pursuit of device shrinkage and circuit miniaturization, surface mount technology in itself has vastly evolved over the last couple of decades. With the potent need for small form factor packaging architectures, fine pitch packaging in the range of 0.8mm-1.27mm became a reality which gave rise to the conception of ball grid array (BGA) packages. Manufacturing of fine pitch leaded chip carriers was a major issue which was one of the instrumental factors in pushing BGA packaging in the mainstream electronic manufacturing. BGAs appear to be the answer to the high pin count packaging trend since they can accommodate high I/O in a very small form. Fine pitch packages with their fragile leads pose serious handling problems and are difficult to place and solder. BGAs became popular because during placement and reflow, robust balls outperform fragile leads as they self align and provide better control during reflow at ultra-fine pitches.

In surface mount devices (SMDs) like BGA packages, solder joints not only provide electrical connectivity but also ensure mechanical integrity between the package and the printed circuit board (PCB). The major reliability issue with BGA package is the thermal mismatch between the BT substrate and the printed circuit board (PCB). The difference in the coefficient of thermal expansion (CTE) of the BT substrate and the PCB induces shear stress in the second level solder interconnects due to disparity in the rate of expansion and contraction of the two materials when exposed to thermal loads. Repeated shearing of solder joints lead to cyclic stress or fatigue build-up in the solder joints causing them to fail eventually. Different techniques are employed to reduce cyclic thermal fatigue of solder joints as the solder joint reliability is directly proportional to the overall package reliability.

2.1.1 Reliability of BGA Packages

[Chiang 2000] proposed that a better reliability characteristic of BGA type packages can be achieved by using the 2nd reflow process. He showed 2X increase in the characteristic life of BGAs under thermal cycling due to significant reduction in equivalent plastic strain, the energy density and the Von-Mises stress of the solder joint. [Syed 1996] reported on package architecture variables affecting the solder joint reliability of BGA packages. He showed that perimeter array packages had a better solder joint reliability than full array packages. He also showed that the BT thickness had a direct impact on solder joint reliability with thicker BT substrate enhancing the solder join reliability.

[Charles 1990] reported that increase in fatigue life under power cycling can be attained by fabricating solder joints with large fillets and low standoff heights. The large

fillet geometry significantly reduces harmful stress concentrations while increasing the net cross-sectional area within the joint. Both factors tend to improve the fracture toughness of the joint. Temperature cycling studies indicate joints with slightly higher standoffs and low fillet angles are more resistant to cyclic fatigue than pillar type joints which tend to focus shear strains at the interfaces.

Generally, for enhanced solder joint reliability of stacked die BGA, it is recommended to have smaller top and bottom dice sizes, thicker top or bottom die, thinner PCB, thicker substrate, higher solder ball standoff, larger solder mask opening size, smaller maximum ball diameter, smaller PCB pad size, smaller thermal cycling temperature range, longer ramp time, and shorter dwell time. It is possible to greatly enhance the solder joint performance through simple optimization in mold compound material and package thickness. The layout of solder balls is important as it affects the load distribution on critical solder ball [Tee 2004].

[Zhong 1999] presented the effects of solder ball pad metallurgy, intermetallic compound (IMC) thickness and thermal cycling on the shear strengths of PBGA package solder balls. The study of the microstructures of solder balls revealed that only a very thin layer of intermetallic compound existed between solder balls and Ni or Ni alloy barrier layers immediately after ball placement and reflow. [Bradley 1996 and Suhling 2002] showed superior HASL pad finish thermal reliability performance over immersion nickel and palladium based pad finishes for BGA packages.

2.1.2 Lead-Free (Pb-Free) Solders

Recent global environmental projects like Restriction of Hazardous Substances (RoHS) and Waste from Electrical and Electronic Equipment (WEEE) has put a full stop

on further use of tin-lead components in electronic manufacturing industry which gives a call for all the possible Pb-free alloys. There are hundreds of lead-free alloy compositions that are been studied for their applicability in electronics. The tin-silver-copper (Sn/Ag/Cu or "SAC") family of alloys is one of the leading contenders which have been accepted by electronics industry as a substitute for tin-lead solders.

[Syed 2001, Zhang 2003 and Vandevelde 2004] have shown that the SAC alloy performance varies with different packaging architectures and has strong temperature dependence. The experimental studies have confirmed that the use of lead free solders with low Ag content significantly improves board level reliability during drop test when compared with high Ag content SAC alloys. On the contrary it has been reported by [Zhang 2008 and 2009] that higher Ag content SAC alloys enhance thermal reliability.

[Schubert 2003 and Clech 2005] reported on the relative SAC solder alloy performance over conventional tin-lead solders. Their experimental studies have shown that there is significant enhancement in solder-joint reliability of second level interconnects with SAC alloys than tin-lead when used with compliant plastic substrates.

As the SAC alloys are ternary system alloys the microstructure is pretty complex compared to binary system solder alloys. In case of eutectic tin-lead solders the intermetallic compound formation is so fast that the solder attains equilibrium condition quickly. The biggest problem with SAC alloys is that the intermetallic formation is very slow compared to eutectic tin-lead due to high percentage of tin [Henderson 2004]. [Zhang 2003] reported that the fine microstructure of SAC alloys right after reflow help prevent grain boundary sliding and hence SAC alloys perform better than tin-lead in low stress regimes. [Dutta 2004] emphasized on the need for incorporating coarsening kinetics in the existing solder creep models as the microstructure of SAC alloys evolves rapidly during thermal cycling and creep behavior is related

with microstrucure. [Liu 2004 and Tsai 2005] have reported on the difference in the mechanical behavior and characterization of intermetallic compounds found in SAC and Sn-Pb alloys and its effect on solder joint reliability.

Apart from SAC alloys other potential metals that can be used as lead-free alloys are Indium, Zinc, Bismuth etc. [Seelig 2003] reported that Bismuth poses a potential supply problem since it is a by-product of lead mining, and also has embrittlement problems. Bismuth is also a poor conductor, both thermally and electrically. [Lung 2004] reported on potential Pb-free Sn-Zn and its relative performance with SAC alloys. [Shimizu 1995] showed that Indium-alloy solders have better mechanical properties for solder joints, and their flip-chip interconnection models showed a longer fatigue life than that of Pb-Sn solder in thermal shock tests between liquid nitrogen and room temperatures. He proposed lead-free solders such as indium (In)-alloy solders are a possible alternative to conventional lead-tin (Pb-Sn) solders and are suitable for fabricating reliable interconnections.

2.2 Life Prediction Models

Electronics is a fast paced industry and because the market life of individual commercial electronic product is typically 6-12 months it is impractical for any electronic manufacturing company to test every new product in the real field environment and evaluate mechanical reliability or life of the product. Instead, accelerated tests such as Highly Accelerated Life Tests (HALT) or Highly Accelerated Stress Tests (HAST) are used which impose harsher conditions on the electronic product causing them to fail in a shorter time to make reliability predictions in the actual field applications. There are number of life prediction techniques for electronics ranging from simple analytical

methods to complex damage mechanics based finite elements models that are available in literature especially based on solder joint reliability mechanics.

2.2.1 Physics of Failure (POF) Models

Classical [Coffin 1954, Manson 1964 and Goldmann 1969] models have proposed physics of failure based life prediction equations that relate the plastic strain in the solder joints with failure life of the package. [Norris 1969, Lau 1995] studied the effect of cycling frequency and maximum temperature of cycling on fatigue failure of solder joints.

[Wong 1990] proposed a mechanistic model for eutectic Pb/Sn solder life predictions wherein he studied crack initiation, crack propagation, microstructure coarsening and deformation kinetics models of the solder during thermal cycling. By merging these models together he predicted the time to crack initiation and the time to failure of the solder joints.

Low cycle fatigue testing of a eutectic alloy 63Sn/37Pb was carried out by [Shi 1999] to study Morrow energy-based model, the frequency-modified Coffin-Manson model, and the frequency-modified energy-based model by [Solomon 1986] for life prediction.

[Engelmaier 1982 and 1984] developed a surface mount solder joint reliability prediction model containing all the parameters influencing the shear fatigue life of a solder joint due to shear displacement caused by thermal expansion mismatch between component and substrate. [Wong 1988 and Yamada 1989] implemented fracture mechanics concept to study solder joint cracking and compute time to failure.

[Choi 2003, Ye 2003 and Chiu 2006] studied the effect of joule heating, electro-migration and thermo-migration on flip-chip solder joints. They proposed damage mechanics of flip-chip joints under high current densities and have related mean time to failure using Black's equation. Overwhelming mechanical property degradation of solder joints was observed due to current stressing. Mass accumulation was reported to be primary reason for void formation and subsequent crack propagation in such high current density applications.

[Lau 2002 and 2003] developed empirical equation for predicting the thermal-fatigue life of wafer level chip scale package (WLCSP) solder joints. It is derived by combining the measured thermal-fatigue crack growth rate of the corner solder joint and the simulated nonlinear fracture characteristics i.e. average strain energy density per cycle around the crack tip of the corner solder joint with various crack lengths.

2.2.2 Finite Element Analysis (FEA) Models

Numerous researchers in the field of electronic packaging have used the power of finite element methods to make solder joint life predictions under different operating conditions like thermal and power cycling, drop and shock, vibration and bending. Majority of finite element life prediction models are based on accumulated field quantities and derivatives of field quantities like creep strain, inelastic strain energy density and nonlinear plastic work etc.

[Amagai 1998 and Popelar 1997] proposed a viscoplastic constitutive model to analyze thermally induced plastic and creep deformation and low cycle fatigue behavior of the solder joints in Chip Scale Packages (CSP).

[Frear 1997 and Vianco 1999] developed a finite element simulation methodology to predict solder joint mechanical behavior that includes micro-structural evolution. The micro-structural evolution was incorporated through a series of mathematical relations that describe mass flow in a temperature/strain environment.

[Wang 2001] applied [Anand 1985] unified creep model to represent viscoplastic deformation behavior of solders. He concluded that inelastic deformation behavior calculated by the model can be applied for solder joint reliability predictions. [Zhang 2000] proposed a novel life prediction model that takes into account the damage evolution to accurately predict solder joint reliability.

[Darveaux 2000] established 63Sn37Pb eutectic alloy damage relationships correlating crack growth rate with inelastic strain energy density per cycle. This relationship is widely incorporated by other researchers in their life prediction frameworks to compute the characteristic life of ceramic BGAs on solder masked defined pads using finite element simulations. Later [Lall 2004] widened the scope of Darveaux's work by updating damage relationship constants and applied that for life prediction of plastic BGAs with non-solder masked defined pads. [Syed 2004] proposed accumulated creep strain and energy density based thermal fatigue life prediction models for lead-free SAC solder alloys using advanced finite element modeling and analysis. He used different constitutive equations proposed by [Wiese 2003, Schubert 2003, Zhang 2003 and Morris 2003] to model solder creep and studied its effect on life prediction accuracy.

[Zahn 2003] presented a three-dimensional finite element analysis methodology which explored global, sub-structure, and sub-modeling solution options using both slice and symmetry models for the purpose of deriving life prediction equations that determine

the fatigue response of microelectronic package structures using both eutectic (63Sn37Pb) and lead-free (95.5Sn4Ag0.5Cu) solder materials.

[Tee 2004] presented a life prediction model to estimate number of drops to failure for a package subjected to board level drop test. The maximum normal peel stress of the critical solder joint extracted from finite element simulation was used as the failure criteria to predict mean number of drops to failure.

One of the potential causes for mechanical failure of component interconnects is the bending of the PCB. [Shetty 2003] demonstrated the application of three-point and four-point bending tests for evaluating the reliability of chip scale packages under curvature loads. He proposed deformation energy based empirical reliability model to calculate mean life time to failure of solder joints under mechanical bending. The relationship between average cycles to failure and average strain energy density is established in this reliability model by volume averaging the strain energy density over the top layer of the solder joint, volume average technique proposed by [Zhan 20003, Darveaux 1992 and 2000].

2.3 Diagnostic Models

Life prediction models discussed in previous section are based on fear of failure, i.e. they provide estimate on failure life, which are only useful in making reliability predictions upfront i.e. before deployment in the intended field. Although these models help in benchmarking the overall life of electronics, they are of no use in the need of in-field fault detection during the service life. This is especially important for hi-reliability, mission critical applications wherein the characteristic life of the component is important before deployment but also continuous monitoring of system is equally important. Thus

condition monitoring leading to fault diagnosis has attracted researchers in the past few years because of its considerable influence on the operational continuation of many industrial processes. Correct diagnosis and early detection of incipient faults result in fast unscheduled maintenance and short downtime for the process under consideration. They also avoid harmful, sometimes devastating, consequences and reduce financial loss. An ideal diagnostic procedure should take the minimum measurements necessary from a machine and by analysis extract a diagnosis, so that its condition can be inferred to give a clear indication of incipient failure modes in a minimum time [Bellini 2008].

The diagnostic methods can generally be classified into the three basic categories. The model-based diagnostics checks how the system responds to inputs. It relies on some model of correct behavior of the diagnosed system. Using the inputs the model makes predictions of correct outputs; the differences between the actual outputs and the predictions are diagnostic variables called residuals. The latter are usually compared with certain threshold values and the results of the comparisons are the basis for the ultimate diagnostic decisions. The reference-band diagnostics is only applicable to closed-loop control systems. As the closed-loop system outputs should follow the commanded values, excessive discrepancies between the outputs and commanded values can be indicative of faults. In other words, the reference-band diagnostics checks how the system tracks the reference values. The signal-based diagnostics disregards any input–output relationships and exploits the fact that the output signals themselves can convey information about the health of a system [Sleszynski 2009].

The very first efforts in this area is the usage of Built- In-Self Test (BIST) circuit, which is an onboard hardware and software diagnostic means to identify and locate faults

and includes error detection and correction circuits [Drees 2004]. BIST is a methodology that embeds additional functionality in the product to give it the ability to test and diagnose itself with minimal interaction from external test equipment [Chandramouli 1996, Hassan 1992, Williams 1983, Zorian 1994]. BIST, when effectively designed in a chip / board / system, can yield an enormous amount of diagnostic information. BIST controllers can also output failure data that can be correlated to show exactly when the failure occurred. This data can then be interpreted by diagnostic software to analyze the cause of failure. For example, Pseudo-Random Binary-Sequence (PRBS) test pattern generators, apply input vectors to digital or analog [Al-Qutayri 1992] modules. Self-Checking circuit designs provide on-line test for digital [Lala 1985] as well as for analog circuits [Kolarik 1993]. The obtained output is then compared with a golden response. The results obtained from BIST functions can generate diagnostic information which in turn provides additional confidence in the measurement result and confirm the device availability.

Though BIST helps in minimizing the interaction with external automated test equipment (ATE) as well as provides the advantage of a more robust "at-speed" test of the circuitry, the current form gives little insight about the system level reliability or the remaining useful life of the system. Also, several studies conducted [Allen 2003, Drees 2004, Gao 2002, Rosenthal 1990] have shown that BIST can be prone to false alarms and can result in unnecessary costly replacement, re-qualification, delayed shipping, and loss of system availability.

Also, Fuses and Canaries are mounted on the part to provide advance warning of failure due to specific wear out failure mechanism. The basic procedure here is to take

some form of action, after an initial failure or malfunction, to prevent additional or secondary failures. By reducing the number of failures, techniques such as enhancing product reliability can be considered, although they also affect availability and product effectiveness. However, replacement of fuses and canaries does impact the maintenance, repair and part replacement making it difficult to integrate these systems with host system.

Although diagnostic models are able to detect faults in the system but they are unable to provide any information about the ongoing damage such as damage initiation and damage progression. In other words a fault is detected or diagnosed only when failure occurs. It also lacks insight about the remaining useful life of the systems. There is a growing need to develop techniques that can provide information about the impending failure way before the system is about to fail and use this information to predict remaining useful life. Prognostic Health Management (PHM) systems have the ability to perform fault diagnosis before the actual failure occurs and compute remaining useful life, and hence its application is relevant especially in hi-reliability applications.

2.4 Applications of Prognostic Health Management (PHM) Systems

Maintenance has evolved over the years from corrective maintenance to performing time-based preventive maintenance. Future improvements in reduction of system downtime require emphasis on early detection of degradation mechanisms. Incentive for development of prognostics and health management methodologies has been provided by need for reduction in operation and maintenance process costs [Jarell 2002]. New advances in sensor technology and failure analysis have catalyzed a broadening of application scope for prognostication systems to include large

electromechanical systems such as aircraft, helicopters, ships, power plants, and many industrial operations. Current PHM application areas include, fatigue crack damage in mechanical structures such as those in aircraft [Munns 2000], surface ships [Baldwin 2002], civil infrastructure [Chang 2003], railway structures [Barke 2005] and power plants [Jarrell 2002].

2.4.1 General PHM Applications

Previously PHM of mechanical structures has been done by dynamic analysis based on natural frequencies, mode shapes, damping factors, and static analysis based on deformation or changes in structure orientation due to load or unexpected damage using innovative signal processing, new sensors, and control theory [Kok 2005].

PHM systems for fault detection and characterization such as BEAM have also been proposed for spacecrafts which involves system characterization using all available observation followed by training of the characterization with respect to normal phase operation [Park 2002]. The use of multiple sources of information for the interrogation of system state and fault detection in aircrafts has been proposed in which predictions from various subsystems is used for fault diagnosis [Oza 2003].

Wayside detection involving fault identification using interrogating sensors placed along the sides of railway tracks has been used in the railway industry for gathering information about the vehicle performance. Information on the vehicle condition and performance over an extended period of time is recorded in an online database, which is interrogated for critical performance parameters to provide information on condition of in-service railway vehicles [Barke 2005].

A model-based method has been used for the on-line identification of cracks in a rotor of aircraft engines which start and stop quite frequently and run at high speeds [Sekhar, 2003].

Detection of surface corrosion has been used to reduce the maintenance required, and trigger preventive repair for increased aircraft availability and significantly reduced cost of ownership. Fluorescent fiber optic sensors that detect aluminum coating from the early stages of the corrosion process have been used for providing early warning of corrosion in susceptible areas of an aging aircraft [Maalej 2004].

Crack modeling approach in beam has been used to demonstrate the structural HM using low frequency vibration; simple models of crack flexibility based on beam elements are adequate [Friswell 2002].

Optical fiber based sensor system has been used on concrete structure to evaluate its performance for health monitoring [Fernando 2003]. Monitoring bridge performance has been done to answer questions on the performance of existing bridges, refine techniques needed to evaluate different bridge components, and develop approaches that can be used to provide a continuous picture of a bridge's structural integrity using structural health monitoring [DeWolf 2002]. These techniques help in detection of damage of bridges or building to avoid the economic and social effect of aging and deterioration [Chang 2003]. In other applications, signal feature analysis is used to detect abnormalities related to impending failure indication by an inference system using an historical database [Hess 2001].

2.4.2 PHM for Electronics

Implementation of PHM algorithms in electronics for the interrogation of system state and residual life calculations is still relatively at a latent stage compared to its application in other domains. Prognostics based health monitoring of electronics require leading indicators in the system for fault detection and decision support. A prognostic feature provides an advanced warning of impending failure to predict remaining useful life (RUL). Prognostic features may be extracted from a combination of device, circuit, or system parameters sensitive to damage accumulation [Brown 2007].

Modern aircrafts are increasingly dependent on avionic systems for a variety of roles ranging from effective communication and navigation to flight control, engine control and fuel management. Most of the avionics are intended for flight safety and thus the reliability associated with it can not be compromised at any point of time. Routine maintenance of such high reliability equipments requires advance planning and high expertise. On board diagnostic systems are intended to identify and localize component failures but it is well known that electronic parts can fail in number of different modes at different times resulting in ambiguous diagnosis. There is a growing need to develop prognostic techniques for such high reliability applications which can provide early device degradation warning for maintenance with considerable reduction in variability. Some of the damage indicators that have been incorporated in the development of the prognostic techniques for avionics include power dissipation, output degradation and aging of semiconductors [Hecht 2006].

In case of mission critical applications like space explorations the reliability of the spacecraft is extremely important as they are away from the earth for considerably long periods of time. Effective on-board prognostic systems not only increase safety by detecting problems before they become serious and prevent major failures but also help schedule efficient maintenance [Schwabacher 2005].

Switch mode power supplies (SMPS) commonly used aboard aircraft for various electrical power requirements are susceptible to malfunction due to component failures. Previously prognostic approach dealing with SMPS health management has been developed in which components like switching transistors, filtering capacitors and rectifying diodes inside SMPS have been indentified as critical components for prognosis [Orsagh 2005].

Reliability of the electronic power modules used in vehicles has always been a concern as it consists of numerous electronic components which undergo thermal stresses and fatigue due to power dissipation during usage. The nature of the gradual degradation of these power modules has enabled the development of prognostic systems for the same. Some of the signatures of impending failures including increase in forward on-voltage, leakage current and thermal impedance have been used as the damage proxies for the on-board prognostic system [Xiong 2008].

Field data from aircraft has been evaluated for the continuous health assessment of avionics and a prognostic software has been developed that involves mining of data from multiple sources, trending and ranking of anomalous indicators, development of on-board built-in-test (BIT) data and automated advanced reasoning for reduced ambiguity [Dussault 2006].

For many years, commercial telecom systems have adopted many forms of reliability enhancements all intended to improve system up-time. While these changes have been effective, the surprise factor is still prevalent in systems carrying vitally important traffic over the network. Providers and technicians alike often wish there was some signal or other indicator of an upcoming problem in order to take some action in advance of a system shutdown [Wood 2006].

Electronics systems may be subjected to prolonged periods of thermal exposure over wide temperature extremes and long periods of thermal aging at often high ambient temperatures. High-rel systems may have very long operating life times with low downtime during operation. Historical environmental conditions to which the systems may have been subjected may be often unavailable. PHM for electronics has wide applicability spanning a number of different areas. Electronics used in critical applications like space, military and avionics require multiple deployments with sequential thermal stresses. Systems may also be subjected to long term dormant storage in uncontrolled thermal environments. Ultra high reliability is needed to ensure predictable operation when needed and avoid any catastrophic damage during the service life.

There is need for tools and techniques which will enable the spot-assessment of the system's health and provide method for estimation of remaining useful life. Prognostication of sequential thermo-mechanical damage under thermal aging and thermal cycling based on damage pre-cursors is currently beyond the state of art.

Previously [Lall 2005, 2006[a,b], 2007[a,b] and 2008] has developed leading indicators based prognostic and health management methodologies for residual life computation of

electronics subjected to single thermal environments comprising of isothermal aging and thermal cycling. Examples of damage pre-cursors include micro-structural evolution of second level solder interconnects, inter-metallic compound growth, stress and stress gradients. Pre-cursors have been developed for both eutectic 63Sn37Pb and various lead-free alloy compositions like Sn4Ag0.5Cu, Sn3Ag0.5Cu, Sn1Ag0.5Cu, Sn0.3Ag0.7Cu, Sn3Ag0.5Cu-Bi, Sn3Ag0.5Cu-Bi-Ni, 96.5Sn3.5Ag alloy systems on a variety of area-array architectures.

In this thesis, PHM models have been developed and implemented for the interrogation of system state and the estimation of remaining useful life of electronic systems subjected to single steady-state environment and multiple thermal environments of isothermal aging and thermal cycling. Data on damage pre-cursors has been collected and analyzed for both aging and cycling to develop a technique that can map aging time into number of cycles and thus account for reduction in life due to dormant storage. The methodology involves the use of condition monitoring devices which have been interrogated for aging, cycling and different combinations of aging + cycling for residual life predictions. Developed PHM technique is based on non-linear least-squares method called Levenberg-Marquardt (LM) algorithm which has been developed for two different damage proxies. Prognostic model performance based on standard prognostic metrics has also been evaluated for both the damage proxies to determine which leading indicator of failure can be employed for accurate life prediction. Results of interrogation of system state have been compared with a second set of experimental-matrix to validate the proposed methodology.

CHAPTER 3

PROGNOSTIC MODEL FOR LIFE ESTIMATION OF ELECTRONICS SUBJECTED TO STEADY-STATE ISOTHERMAL AGING

3.1 Introduction

Electronic systems may often be subjected to high temperature steady-state aging environments depending upon the usage profile or during storage. It is well known that even the steady-state temperature has a detrimental effect on life of electronics. The presented PHM model enables life estimation of electronics subjected to single isothermal aging environments. The proposed methodology enables spot assessment of life consumed due to isothermal aging environments in the pre-failure space, without any knowledge of prior stress histories. This technique eliminates the need for continuous monitoring of the system state to make life predictions, which considerable saves the overhead associated with data acquisition systems. The prognostic model is based on physics-of-failure of lead-free second level solder interconnects commonly found in today's high I/O packaging architectures.

3.2 Test Vehicle

Two most popular lead-free solder alloy compositions viz. 98.5Sn1.0Ag0.5Cu (SAC 105) and 96.5Sn3.0Ag0.5Cu (SAC 305) on ball grid array packaging architecture have been used in this study. These two solder alloy compositions were chosen as industry has widely accepted these two solder alloy compositions as the drop-in

replacement for eutectic Sn/Pb for drop/shock and thermo-mechanical applications respectively. The packaging architecture used for this study is chip-array ball grid array CABGA with 100 I/O. The primary motivation behind choosing this packaging architecture was that plastic ball grid arrays PBGAs are replacing leaded packages in the commercial sector due to its small form factor. The test vehicles were imported from practical components which consist of Amkor CABGA100 packages as shown in Figure 3. The test board is a 132 mm X 77mm JEDEC drop test board as shown in Figure 4. SAC 105 and SAC 305 solder pastes were provided by Cookson Electronics. Table 2 summarizes other package attributes. Test boards were subjected to single accelerated thermal aging environment only. The isothermal aging temperature chosen for this accelerated testing was 125ºC so that substantial amount of damage is accrued in short period of time.

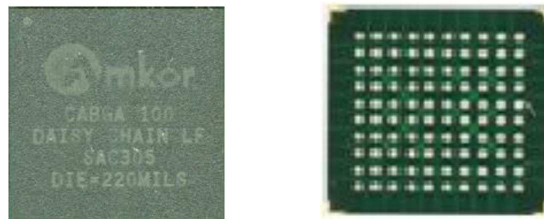

Figure 3: CABGA 100 Package Front and Back View

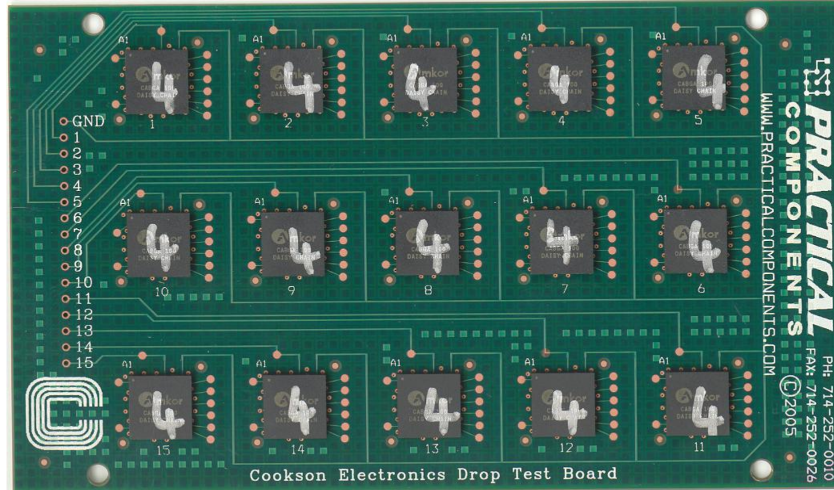

Figure 4: Test Vehicle

Table 2: Package Attributes (All Dimensions are in mm)

Body Size	**Solder**	**Package Type**	**Ball Count**	**Ball Pitch**	**Die Thick**	**Die Size**	**BT Thickness**	**BT Pad Type**	**Ball Diameter**
10	SAC 305	CABGA	100	0.8	0.26	6.4	0.26	NSMD	0.50
10	SAC 105	CABGA	100	0.8	0.26	6.4	0.26	NSMD	0.50

Multiple sets of test vehicle have been used in this study for experimental and prognostication respectively. Two condition monitoring cells of test vehicles were created viz. CM#1 and CM#2 where, CM#1 was allotted for experimental part and was subjected to multiple of hours of aging at 125ºC. Test vehicles in CM#2 were allotted for the development and implementation of the prognostic model.

3.3 Inter-Metallic Compound (IMC) Growth as Leading Indicator of Failure

The leading indicator of failure used for developing this prognostic model is called the inter-metallic compound (IMC) growth which is formed between the solder ball and board-side copper pad as shown in Figure 5. Typically in electronics manufacturing the solder paste is first printed on a copper pad footprint on a printed circuit board (PCB), components are placed on this solder print and the assembly is allowed to undergo high temperature reflow.

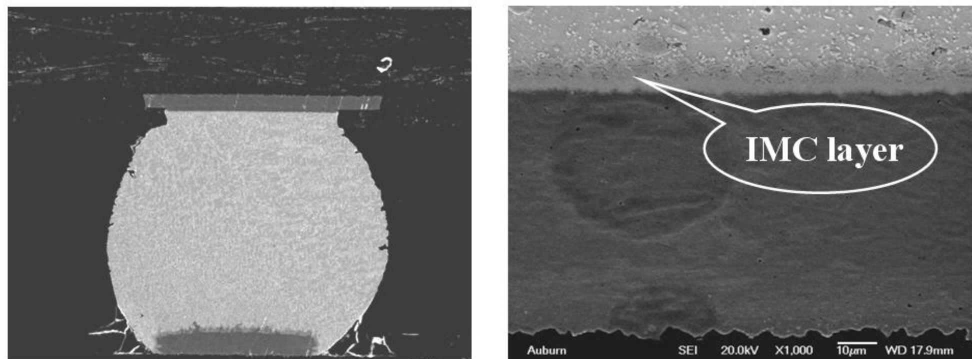

Figure 5: Inter-metallic Compound (IMC) at Solder Ball, Copper Pad Interface

During the soldering process when solder is in the molten stage, the formation of an inter-metallic compound between Sn-based solders and substrates is inevitable and then it continues to grow during solid-state aging. High temperature accelerates the diffusion of metal atoms across the interface, causing the formation of inter-metallics. The initial formation of these inter-metallic compounds at the interface between the solder and the substrate during soldering ensures a good metallurgical bond. However, the growth of these inter-metallic compounds influence the strength and can result in mechanical failure of the joints.

Most lead free alloys are Sn-based. Eutectic alloy is preferred due to its single and low melting point. Eutectic Sn alloys have higher melting points than Sn-Pb. Hence the

corresponding reflow temperatures are also higher, typically by about 30°C. This increases the rate of IMC formation with Cu. Furthermore it is not possible to develop a high temperature solder with SAC alloys as adding high percentages of Ag or Cu tend to have a large temperature gap between liquids and solidus points which is highly undesirable.

Examining the microstructure of SAC alloys suggests that it is a mix of Sn and IMC, unlike eutectic Sn-Pb which has no equilibrium IMC. Also the Sn-Cu reaction rate during the high reflow temperatures is very intense; hence even the small amount of Ag leads to large amount of IMC formation. The properties and thickness of IMC's formed at the solder pad interconnects directly affects the reliability of solder joints [Tz-Cheng 2004, Tu 2002, Lehman 2005]. Understanding the effects of IMC formation in Pb-free solder joints and how this formation can be limited is crucial in obtaining solder joint reliability.

3.3.1 Formation of Different Inter-metallic Compounds:

Immediately after the flux reduces surface oxides and permits metallurgical contact of solder to Cu, the solid Cu starts to dissolve into the molten solder. The formation of Cu6Sn5 takes Cu out of the saturated solder and causes some further dissolution of Cu from the solid Cu pad. The Cu6Sn5 crystallizes and joins together to form a continuous layer on the Cu, blocking the channel for further liquid solder dissolution of Cu. However, Cu is not in equilibrium with Cu6Sn5. There is another IMC, Cu3Sn, between Cu and Cu6Sn5. This implies that the interface between the Cu6Sn5 IMC and Cu pad is not stable. Consequently, the solder reaction will continue through solid state diffusion to form Cu3Sn IMC between Cu and Cu6Sn5 if the temperature is

high enough to activate the reacting atoms of Cu and Sn. The Cu-Sn inter-diffusion process does not stop even after the Cu3Sn layer is in place. In the Cu-SnAgCu solder system, the diffusing Cu atoms arrive at Cu3Sn-Cu6Sn5 and Cu6Sn5- solder interfaces and result in the growth of both IMC layers towards the solder. Because of the unbalanced Cu-Sn inter-diffusion through interface, Cu atoms on the bare Cu side are not filled by Sn atoms. This result in the formation of something called as voiding at the IMC interface. The voiding process is initiated at as low as 100°C which is the main mechanism for joint strength degradation under thermal aging which can be detrimental in high temperature applications [Dunford 2004].

3.3.2 Inter-Metallic Compound (IMC) Measurement and Analysis

The inter-metallic compound has been empirically observed to grow when the electronic assembly is subjected to high temperature isothermal aging for increasing time intervals [Lall 2004, 2005, 2006]. The compositions of the IMC layer closer to solder interconnect has been identified as Cu_6Sn_5 and that near to copper pad has been identified as Cu_3Sn using energy dispersive X-ray (EDX). It has been observed that with the increasing aging time, the IMC layer thickens, and the local irregularities appear to gradually smooth out.

Previously, empirical analysis of inter-metallic compound (IMC) thickness growth at various intervals of time has indicated a square root dependence of inter-metallic thickness on aging time.

$$y(t) = y_0 + k\sqrt{t} \qquad (1)$$

Where y (t) is inter-metallic compound growth thickness during aging at time t, y_0 is the initial thickness of inter-metallic compounds, k is the coefficient standing for the square

root of the diffusivity at aging temperature, and t is the aging time. The exponent value, n = ½ has been used in $y(t) = y_0 + k\sqrt{t}$ (1 above, which reveals a diffusion-controlled mechanism during aging. The IMC growth data indicates that growth rate stays fairly uniform during the thermal aging. It is observed that for Sn-Ag solder systems, the inter-metallic compound thickens roughly as $t^{1/2}$ in a linear manner, where t is the aging time as expected for diffusion-controlled growth. This trend has been cross checked in the case study section for both SAC 105 and SAC 305 test vehicles.

In order to measure the inter-metallic compound (IMC) growth, samples were withdrawn at various aging time intervals. The withdrawn samples were cross-sectioned, potted using epoxy resin and finely polished using grinding papers and collidal silica solution so that the inter-metallic layer was clearly visible under the microscope. The inter-metallic thickness was measured using pictures taken from Scanning Electron Microscope (SEM), JEOL JSM-7000F operated at an accelerating voltage of 20V and magnification of 1000X.

3.4 Problem Definition and Prognostication Methodology

In real world setting it is often required to know during the service life of the system what is the amount of life consumed well before the actual failure occurs especially for mission critical applications. The problem defined in this chapter is a real world application problem wherein the electronic system is already deployed in some isothermal aging environment for unknown time period and one has to compute the life consumed in terms of hours of aging well before the failure takes place. Figure 6 depicts the problem definition. Here the timeline is defined by START and END or t=0 and t=FAILURE. It means that electronic system is deployed in isothermal aging

environment (125°C) at t=0 and has an active field life until t=FAILURE. The primary objective of the prognostic model is to assess life consumed at any point of time between START and END.

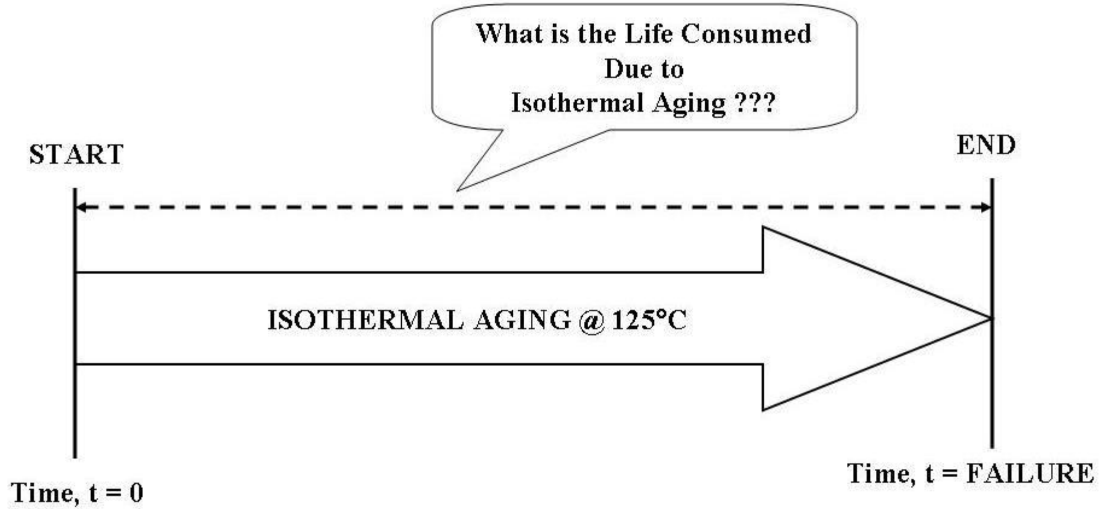

Figure 6: Problem Definition

The framework adopted to compute the life consumed due to aging is shown in the form of a flowchart as shown in Figure 7. The prognostic model proposed in this chapter predicts the life in terms of aging based on inter-metallic compound growth as the leading indicator of failure discussed earlier in the chapter. A detailed case-study has been presented later in this chapter.

The equation relating IMC growth of the solder interconnect with aging time 't' the system has been exposed to a isothermal aging environment is given by,

$$y(t) = y_0 + k\sqrt{t} \qquad (2)$$

Where, 'y(t)' is the IMC thickness measured after t hours of thermal aging, 'y_0' is the IMC thickness measured after reflow, 't' is the aging time the system is exposed to in a

isothermal aging environment and 'k' is a constant. The damage incurred during aging is reflected in the IMC thickness of the solder which can be measured by cross-sectioning the sample. Thus in real time, without the knowledge of prior stress histories one can only find IMC thickness y(t) in the above equation while rest of the variables y_0, k and t are unknowns.

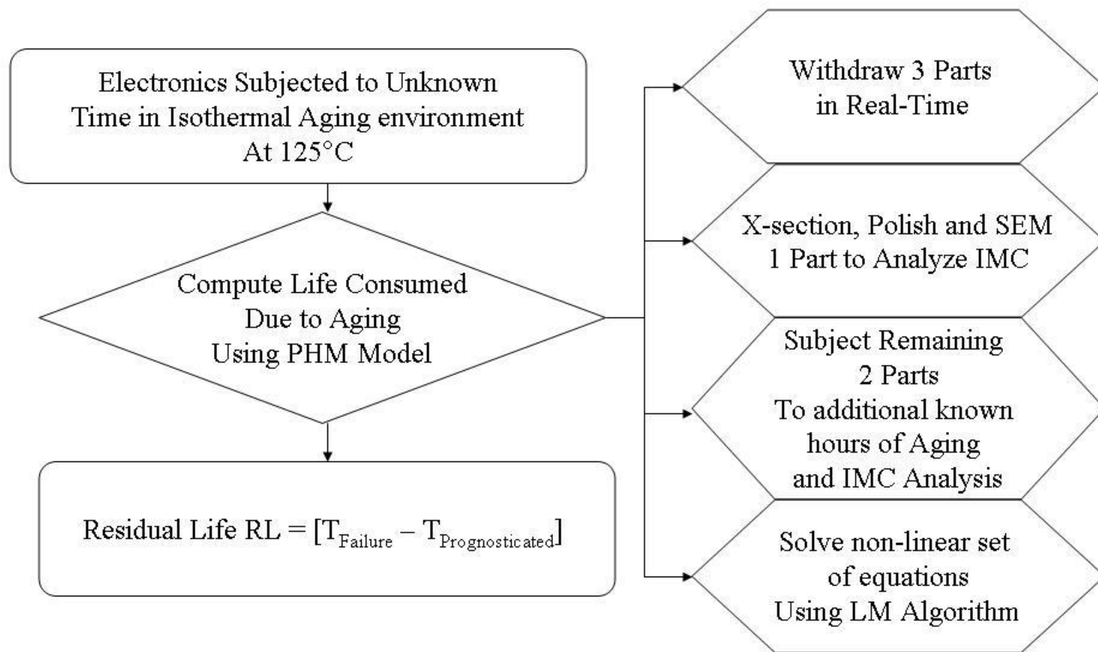

Figure 7: Flowchart for Life Estimation of Electronics Subjected to Single Isothermal Aging Environment

The prognostic model has been developed to predict the aging time't' the system has been exposed to in a isothermal aging environment based on the real time IMC measurement 'y'. In order to compute the aging time, the non-linear IMC growth equation (Equation 2) has been solved for the 3 unknown's viz. t, k and y_0. To solve 3

unknowns we need 3 equations and therefore the system has to be subjected to known additional hours of aging (t + Δt, t + 2Δt), followed by IMC thickness measurements $y_{t+\Delta t}$ and $y_{t+2\Delta t}$ for additional aging times respectively as depicted in the flowchart (Figure 7). The following 3 equations are solved to compute t, k and y_0.

$$y(t) = y_0 + k\sqrt{t} \quad (3)$$

$$y(t+\Delta t) = y_0 + k\sqrt{t+\Delta t} \quad (4)$$

$$y(t+2\Delta t) = y_0 + k\sqrt{t+2\Delta t} \quad (5)$$

As there exist a non-linear relationship between the IMC growth and time t, thus a non-linear least square technique has been employed to minimize error in the solution space. All the prognostic models proposed in this thesis are based on non-linear least square (NLLSQ) method called Levenberg-Marquardt algorithm which has been discussed in the next section.

3.5 Levenberg-Marquardt Algorithm (LMA)

A non-linear set of equations does not have a trivial solution which means that when non-linear equations like the three IMC growth equations are solved to compute three unknowns ($y(t) = y_0 + k\sqrt{t}$ (**3**,

$y(t+\Delta t) = y_0 + k\sqrt{t+\Delta t}$ (**4** and

$y(t+2\Delta t) = y_0 + k\sqrt{t+2\Delta t}$ (**5**), we get multiple solutions for all the three unknowns. In order to find the exact solution from a multidimensional solution space or in other words to reduce multiple solutions to a single solution for each unknown a technique like Levenberg-Marquardt (LM) algorithm has to be implemented.

Typical output from a LM algorithm is depicted in Figure 8. Each dot in the solution space represents a solution of non-linear equations. The algorithm iteratively minimizes error in each step and selects the final solution corresponding to the minimum error as shown by the red dotted lines.

Levenberg-Algorithm is a higher order non-linear least square method which is a combination of Gauss-Newton method and Steepest Descent method. It is a hybrid method which combines the speed of the Newton algorithm with the stability of the Steepest Descent method. The primary reason for incorporating two non-linear least square methods into one algorithm is because it eliminates the individual weaknesses of Newton method and steepest descent method.

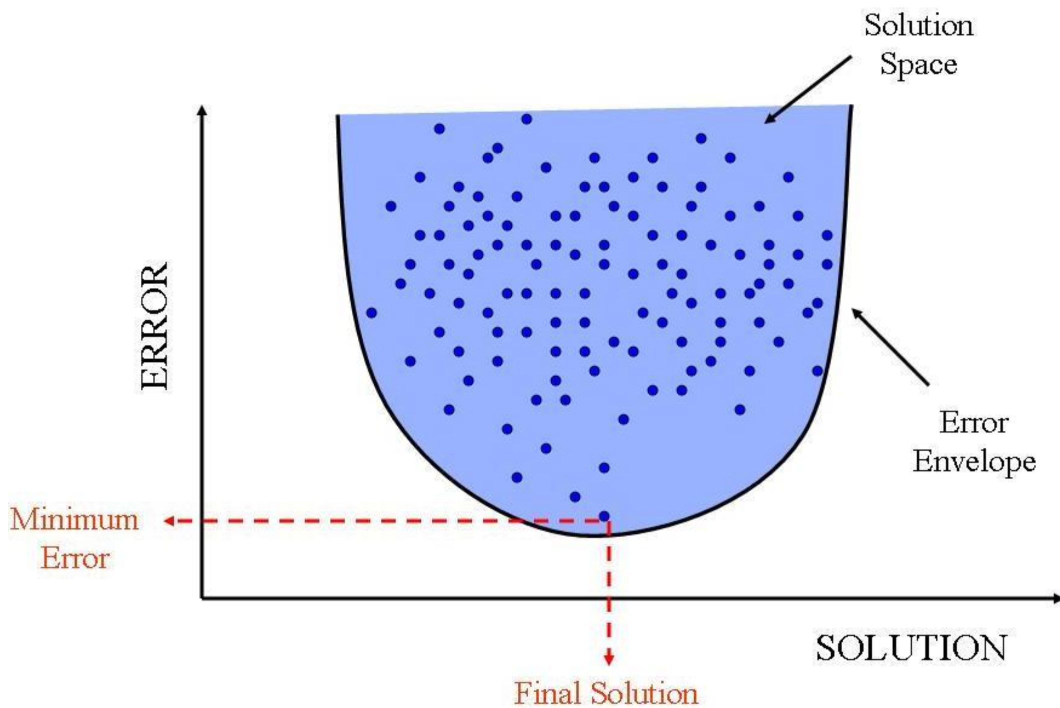

Figure 8: Schematic of a Multidimensional Solution Space

Solution of a non-linear system largely depends upon the guess values which vary according to the problem. The main obstacle in using steepest descent method alone is

that if the error curvature is in different directions i.e. if the error envelope is zigzag, there is a high probability that the steepest descent method would get stuck in the local minima and would never converge to the global minima as shown in Figure 9. Or even if it does converge the entire process can be extremely inefficient and time consuming. On the contrary the disadvantage of using Gauss-Newton method alone is that it does not guarantee the convergence even to the local minima especially when we are away from the solution or at the start of the solution. If the initial guess value is far from the minimum there is a high probability that the Gauss-Newton method will not converge at all.

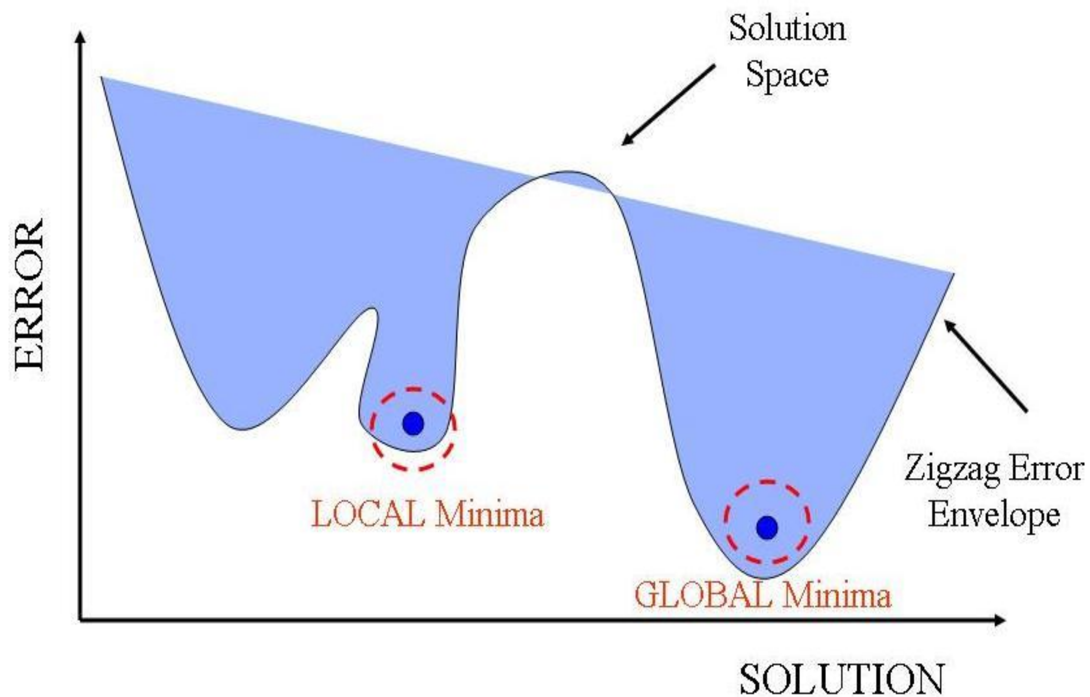

Figure 9: Schematic highlighting drawbacks of Steepest Descent Method

Levenberg-Marquardt algorithm has been developed to exploit the advantages of both the methods at the same time and eliminate the individual drawbacks of the two methods. It effectively switches between these two methods using a learning parameter or

a damping parameter. When the solution is away from the minima it becomes steepest descent method and switches to Gauss-Newton when it is close to the final solution. The equation used to minimize the multidimensional solution space is given by,

$$(J^T J + \mu I)\, h = -J^T e \qquad (6)$$

Where J is the Jacobian matrix which is used to minimize the error in the each iteration step, μ is the damping parameter which governs the switching of the two methods, I is the identity matrix, h is the descent direction which controls the step size in each iteration and e is the error vector. Jacobian is a partial derivative of the governing equation with respect to each unknown. The governing equation for this problem is given by $y(t) = y_0 + k\sqrt{t}$ (2. It relates IMC growth with the aging time. Thus the partial derivatives of $y(t) = y_0 + k\sqrt{t}$ (2 with respect three unknowns viz. y_0, k and t is given by,

$$\frac{\partial y}{\partial y_0} = 1 \qquad (7)$$

$$\frac{\partial y}{\partial k} = \sqrt{t} \qquad (8)$$

$$\frac{\partial y}{\partial t} = \frac{1}{2}\frac{k}{\sqrt{t}} \qquad (9)$$

As we have 3 unknowns the size of the Jacobian matrix is 3X3 as shown below,

$$J = \begin{matrix} \frac{\partial y_1}{\partial y_0} & \frac{\partial y_1}{\partial k} & \frac{\partial y_1}{\partial t} \\ \frac{\partial y_2}{\partial y_0} & \frac{\partial y_2}{\partial k} & \frac{\partial y_2}{\partial t} \\ \frac{\partial y_3}{\partial y_0} & \frac{\partial y_3}{\partial k} & \frac{\partial y_3}{\partial t} \end{matrix} \qquad (10)$$

3.6 Case Study: Prognostication of Life Consumed Due to Steady State Aging

The primary objective of this case study was to develop and implement the prognostic model for the life prediction of electronics subjected to isothermal aging environments. The model has been implemented on the test vehicle discussed in the previous section. Case study has been divided into two parts viz. IMC growth measurement and analysis followed by implementation of the PHM model for prognostication of life using IMC growth as the leading indicator of failure.

3.6.1 Inter-Metallic Compound (IMC) Growth Measurement and Analysis

For this a condition monitoring cell was created consisting of 100 CABGA packages with SAC 105 and SAC 305 solder alloys. This condition monitoring cell was subjected to several hours of isothermal aging at 125°C to study the damage progression in steady state thermal environments. The aged components were withdrawn at regular intervals of aging time to measure the intermetallic compound growth at board side copper interface. The withdrawn samples were cross-sectioned, potted using epoxy resin and finely polished using grinding papers and collidal silica solution so that the inter-metallic layer was clearly visible under the microscope. Figure 10 and Figure 11 show SEM backscattered images exhibiting examples of IMC growth with aging time for 100 I/O, BGA solder ball for SAC 105 and SAC 305 solder alloys respectively. The IMC

thickness has been measured in commercial image processing software using these SEM images. It is evident from the SEM images that the IMC thickness tends to grow as the electronic packages are exposed to long durations of thermal aging. The IMC growth has been plotted against aging time for both SAC 105 and SAC 305 solder alloys as shown in Figure 12 and Figure 13. The trend analysis does show a square root dependence of IMC growth over time as mentioned in the previous section.

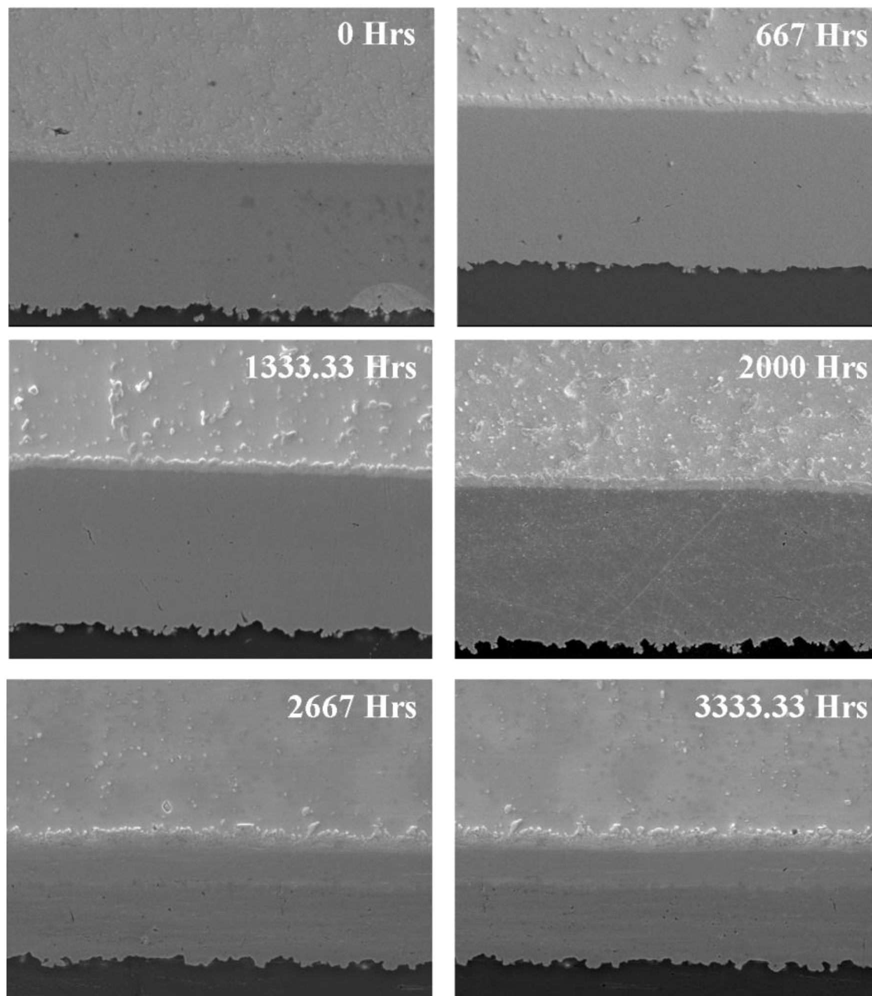

Figure 10: SEM Back-scattered images of IMC Growth versus Thermal Aging for Sn1Ag0.5Cu (SAC 105) (Magnification 1000x)

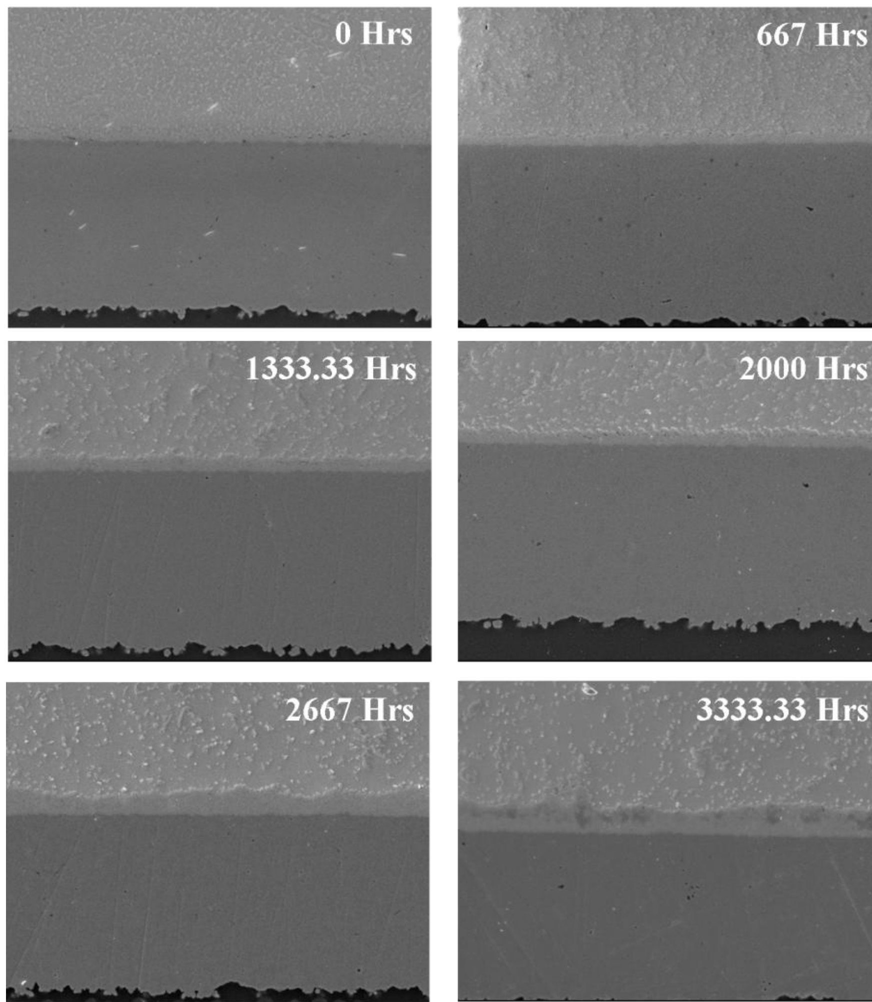

Figure 11: SEM Back-scattered images of IMC Growth versus Thermal Aging for Sn3Ag0.5Cu (SAC 305) (Magnification 1000x)

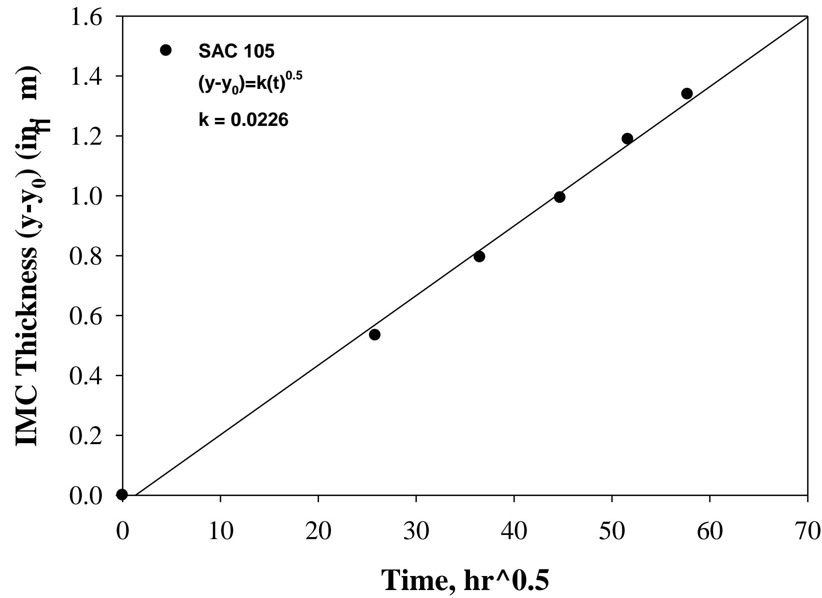

Figure 12: IMC Growth, at various levels of time for CABGA 100 with Sn1Ag0.5Cu alloy (SAC 105)

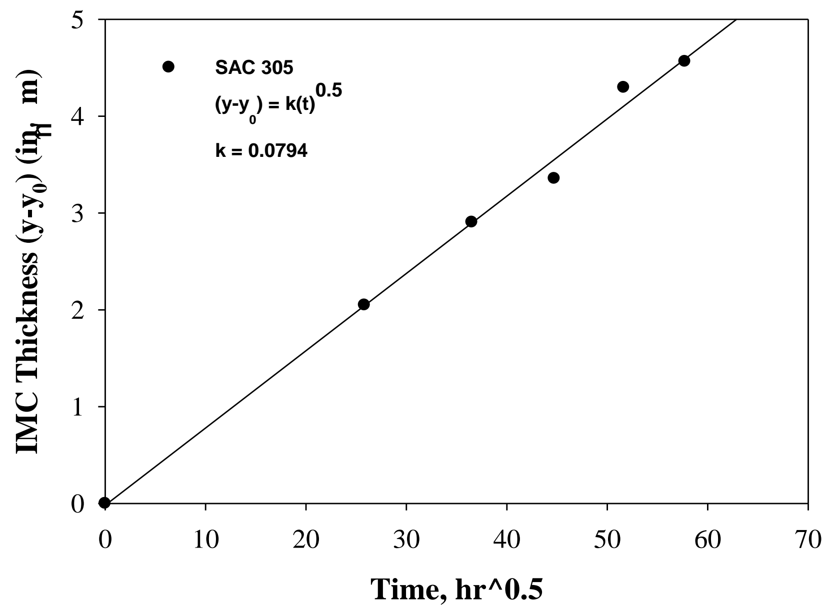

Figure 13: IMC Growth, at various levels of time for CABGA 100 with Sn3Ag0.5Cu alloy (SAC 305)

3.6.2 Life Prediction using PHM Model

Test assemblies were subjected to unknown hours of isothermal aging and the consumed life was predicted using the framework summarized in Figure 14. Two aging times have been prognosticated to prove the viability of the PHM model.

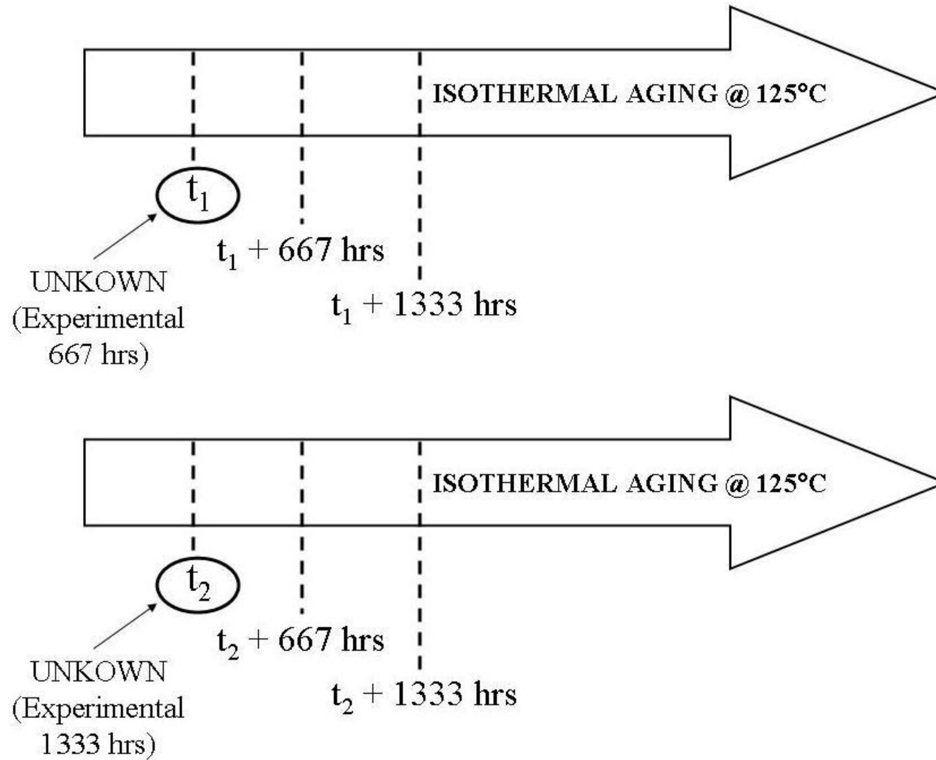

Figure 14: Prognostication Approach

As IMC growth has been used as the leading indicator of failure in the model, we need 3 equations to solve 3 unknown's viz. y_0, k and t as explained in the earlier section. In order to solve 3 unknowns we need 3 equations and hence the test assembly has to be subjected to additional (known) hours of aging at 125°C. Therefore to prognosticate two unknown aging time t_1 and t_2, some of the 100 CABGA packages from the condition monitoring cells were subjected to additional 667 hours and 1333 hours of aging as shown in Figure 14. The packages were cross sectioned for IMC growth measurement at each interval and the following sets of equations were solved using Levenberg-Marquardt algorithm to compute t_1 and t_2 respectively.

$$y(t_1) = y_0 + k\sqrt{t_1} \quad (11)$$

$$y(t_1 + 667) = y_0 + k\sqrt{t_1 + 667} \quad (12)$$

$$y(t_1 + 1333) = y_0 + k\sqrt{t_1 + 1333} \quad (13)$$

$$y(t_2) = y_0 + k\sqrt{t_2} \quad (14)$$

$$y(t_2 + 667) = y_0 + k\sqrt{t_2 + 667} \quad (15)$$

$$y(t_2 + 1333) = y_0 + k\sqrt{t_2 + 1333} \quad (16)$$

Figure 15 and Figure 17 shows the model outputs for t_1 and t_2 respectively for SAC 105 CABGA 100 test vehicle. Similarly Figure 16 and Figure 18 show the model outputs for t_1 and t_2 respectively for SAC 305 CABGA 100 test vehicle. It's a 2D plot of error Vs aging time in hours. Each and every blue dot in the solution space represents the solution of a non-linear set of equations. Levenberg-Marquardt algorithm iteratively minimizes the error in the solution space and selects the final solution corresponding to the minimum error indicated by red dotted line in all the figures. Thus for the experimental value of 667 hours, proposed prognostic model predicts 621 hours for SAC 105 CABGA 100 test vehicle (Figure 15) and 625 hours for SAC 305 CABGA 100 test vehicle (Figure 16). It should be noted that similar 2D plots can be graphed for the rest of the unknown's y_0 and k respectively. However as aging time is the most important unknown of all and as life prediction has been the chief scope of this thesis only plots pertaining to aging time are retained, although model results for other unknowns have been documented in the subsequent validation section.

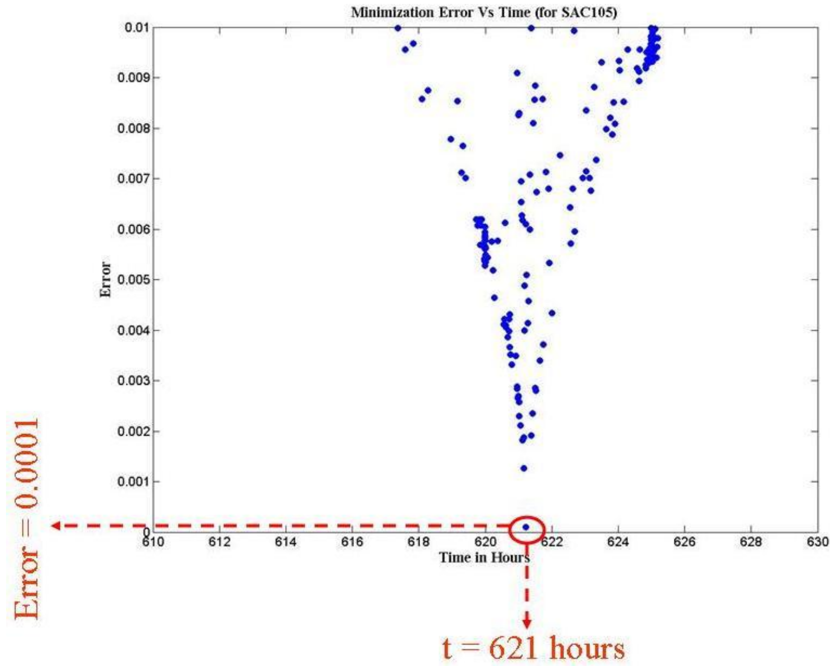

Figure 15: Global Minima for IMC based History Calculation for 100 I/O CABGA, Sn1Ag0.5Cu Solder Alloy Interconnects

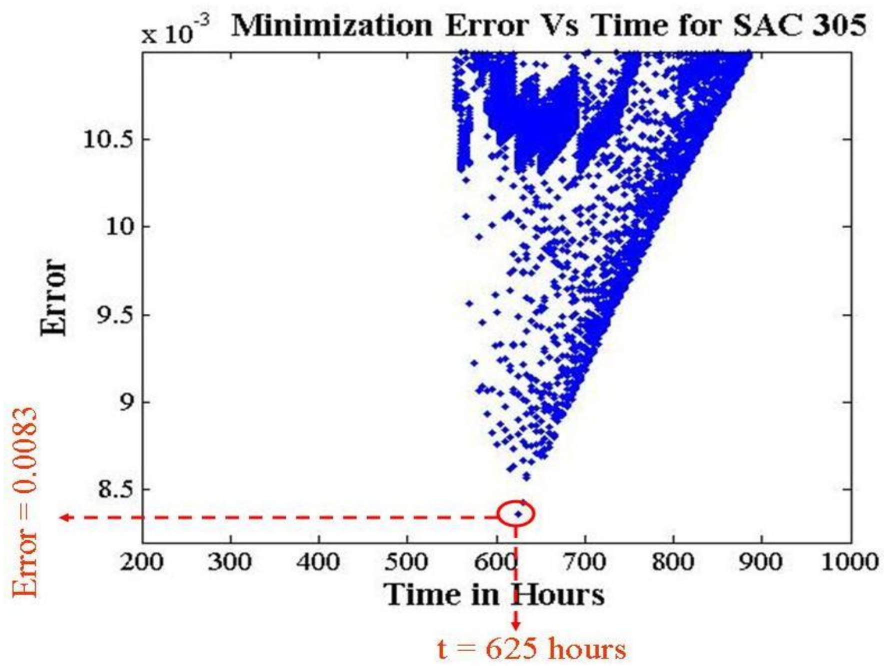

Figure 16: Global Minima for IMC based History Calculation for 100 I/O CABGA, Sn3Ag0.5Cu Solder Alloy Interconnects

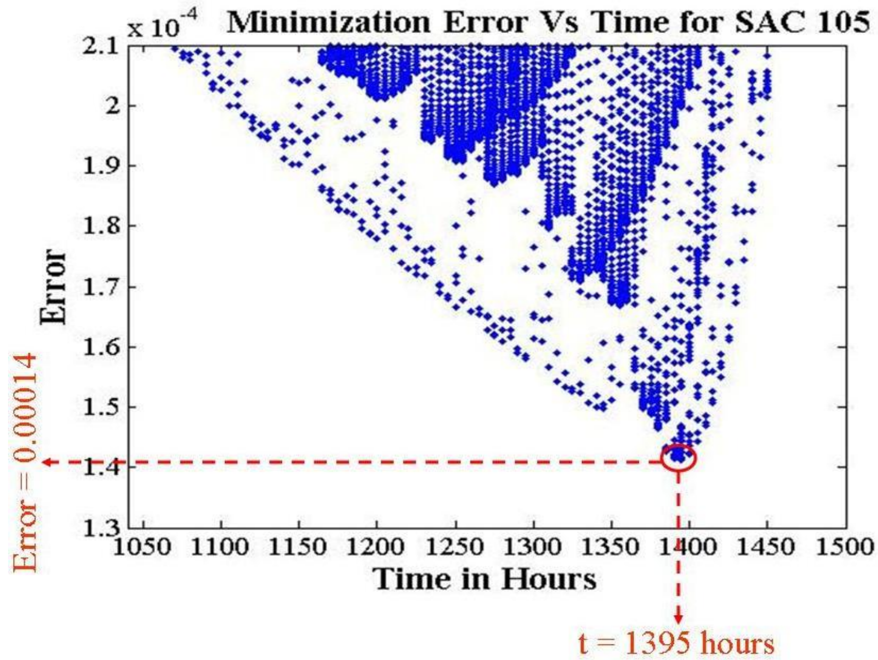

Figure 17: Global Minima for IMC based History Calculation for 100 I/O CABGA, Sn1Ag0.5Cu Solder Alloy Interconnects

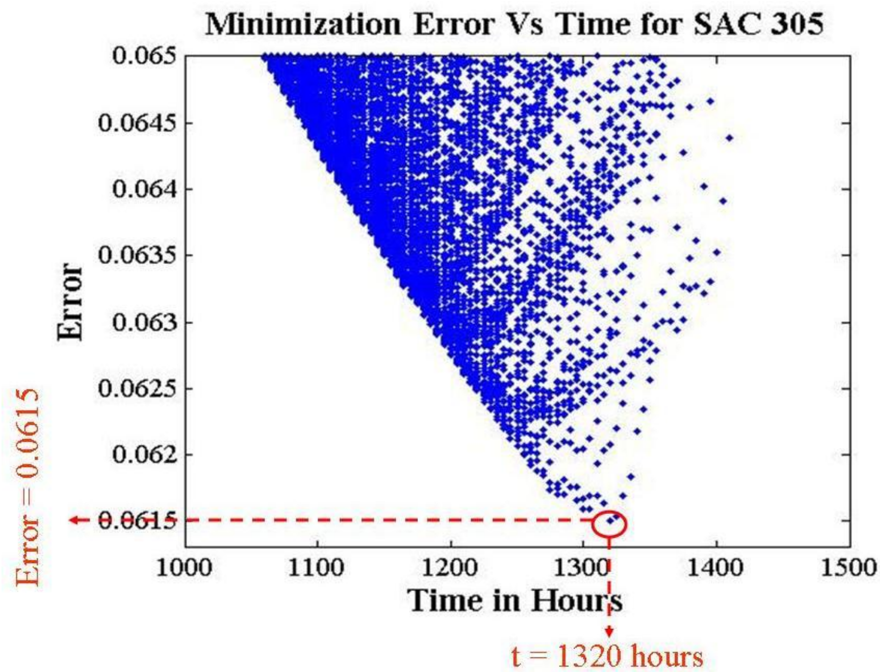

Figure 18: Global Minima for IMC based History Calculation for 100 I/O CABGA, Sn3Ag0.5Cu Solder Alloy Interconnects

3.6.3 Model Validation

Life predicted from the proposed prognostic model has to be checked to study the errors associated with the model. For this model predictions have been correlated with the actual experimental data in this section. Although only the plots corresponding to aging time t are presented in the previous section, but, all the three unknowns have been compared with the experimental values to check individual errors. Two different aging time intervals have been prognosticated and correlated with the experimental data to examine the robustness of the prediction model. Table 3 correlates the model results with the experimental values for all the three unknowns. Error has been computed for all the three unknowns with respect to the experimental values to gain more insight on how individual unknowns are predicted by the prognostic model.

Table 3: Comparison of computed values of t, y_0 and k from prognostication model and experimental result

Solder Interconnect	**Aging Time t (hrs)**			**Initial IMC y_0 (μm)**			**Constant k**		
	EXPT	MODEL	ERROR	EXPT	MODEL	ERROR	EXPT	MODEL	ERROR
SAC 105	667	621	6.9 %	2.89	2.82	2.4 %	0.0226	0.0258	14.2 %
	1333	1395	4.7 %	2.89	2.69	6.9 %	0.0226	0.0215	4.8 %
SAC 305	667	625	6.3 %	2.68	3.03	13 %	0.0794	0.0790	0.5 %
	1333	1320	0.98 %	2.68	2.28	14.9 %	0.0794	0.0781	1.6 %

The model predictions for unknown t for both the time intervals and solder interconnect lay in the range of 1 % to 7 % which is very good from a life prediction model perspective. Initial IMC y_0 predicted by the model for SAC 105 interconnects is better than that for SAC 305 solder interconnects which is in the range of 13 % to 15 %. As for constant k error envelope is in the range of 1.6 % to 15 % for both the solder

interconnects. As the model results are directly dependent on the input guess values for each unknown, one way of reducing the individual errors is by expanding the guess values for each unknown. However this has a direct impact on the computational efficiency. So like any other life prediction model it is a trade off between the appetite for risk and computational capability.

The other interesting finding was that the IMC thickness calculated from the prognosticated values of y_0 and k correlate well with the measured experimental value. The primary reason for this correlation was to find out how well the extrapolated IMC thickness match with the actual experimentally measured IMC thickness so that the extrapolated value can be used for further life predictions. This by passes the need to cross section the samples in real time for IMC measurement which can be thought of as a big leap forward in the implementation of the proposed PHM model. Figure 19 and Figure 20 shows the correlation plots for SAC 105 and SAC 305 solder interconnects respectively.

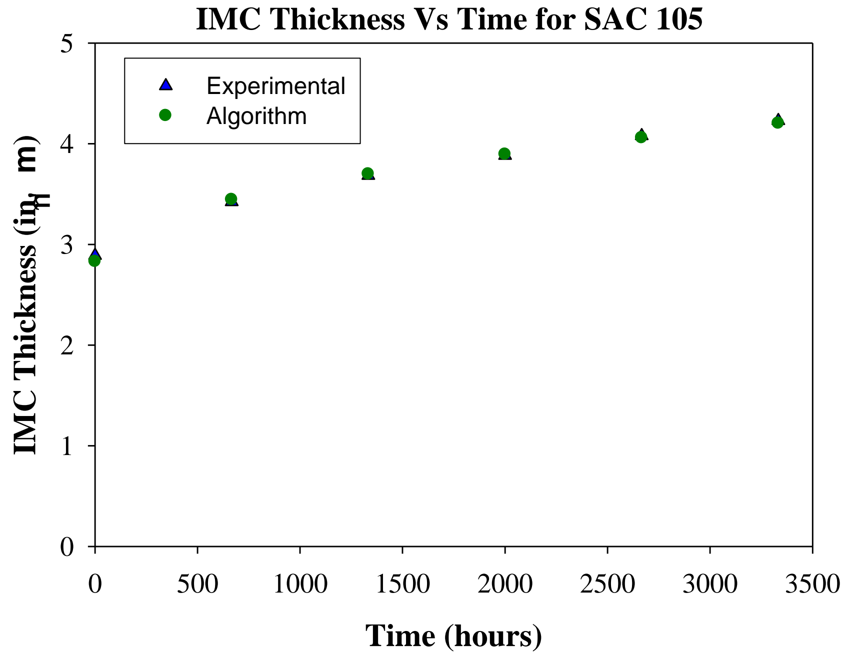

Figure 19: Computation of IMC Thickness (based on prognosticated y_0 and k) vs. IMC from experimental values for 98.5Sn1.0Ag0.5Cu alloy

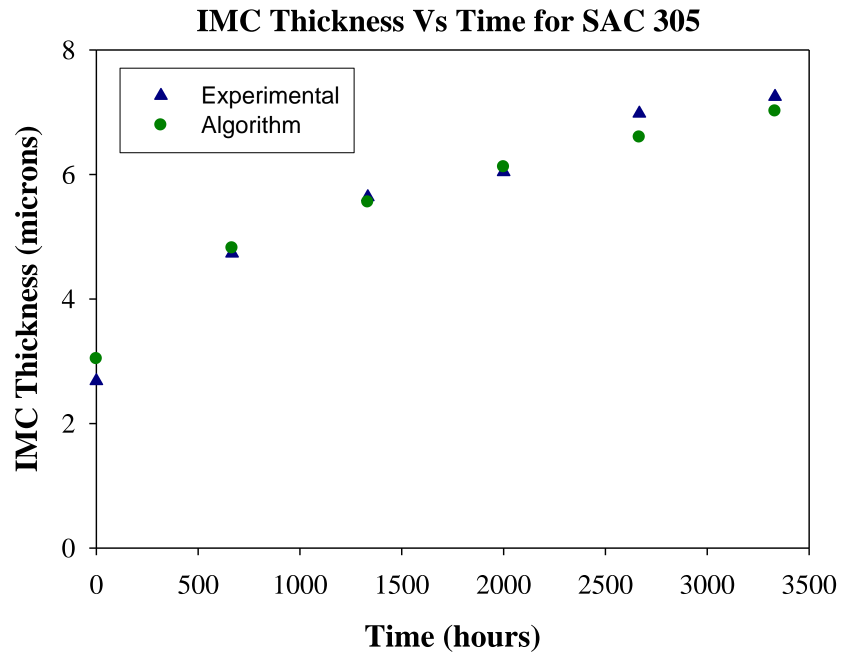

Figure 20: Computation of IMC Thickness (based on prognosticated y_0 and k) vs. IMC from experimental values for 96.5Sn3.0Ag0.5Cu alloy

3.7 Conclusion

In this chapter a prognostic health management model was developed and successfully implemented on electronic components exposed to single isothermal aging environments for accurate life prediction. It has been shown that the physics-of-failure based damage proxy identified as inter-metallic compound (IMC) growth, formed between the second level solder interconnect and copper pad at the board side interface can be used as a leading indicator of failure. Levenberg-Marquardt algorithm which has been as used as a non-linear least square method in this model has been explained in detail followed by its application to this particular problem. A comprehensive methodology has been explained through prognostication equations at each step for easy understanding. The practicality of this model has been demonstrated in the form of a detailed case study on the commercially available packaging architecture with lead-free SAC solder interconnects. The model predictions have been compared with the experimental results for multiple aging time intervals to study the robustness of the proposed model. The correlations indicate that the proposed PHM model can be used to interrogate the system state and thus estimate the residual life of a electronic component.

The prognostic model finds its application in a real world setting where one has to find the remaining useful life of the electronic system in the same isothermal environment well before the actual failure occurs i.e. in the pre-failure space without any knowledge of prior stress histories. In such scenario the proposed prognostic model can be implemented using condition monitoring devices which would be used to interrogate the damage progression in the form of IMC growth data. This data can be fed to the Levenberg-Marquardt algorithm developed for this model for accurate life predictions.

CHAPTER 4

PROGNOSTIC MODEL FOR THE QUANTIFICATION OF REDUCTION IN CYCLIC LIFE DUE TO LONG-TERM DORMANT STORAGE

4.1 Introduction

Electronic systems are often stored for a very long time before they are deployed in the intended environment. It is extremely important to quantify the expended life during storage especially for electronic systems used in mission critical applications. Although ambient temperature storage does not lead to any macro indicators of failure like cracks or de-lamination but it is well known that aging has an adverse effect on the life of electronics. Thus the primary objective of the presented PHM framework is to account for the damage incurred during dormant storage and map this damage in terms of life in the intended environment without any knowledge of prior stress history. Applications for the presented PHM framework include defense applications such as avionics systems, naval electronic warfare systems wherein the electronics is subjected to thermo mechanical loading after long term dormant storage.

In this chapter a PHM model has been developed and implemented for the interrogation of system state and life estimation for sequential thermo-mechanical stresses. Dormant storage has been simulated by isothermal aging environment as typically electronics are stored in a temperature controlled storage facilities before field deployment. Field application has been simulated by a conventional harsh thermal cyclic

environment used for reliability qualification under accelerated stress testing. Two physics-of-failure based damage proxies of second level solder interconnect have been examined and incorporated in this prognostic model. Damage proxies have been extracted and analyzed for isothermal aging, thermal cycling and combination of aging + cycling to study their dame progression in single and sequential thermo-mechanical stress scenarios. Measured damage proxies have been identified as the leading indicators of failure and have been used for damage mapping as well as prognostication of life in multiple thermal environments of thermal aging and thermal cycling. Life has been prognosticated using Levenberg-Marquardt algorithm discussed in the previous chapter. Model predictions have been validated using another set of experimental results. As this model incorporates two damage proxies, standard prognostic metrics such as (α-λ) curve have also been evaluated to study the relative performance of both the damage proxies with respect to life prediction.

4.2 Test Vehicle

Test vehicle used for the development and implementation of the prognostic model is plastic ball grid array (PBGA) type area array package with 676 I/O's assembled on a FR4 printed circuit board with Sn3.0Ag0.5Cu (SAC 305) solder paste. PBGA 676 package was chosen for this study because typically this kind of high I/O packaging architecture serves as the primary component on the commercially offered electronic systems such as engine control unit installed in today's automobiles. PBGA 676 electronic package with SAC 305 solder balls was imported from practical components. It is a AMKOR dummy component as shown in Figure 21. The package attributes have been summarized in Table 4. SAC 305 solder alloy composition was selected as it has

been a major contender for interconnecting small form factor type components due to its acceptable mechanical properties in harsh thermal applications and ready availability. SAC 305 solder paste was imported from Multi-Core$^{TM.}$ Test vehicle was assembled at an in-house SMT laboratory at Auburn University. The novelty in this test vehicle is that custom PCB's were designed to accommodate 4 daisy chain patterns instead of conventional 1 daisy chain pattern for resistance monitoring. The primary reason for incorporating this change was for effective fault detection and isolation followed by systematic failure analysis.

Figure 21: PBGA 676 Front and Back Side

Table 4: Package Architecture Details

Solder	Sn3Ag0.5Cu
Package Size (mm)	27 x 27
Package Type	PBGA
I/O Count	676
I/O Pitch (mm)	1
Ball Diameter (mm)	0.63
Mold thickness (mm)	1.17
Substrate Pad	SMD

4.2.1 Custom PCB Design

The first step in PCB footprint design to create 4 daisy chains was to check the component side daisy chain pattern. For this PBGA 676 daisy chain pattern was downloaded from practical components website as shown in Figure 22. The 4 daisy chains were laid out into 4 quadrants as shown in Figure 23. As we do not have any control over the component side daisy chain pattern the only way of creating 4 daisy chain patterns was to route copper traces on the PCB footprint such that we get 4 daisy chain quadrants as shown in Figure 24. If the component side daisy chain and the board side daisy chain are overlaid the 4 daisy chain pattern is vividly seen as shown in Figure 25. PCB footprint was created in ExpressPCB software for JEDEC size board 132 mm X 77 mm. This design was sent out to a PCB manufacturing vendor for manufacturing. The actual PCB with PBGA 676 footprint for 4 daisy chain patterns is shown in Figure 26. The printed circuit board pads were solder mask defined (SMD) with immersion silver finish.

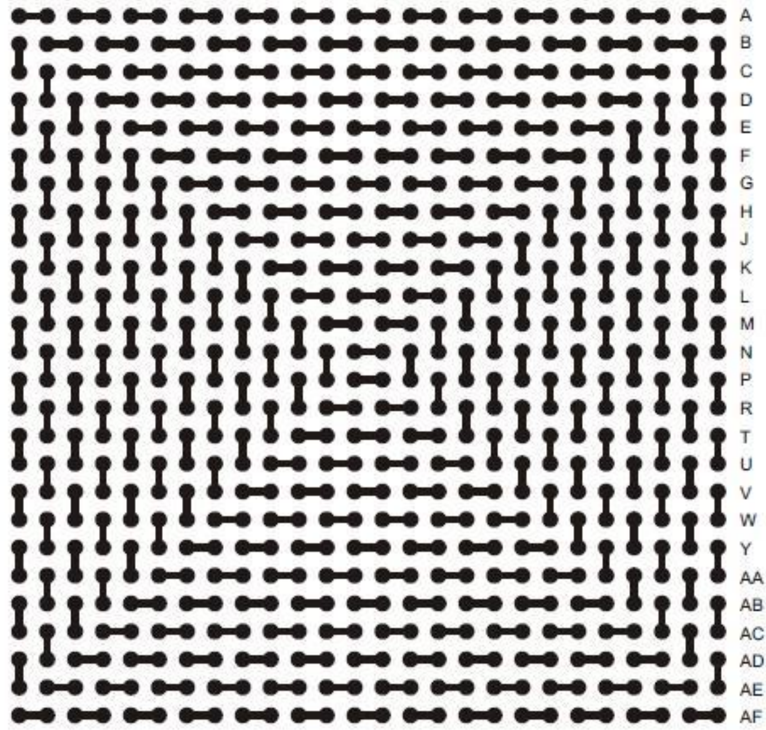

Figure 22: PBGA 676 Component Side Daisy Chain Courtesy: Practical Components

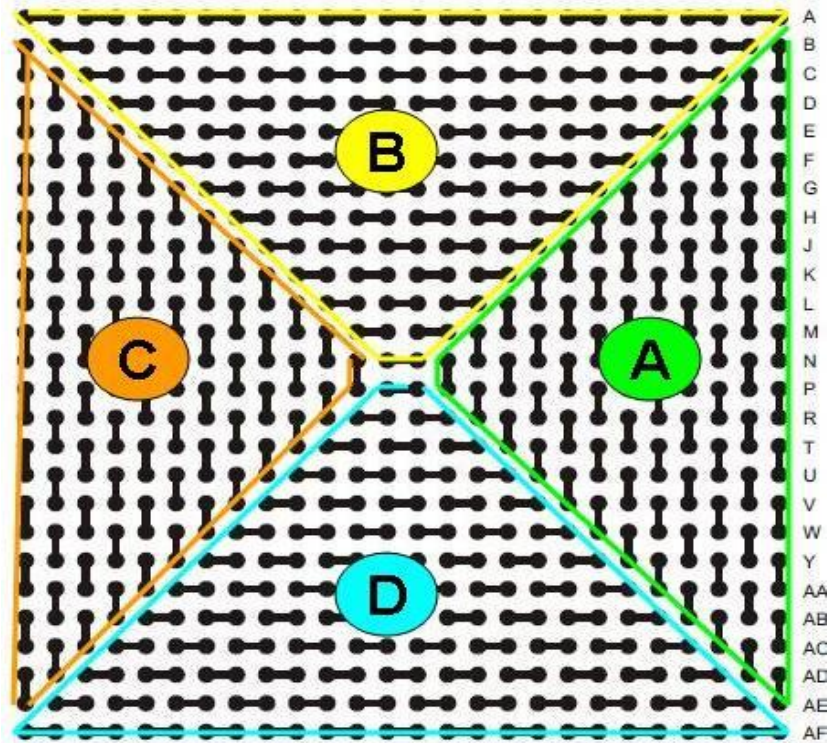

Figure 23: 4 Daisy Chain Schematic

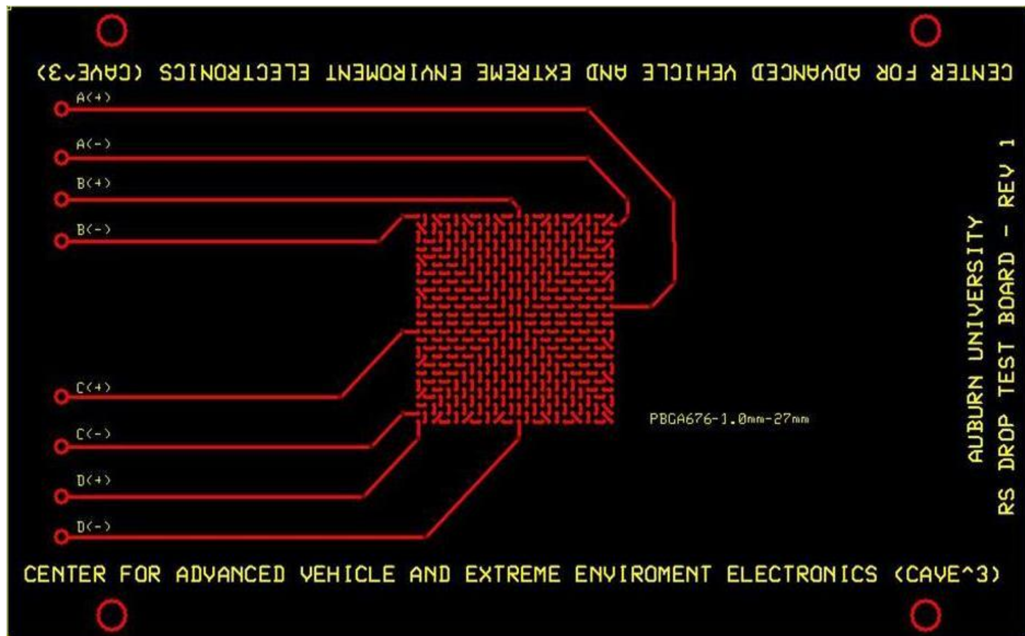

Figure 24: ExpressPCB Snapshot for PBGA 676 Daisy Chain Pattern

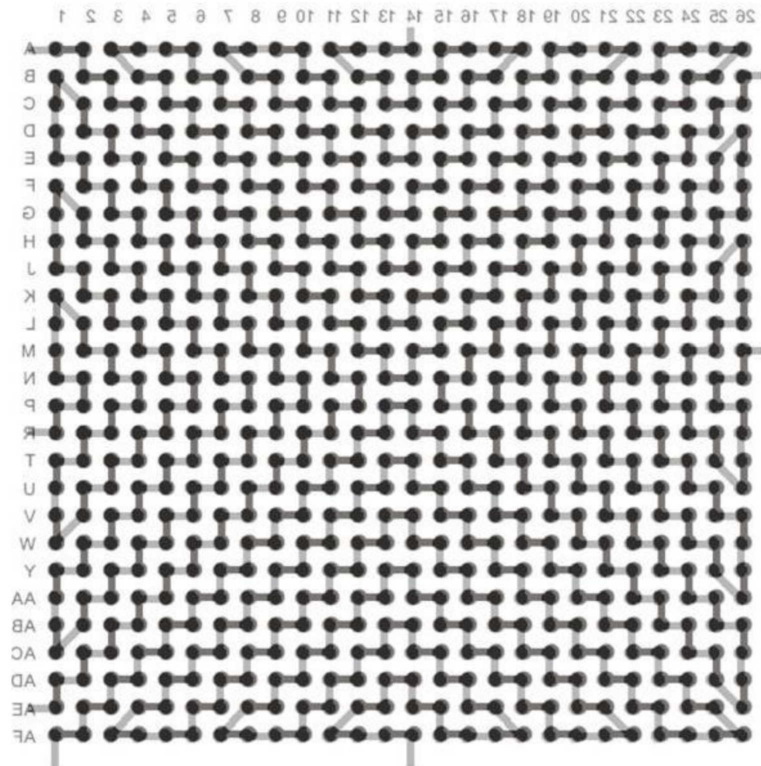

Figure 25: Component Side Daisy Chain (BLACK) and Board Side Daisy Chain (GRAY) Overlaid to Show 4 Daisy Chain Patterns

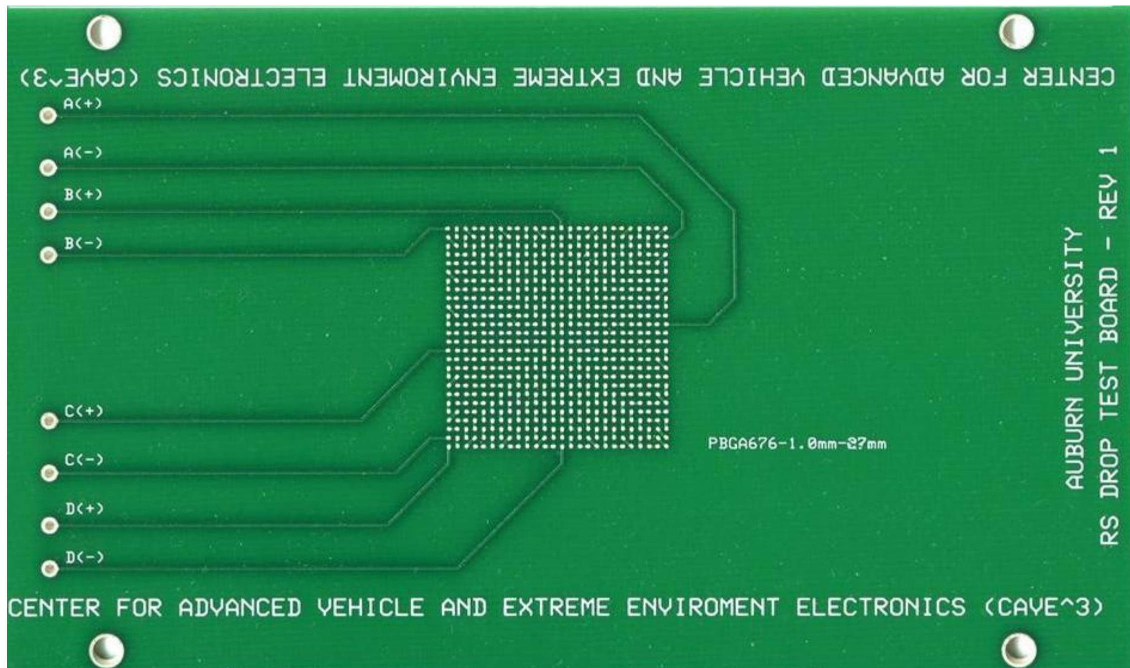

Figure 26: Actual PCB with PBGA 676 Footprint Accommodating 4 Daisy Chain Patterns

Once the custom PCBs were manufactured multiple sets of test vehicles were assembled in-house at NSF CAVE^3 SMT laboratory. Stencil for solder printing was obtained from practical components. Manncorp SP-5500 machine was used for SAC 305 solder paste printing, manual pick and place was used for placing PBGA 676 package onto PCB (Manncorp optical Mounter (FP-100)) and the assembly was reflowed in a single stage lead free convection reflow oven (X-Reflow 306 LF). Different reflow profiles were designed and tested on dummy assemblies to ensure high quality finished boards. After multiple trials the profile shown in Figure 27 was used to reflow multiple sets of test vehicles. The final board after reflow is shown in Figure 28. The daisy chain resistance was measured on all the 4 quadrants after reflow to check for manufacturing failures and defects such as warpage during high temperature reflow and misalignment

during print and place. Also solder joints were inspected under optical microscopes after each reflow to check the integrity of the joints.

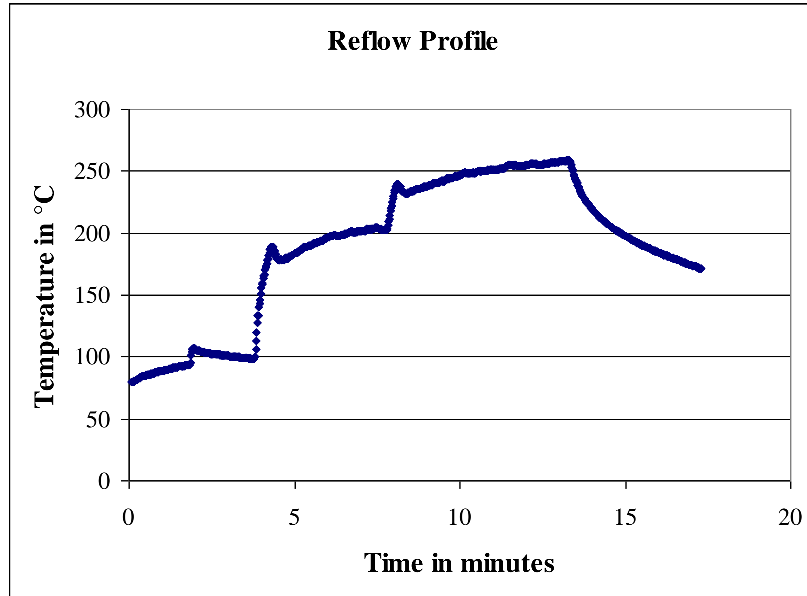

Figure 27: Reflow Profile for SAC 305 Solder

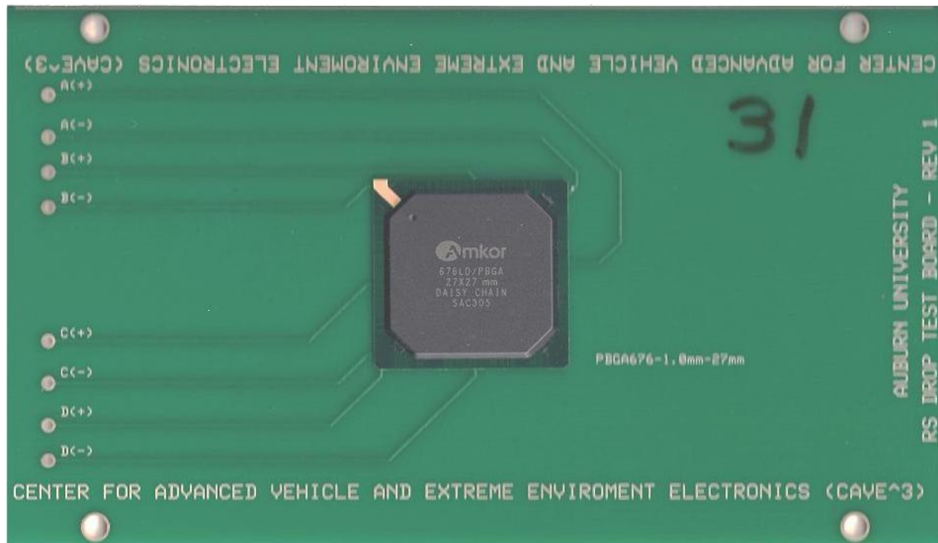

Figure 28: Test Vehicle

4.2.2 Test Conditions

Three different condition monitoring cells were created viz. CM#1, CM#2 and CM#3 as summarized in Table 5. Test vehicles in CM#1 were subjected to air to air thermal cycling (AATC) from –55°C to 125°C and the damage proxies were extracted at different cycling intervals. Thermal cycling profile is shown in Figure 29. It is a hundred minutes cycle with 15 minute dwells at each extreme. The ramp up time is 25 minutes and is less than ramp down time which is 45 minutes as in AATC the thermal chamber takes more time to attend sub-zero temperatures. In CM#2 test vehicles were subjected to isothermal aging at 125°C and the damage proxies were extracted at different aging times. Test vehicles in CM#3 were subjected to some combination of isothermal aging and thermal cycling for the assessment of residual damage in sequential thermo-mechanical environments followed by prognostication of life in such complex environments.

Table 5: Condition Monitoring Cells

Condition Monitoring Cell	**Thermal Cycling (-55°C to 125°C)**	**Isothermal Aging (125°C)**	**Isothermal Aging + Thermal Cycling**
CM # 1	✓	✗	✗
CM # 2	✗	✓	✗
CM # 3	✗	✗	✓

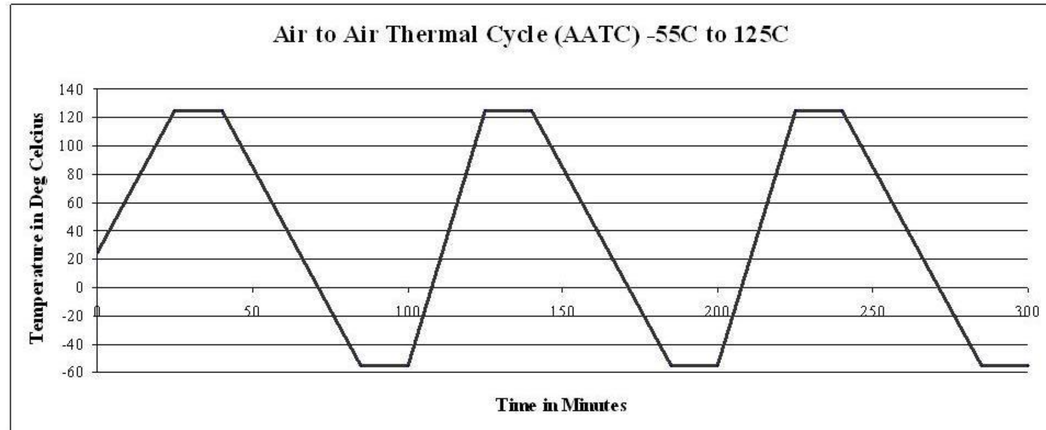

Figure 29: Thermal Cycling Profile

4.3 Leading Indicators of Failure

The change in solder microstructure and its derivatives have been used as the leading indicators of failure for electronics subjected to multiple thermal environments of thermal aging and thermal cycling. The core function of any prognostic health management model is to detect fault in the system and compute residual life at any given time. Typically fault detection involves interrogation of system state for physics-of-failure (POF) based damage proxies that provide information about the ongoing damage and impending failure. These damage proxies are classified as the leading indicators of failure and are used in a PHM model development which directly or indirectly relate to the overall life of the system. There are two damage proxies used in this model which are based on the micro-structural evolution of second level solder interconnects. The first damage proxy has already been discussed in the previous chapter called the IMC growth which is formed at the board-side copper pad solder ball interface as shown in. This damage proxy has been used as the leading indicator of failure for the prognostic model development in Chapter 3. The same proxy has also been used in this model. The damage proxy extraction and analysis details can be referred in Chapter 3.3.

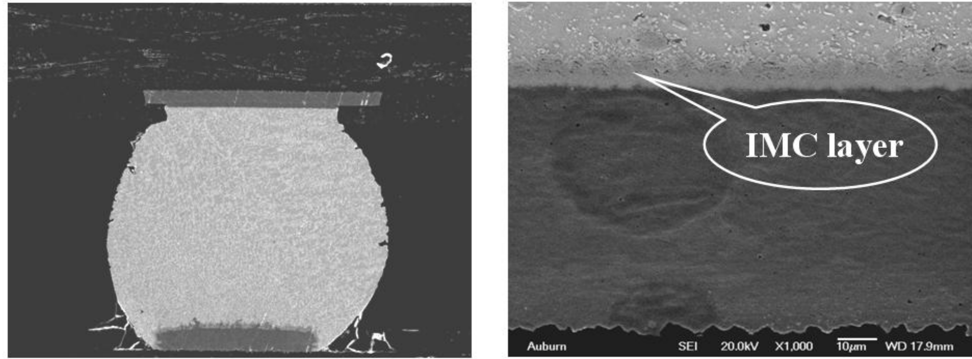

Figure 30: IMC Growth as the Leading Indicator of Failure

4.3.1 Phase-Growth as the Leading Indicator of Failure

Temperature excursions during operation of an electronic circuit are due to both power-cycling and variations in ambient conditions resulting in thermo-mechanical cyclic stresses and strains induced primarily by thermal expansion mismatch between the package and the board assembly. Previous researchers have studied the micro structural evolution of ternary SnAgCu alloys at elevated temperatures using bulk real solder joints with different designs, geometry and process conditions. The SnAgCu microstructure comprises Ag_3Sn and Cu_6Sn_5 dispersed within the tin matrix as shown in Figure 31. The relatively low percentage of alloying elements, 1-4% for Ag and 0.5% for Cu results in phases which comprise a small percentage of the total volume within the solder joint. The microstructural evolution of SnAgCu alloys over time has been found to affect the thermo-mechanical properties and damage behavior [Ye 2000, Allen 2004[a, b], Kang 2004, Xiao 2004, Henderson 2004, Kang 2005, Korhonen 2006, Jung 2001].

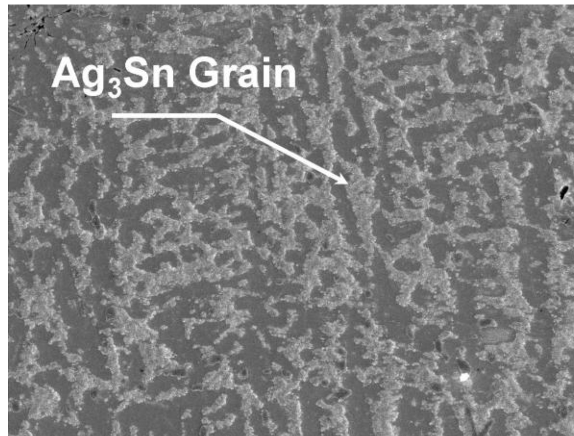

Figure 31: Ag_3Sn Grains in 95.5Sn4.0Ag0.5Cu solder microstructure

Micro-structural coarsening during thermo-mechanical deformation is attributed to the generation of excess vacancies caused by the combined effect of local hydrostatic state of stress, and the instantaneous inelastic strain rate [Dutta 2003[a], 2003[b], 2004; Jung 2001]. Evolution of solder microstructure in 63Sn37Pb and lead-free chip resistor solder joints due to thermal fatigue have been studied previously by previous researchers [Sayama, et al. 1999, 2003] and thermal fatigue correlated with occurrence of micro-structural coarsening in the fatigue damaged region in of 63Sn37Pb solder interconnects [Frear 1990, Morris 1991]. Correlation of grain coarsening with thermal fatigue has also been established for high-lead solders [Bangs 1978, Wolverton 1987, Tribula 1989]. Previously the phase-size evolution and derivatives of phase growth rate have been investigated and classified as prognostics parameters on a wide range of leaded and Sn4Ag0.5Cu devices in underhood applications [Lall 2004[b], 2005, 2006[a,b], 2007[a,b]].

Phase growth under thermal cycling and thermal aging has been identified as the damage precursor to compute the residual life. The relation between phase growth parameter and time for polycrystalline material is given by [Callister 1985].

$$g^n - g_0^{\ n} = Kt \qquad (17)$$

Where g is the average grain size at time t, g_0 is the average grain size of solder after reflow, K and n (varies from 2 to 5) are time independent constants. Senkov and Myshlev [1986] applied the theory of phase growth process in a super plastic alloy and validated the theory for Zn/Al eutectic alloy. They expressed the phase growth parameter S as:

$$S = g^4 - g_0^{\ 4} = Kt \qquad (18)$$

The exponent value of 4 indicates that the phase coarsening kinetics is primarily due to grain boundary sliding under thermo-mechanical loading studied by [Allen 2004]. Previously, it has been shown that the rate of change in phase growth parameter [d(lnS)/d(lnN)] is valid damage proxy for prognostication of thermo-mechanical damage in solder interconnects and assessment of residual life [Lall 2004a, 2005a, 2006c,d, 2007c,e, 2008c,d, 2009c,d]. The damage proxy [d(lnS)/d(lnN)] is related to the micro-structural evolution of damage by the following equation:

$$S = g^4 - g_0^{\ 4} = a(N)^b \qquad (19)$$

Where g is the phase size measured after N number of thermal cycles, g_0 is the phase size measured after reflow, a and b are the constant and exponents respectively. The log-plot of the equation provides a straight line relationship between the phase growth parameter and the number of cycles.

$$\ln(S) = \ln(g^4 - g_0^{\ 4}) = \ln a + b\ln(N) \qquad (20)$$

$$\frac{d[\ln(S)]}{d[\ln(N)]} = b \qquad (21)$$

$$S = g^4 - g_0^4 = a(t)^b \qquad (22)$$

It should be noted that the same equation is valid for the solder alloys subjected to thermal aging as shown in $S = g^4 - g_0^4 = a(t)^b$ (**22** since the fundamental physics of phase coarsening remains the same.

4.3.2 Phase-Growth Measurement

The phase size is measured by cross-sectioning the samples after thermal cycling or thermal aging. The cross-sectioned samples are potted using resin and hardener to form an epoxy. The samples are finely polished using different levels of grinding papers and colloidal silica solution so that the Ag_3Sn phases are clearly visible. Cross-sectioned / polished samples are then gold sputter coated so as to take SEM images at 750x magnification to measure the growth rate of tin and Ag3Sn phases. Phase size is measured using SEM and image analysis. For this the SEM images are cropped in a 60µm X 45µm window (Figure 32) and are converted into a gray scale images as shown in Figure 33. Image processing software called NI-IMAQ Vision Builder is used to measure the average phase size.

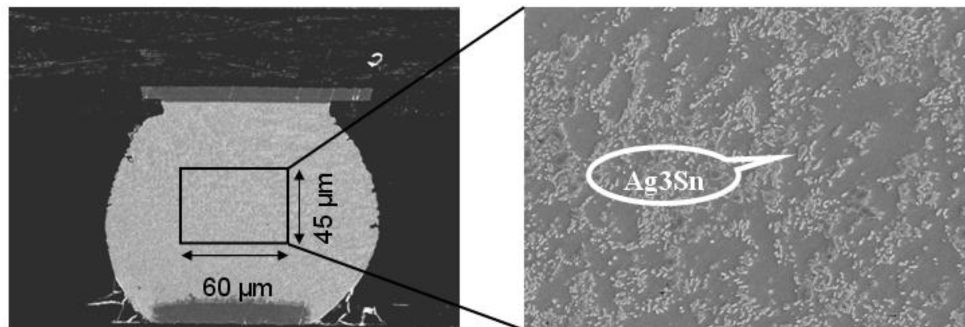

Figure 32: SEM Image for Phase-Growth Analysis

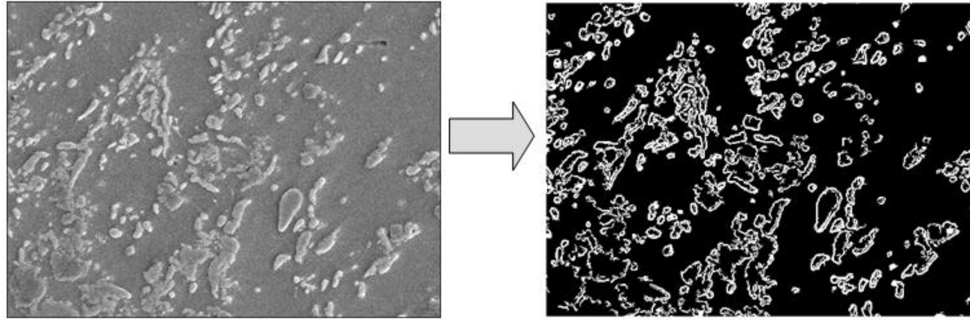

Figure 33: Phase Size Measurement using NI-IMAQ

4.4 Concept of Sequential Thermal Aging and Thermal Cycling

In the real world application not all the electronics that is manufactured on SMT assembly line is deployed in the field right away. Most electronic systems are often stored for some amount of time before their application in the field environment. As aging has an adverse effect on the life of electronics it is extremely important to account for the damage incurred due to storage before the deployment to determine the operational readiness of the system and compute remaining useful life in the intended field. In thermal cyclic field applications, life of the electronic system is measured in terms of number of thermal cycles it has been exposed to. However life in thermal aging environment is always measured in time scale i.e. number of hours, days, weeks or months. So it becomes all the more difficult to relate two different measuring scales, i.e. time for aging and number of thermal cycles for thermal cycling to quantify and map the life consumed due to aging onto the thermal cyclic field.

Figure 34 depicts the concept of storage and deployment encountered in the real world application. Here the storage and field application have been replicated by isothermal aging and thermal cycling respectively. In order to account for life expended due to aging, the life in terms of number of hours ‘t’ has to be converted to life in terms of number of cycles ‘N’ due to the difference in the life measuring scales for two

environments as shown in Figure 35. Therefore in order to develop the damage mapping relationship between number of hours and number of cycles, test vehicles have been subjected to isothermal aging and thermal cycling respectively to plot damage vs number of hours and damage vs number of cycles as shown in Figure 36.

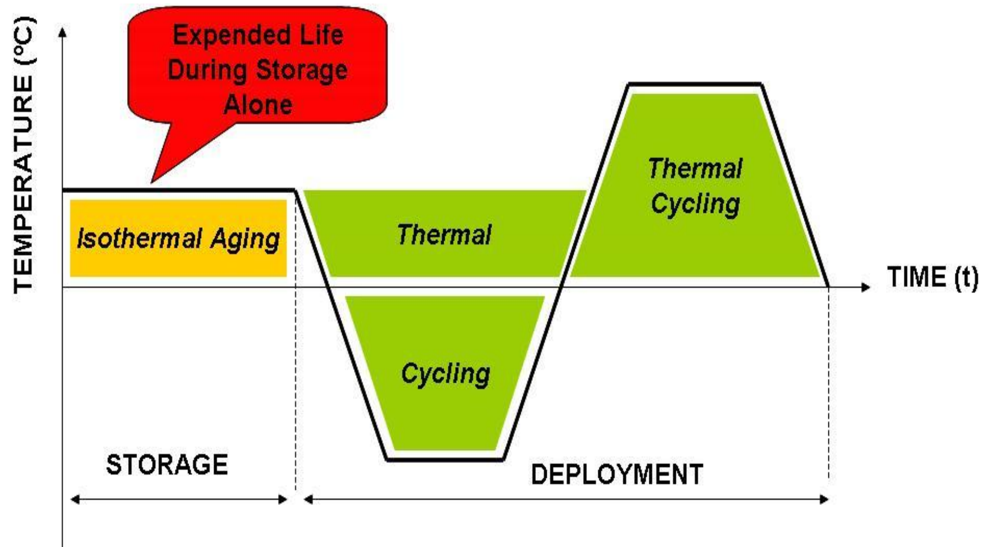

Figure 34: Concept of Sequential Thermal Aging and Thermal Cycling

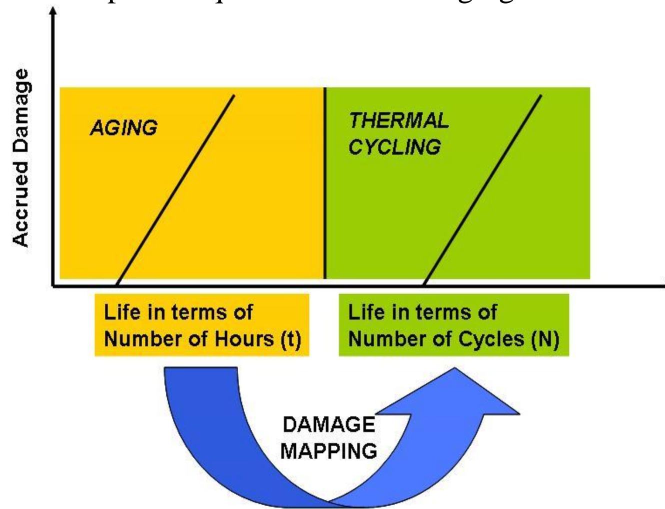

Figure 35: Mapping Reduction in Life Due to Dormant Storage.

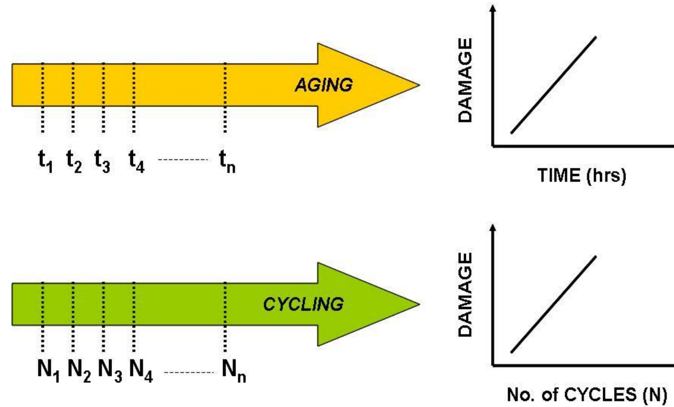

Figure 36: Accrued Damage Due to Thermal Aging and Thermal Cycling respectively.

4.5 Concept of Damage Equivalency Based Mapping

Figure 37 shows the schematic of damage equivalency based mapping of life consumed due to aging in terms of number of cycles. It is a combined plot of normalized phase growth (S_N) as a damage parameter on the vertical axis vs. life on the horizontal axis (in terms of time‘t’ for aging and in terms of number of cycles ‘N’ for cycling). The relationship between time t and number of cycles N can be developed based on the concept of damage equivalency by keeping the damage parameter S constant. It should be noted that the difference in the slopes of the two lines (S vs. t and S vs. N) is because of the different magnitudes of damage incurred due to thermal cycling and thermal aging. It has been previously observed that the phase growth parameter increases more rapidly in thermal cycling than in thermal aging.

In the schematic, point ‘A’ can be thought of as the cross-over point where the electronic system comes out of storage and is ready for deployment. Thus it is essential to find the life consumed during this storage i.e. until point ‘A’. The damage parameter viz. phase growth parameter S_A can be measured at point A or in other words at the end of storage. This damage parameter S_A can be mapped back on the thermal cycling curve

(marked by point B) that corresponds to S_B to find the equivalent number of cycles N_B. The horizontal projection of damage parameter from point A to point B marked by black solid line does not incur any new damage which implies that $S_A = S_B$ which is also evident from the schematic. Thus N_B is the life consumed due to storage in terms of number of cycles based on the concept of damage equivalency. In other words it takes N_B number of cycles in thermal cycling environment to accrue same amount of damage (S_A) that was incurred due to t_A hours of thermal aging.

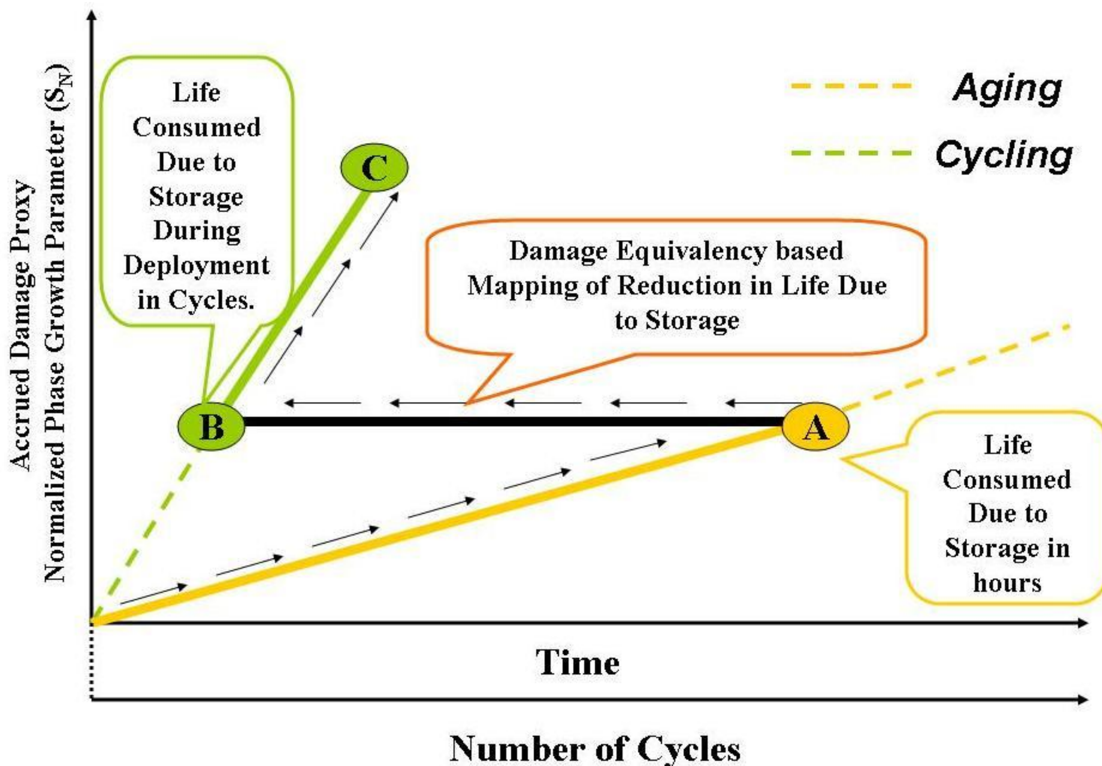

Figure 37: Concept of Damage Equivalency and Mapping of Life Consumed Due to Storage.

4.6 Case-Study: Prognostication of Life of Electronics Subjected to Sequential Stresses

The case study has been divided into two sections for lucid understanding. The first section is an experimental part where the damage equivalency based relationships have been established to account for life consumed due to storage using two damage

proxies. In the later prognostication section the life consumed in sequential thermo-mechanical environments of thermal aging and thermal cycling has been computed and validated using the developed experimental relationships to study how close the model accounts for the life expended due to thermal aging.

4.6.1 Damage Equivalency Relationship between Thermal Aging and Thermal Cycling

The test vehicles have been subjected to thermal aging and thermal cycling respectively to establish damage mapping relationship between number of cycles and aging time. Later in the prognostication section test vehicles have been exposed to some combination of aging + cycling. The function of each condition monitoring cell has been summarized in Table 5. One test vehicle was cross-sectioned and polished right after reflow to measure damage proxies in the pristine condition i.e. un-aged / un-cycled or 0 hours of aging / 0 number of cycles.

It should be noted that as it is a multiple thermal environment problem wherein the damage mapping relationships have been established based on two damage proxies the fundamental equations for phase-growth and IMC growth have been normalized with respect to initial phase-size and initial IMC respectively. This has been done for better representation of equations. If we look at the equation of phase-growth the only variable which is independent of thermal cycles N or aging time t is the initial phase-size g_0 as shown in $S = g^4 - g_0{}^4 = a(N)^b$ (**23** and $S = g^4 - g_0{}^4 = a(t)^b$ (**24**.

$$S = g^4 - g_0{}^4 = a(N)^b \qquad (23)$$

$$S = g^4 - g_0{}^4 = a(t)^b \qquad (24)$$

Similarly for the IMC equation y_0 is the only variable which does not depend on aging time t or thermal cycles N as shown in $y - y_0 = k(t)^m$ (**25** and $y - y_0 = k(N)^m$ (**26**.

$$y - y_0 = k(t)^m \qquad (25)$$

$$y - y_0 = k(N)^m \qquad (26)$$

As both the damage proxies have been extracted and analyzed for both thermal cycling and thermal aging normalization of these equations with respect to g_0 / y_0 eliminates any ambiguity about the damage proxies in thermal aging and thermal cycling environments. The normalized equations used for the damage mapping as well as prognostication of life in sequential thermal environments of thermal aging and thermal cycling are of the form shown in $S_{N\Delta T} = \left[\left(\frac{g}{g_0}\right)^4 - 1\right] = a_{N\Delta T}(N)^{b_{N\Delta T}}$ (**27**, $S_{Nt} = \left[\left(\frac{g}{g_0}\right)^4 - 1\right] = a_{Nt}(t)^{b_{Nt}}$ (**28**, $\left[\frac{y}{y_0} - 1\right] = k_{Nt}(t)^{m_{Nt}}$ (**29** and $\left[\frac{y}{y_0} - 1\right] = k_{N\Delta T}(N)^{m_{N\Delta T}}$ (**30**.

$$S_{N\Delta T} = \left[\left(\frac{g}{g_0}\right)^4 - 1\right] = a_{N\Delta T}(N)^{b_{N\Delta T}} \qquad (27)$$

Where $S_{N\Delta T}$: Normalized phase-growth parameter during thermal cycling

g: Phase-Size measured after N number of thermal cycles

g_0: Initial phase size

$a_{N\Delta T}$: Normalized phase-growth coefficient during thermal cycling

$b_{N\Delta T}$: Normalized phase-growth exponent during thermal cycling

$$S_{Nt} = \left[\left(\frac{g}{g_0}\right)^4 - 1\right] = a_{Nt}(t)^{b_{Nt}} \qquad (28)$$

Where S_{Nt}: Normalized phase-growth parameter during thermal aging

g: Phase size measured after t hours of thermal aging

g_0: Initial phase size

a_{Nt}: Normalized phase-growth coefficient during thermal aging

b_{Nt}: Normalized phase-growth exponent during thermal aging

$$\left[\frac{y}{y_0} - 1\right] = k_{Nt}(t)^{m_{Nt}} \qquad (29)$$

Where y: IMC growth measured after t hours of thermal aging

y_0: Initial IMC growth

k_{Nt}: Normalized IMC growth coefficient during thermal aging

m_{Nt}: Normalized IMC growth exponent during thermal aging (m_{Nt}=0.5)

$$\left[\frac{y}{y_0} - 1\right] = k_{N\Delta T}(N)^{m_{N\Delta T}} \qquad (30)$$

Where y: IMC growth measured after N number of thermal cycles

y_0: Initial IMC growth

$k_{N\Delta T}$: Normalized IMC growth coefficient during thermal cycling

$m_{N\Delta T}$: Normalized IMC growth exponent during thermal cycling

Analysis of Damage Proxies in Thermal Cycling

Condition monitoring cell CM #1 was populated with 7 custom designed PBGA 676 test vehicles which were subjected to thermal cycling from -55ºC to 125ºC. Each of the 7 test vehicles were withdrawn at an interval of 100 cycles for damage proxy measurement and analysis. After every 100 cycles the packages were cross-sectioned and polished to measure two damage proxies' discussed in Chapter 4.3 viz. inter-metallic compound (IMC) and phase-growth. The primary objective of analyzing 7 samples was to study the damage progression of each damage proxy in thermal cycling. Figure 38 and Figure 39 show phase-growth and IMC growth evolution over number of cycles. It is evident from these figures that as the packages are exposed to more number of thermal cycles both the damage proxies evolve over time. The phase growth coarsens from 0 cycles to 700 cycles while there is an obvious increase in IMC growth from 0 cycles to 700 cycles.

Normalized phase-growth and IMC growth have been plotted against number of cycles to study the damage progression. The log plots shown in Figure 40 and Figure 41 indicate linear relationship between the individual damage proxies with respect to number of thermal cycles. The actual equations are shown below.

$$S_{N\Delta T} = 0.015(N)^{0.78} \qquad (31)$$

$$\left[\frac{y}{y_0} - 1\right] = 0.0199(N)^{0.81} \qquad (32)$$

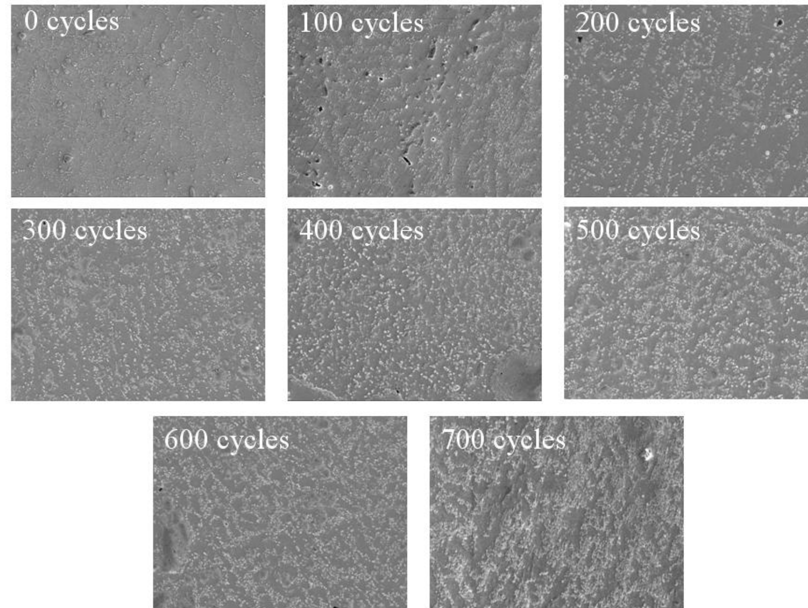

Figure 38: SEM backscattered images of Phase growth versus number of cycles (Thermal cycling -55°C to 125°C, 96.5Sn3.0Ag0.5Cu solder, 676 I/O PBGA, magnification 750x)

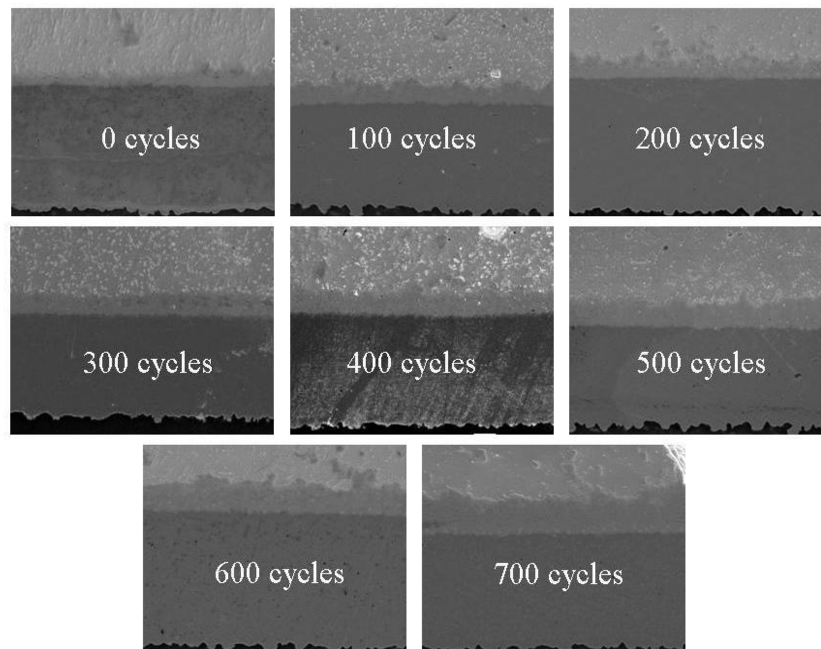

Figure 39: SEM backscattered images of IMC growth versus number of cycles (Thermal cycling -55°C to 125°C, 96.5Sn3.0Ag0.5Cu solder, 676 I/O PBGA, magnification 1000x)

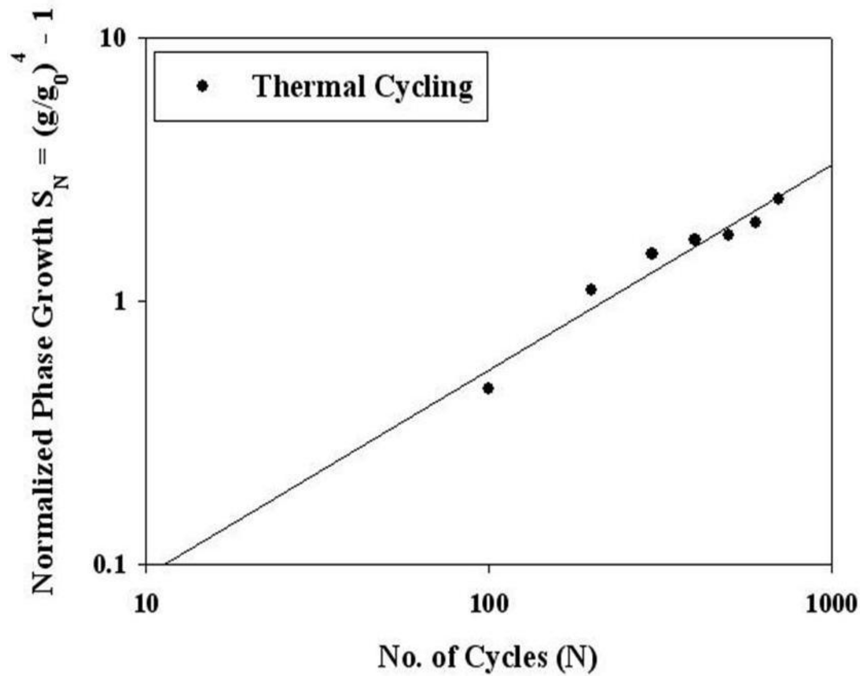

Figure 40: Plot of Normalized Phase growth versus No. of Cycles for 96.5Sn3.0Ag0.5Cu solder, 676 PBGA, subjected to thermal cycling from -55°C to 125°C

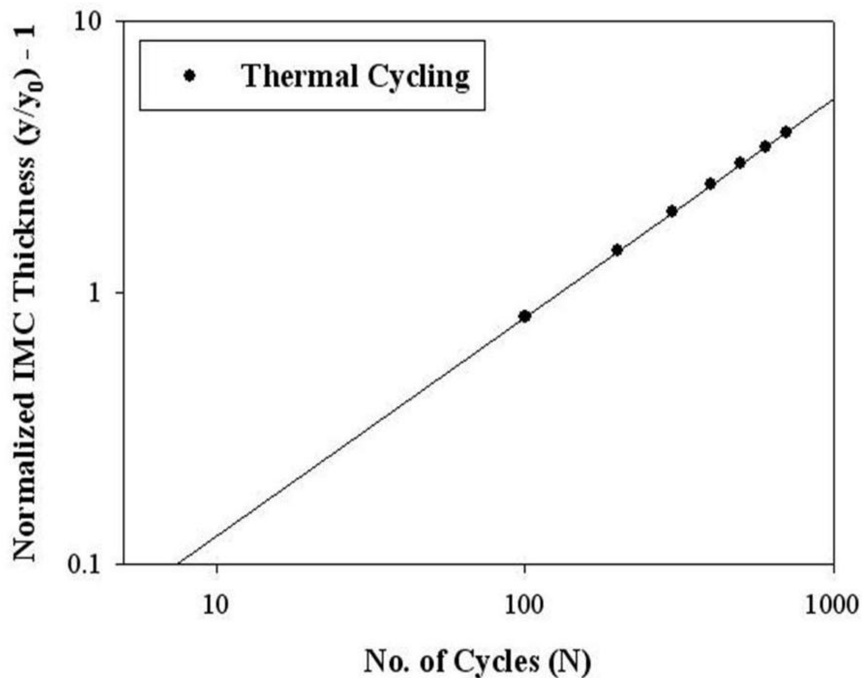

Figure 41: Plot of Normalized IMC growth versus No. of Cycles for 96.5Sn3.0Ag0.5Cu solder, 676 PBGA, subjected to thermal cycling from -55°C to 125°C

Analysis of Damage Proxies in Thermal Aging

To study damage progression in isothermal aging environment condition monitoring cell CM #2 was created consisting of 7 PBGA 676 test vehicles similar to CM #1. The test vehicles were placed in a thermal oven and were allowed to age at steady-state 125°C. The packages were withdrawn after every 48 hours interval for damage proxy analysis. Packages were cross-sectioned and polished followed by SEM imaging for the extraction of both the damage proxies. The extracted damage proxies were analyzed to examine their behavior in isothermal aging environment. Figure 42 and Figure 43 show the damage progression of phase-growth and IMC growth respectively as a function of aging time. It is quiet evident from these figures that both the damage proxies evolve due to isothermal aging. The micro-structure coarsens in the bulk solder while the inter-metallic thickness at the board side copper interface grows rapidly as a function of aging time.

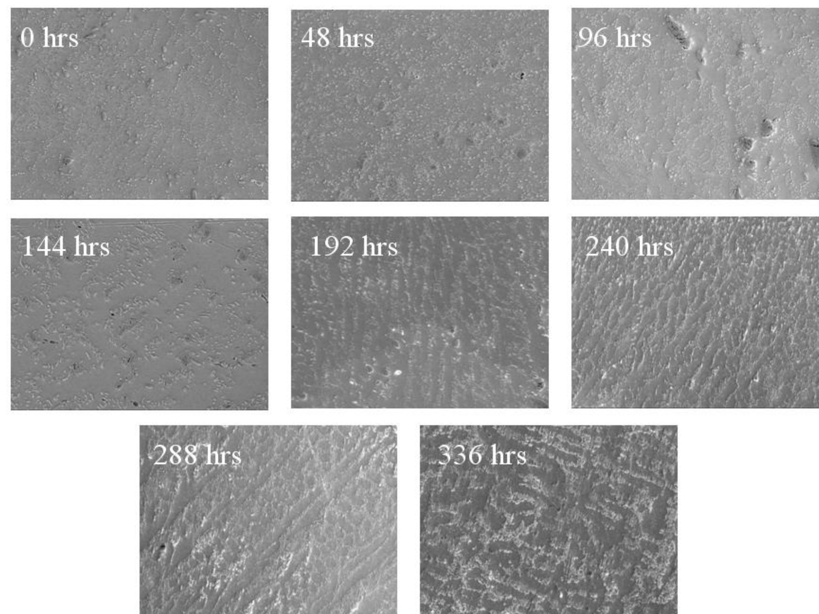

Figure 42: SEM backscattered images of Phase growth at different aging time intervals (Thermal aging at 125°C, 96.5Sn3.0Ag0.5Cu solder, 676 I/O PBGA, magnification 750x)

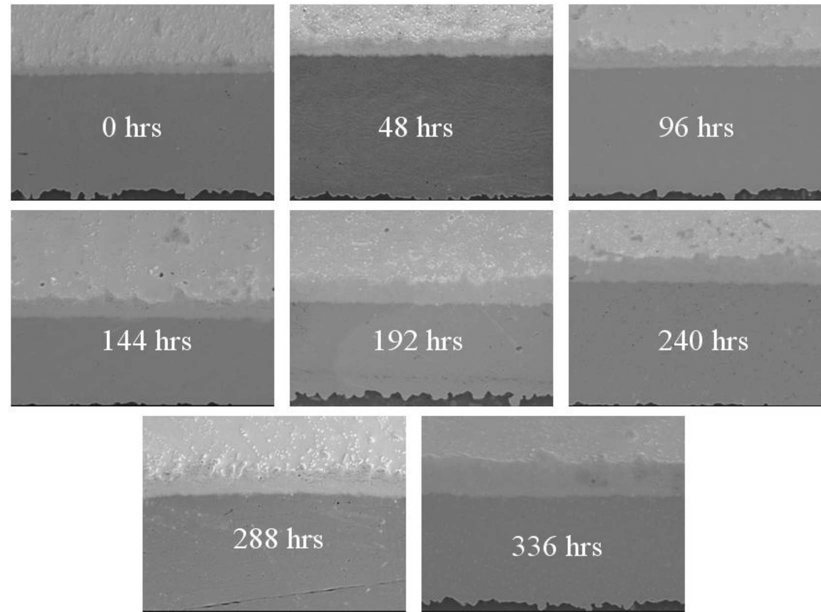

Figure 43: SEM backscattered images of Intermetallic Thickness at different aging time intervals (Thermal aging at 125°C, 96.5Sn3.0Ag0.5Cu solder, 676 I/O PBGA, magnification 1000x)

Normalized plots of phase-growth and IMC growth have been plotted against aging time as shown in Figure 44 and Figure 45. The log plots have been plotted to indicate a linear relationship between the damage progression and aging time for both the damage proxies.

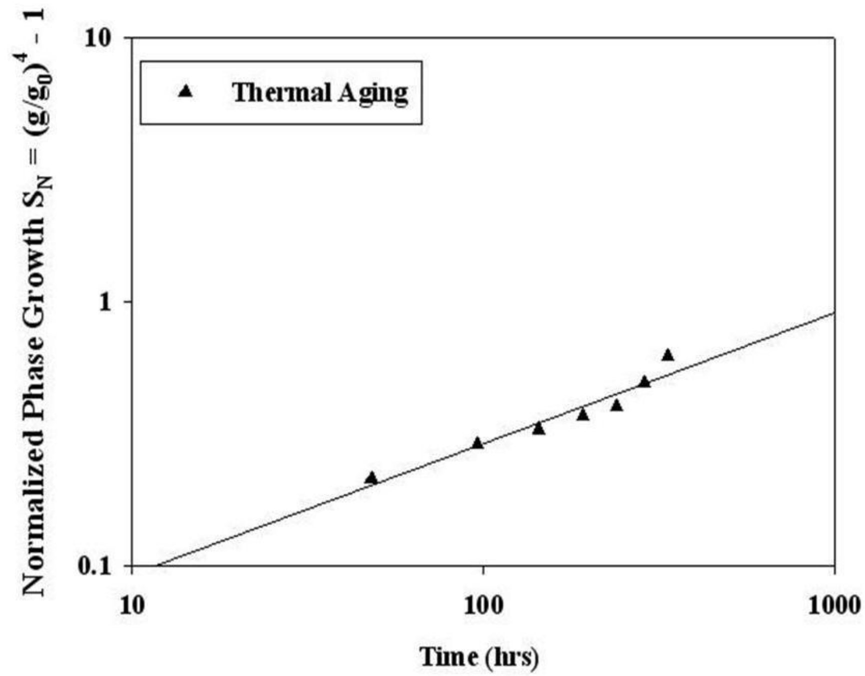

Figure 44: Plot of Phase growth versus Aging Time for 96.5Sn3.0Ag0.5Cu solder, 676 PBGA, subjected to thermal aging at 125°C

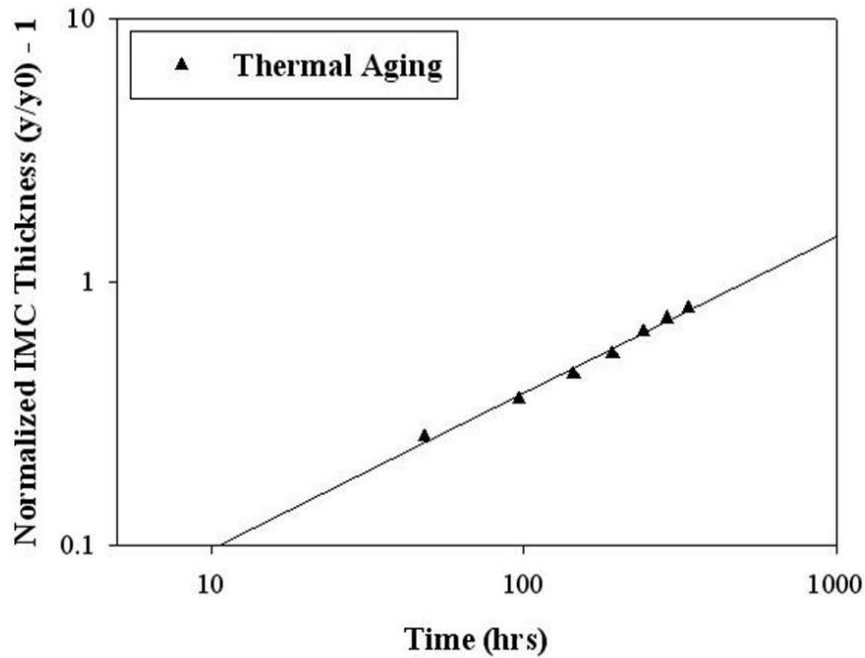

Figure 45: Plot of IMC growth versus Aging Time for 96.5Sn3.0Ag0.5Cu solder, 676 PBGA, subjected to thermal aging at 125°C

The equations of normalized phase growth and IMC growth as a function of aging time are shown below.

$$S_{Nt} = 0.0297(t)^{0.49} \quad (33)$$

$$\left[\frac{y}{y_0} - 1\right] = 0.044(t)^{0.5} \quad (34)$$

Relationship between number of cycles N and aging time t

The relationship between the aging time and number of cycles has been derived using both normalized phase growth and normalized inter-metallic compound (IMC) growth. Both the damage proxies have been used to establish this relationship to capture the true life consumed due to aging and thus eliminate any error contribution from individual damage proxies.

In Figure 46 normalized phase-growth has been plotted against aging time and number of cycles. The plot has two x-axes viz. time in hours and number of cycles. It should be noted that aging time is for isothermal exposure of 125ºC while the number of cycles are corresponding to the thermal cycle ranging from -55 ºC to 125 ºC. It is evident from Figure 46 that same amount of phase coarsening or phase-growth can be obtained by exposure to either thermal cycling or thermal aging. This is the underlying theory of damage equivalency which enables to establish a relationship between two different time scales i.e. number of cycles and aging time. Thus if we equate $S_{N\Delta T} = 0.015(N)^{0.78}$ (**31** and $S_{Nt} = 0.0297(t)^{0.49}$ (**33** based on the concept of damage equivalency for the same normalized phase-growth parameter we get the relationship between number of cycles and aging time ($N = 2.40(t)^{0.63}$ (**37**) as follows,

$$S_{N\Delta T} = S_{Nt} \quad (35)$$

$$0.015(N)^{0.78} = 0.0297(t)^{0.49} \quad (36)$$

$$N = 2.40(t)^{0.63} \quad (37)$$

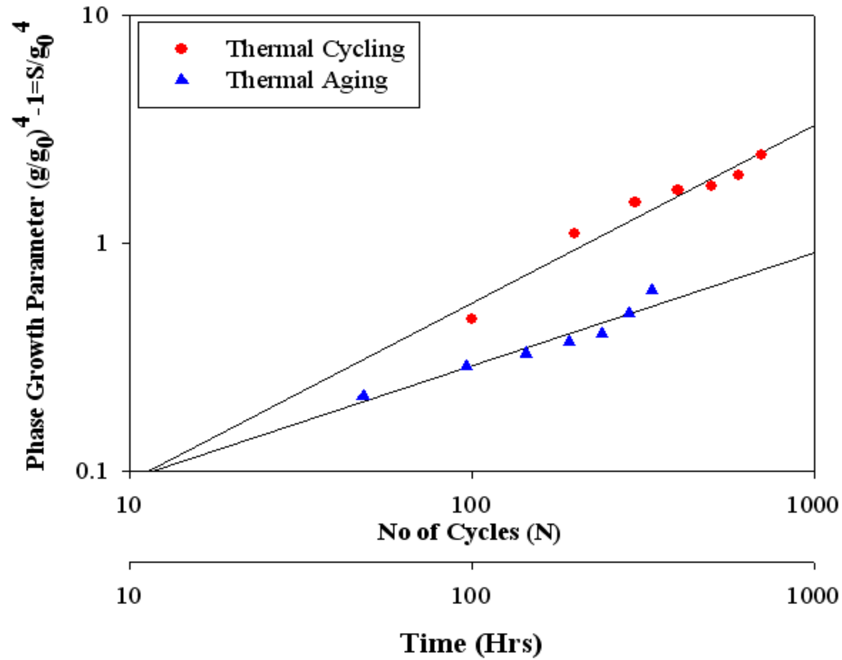

Figure 46: Combined plot Normalized Phase growth versus thermal aging time and thermal cycling

Similar relationship can be derived using normalized IMC growth as the damage proxy. The primary reason for deriving the relationship using both the damage proxies is to validate the relationship and also examine if the fundamental damage mechanics holds true in complex thermal environments. To derive the relationship the normalized IMC thickness has been plotted for thermal cycling and thermal aging as shown in Figure 47. It is a combined plot of normalized IMC thickness vs. aging time and number of cycles where normalized IMC thickness in on y-axis while time in hours and number of cycles have been plotted on dual x-axes.

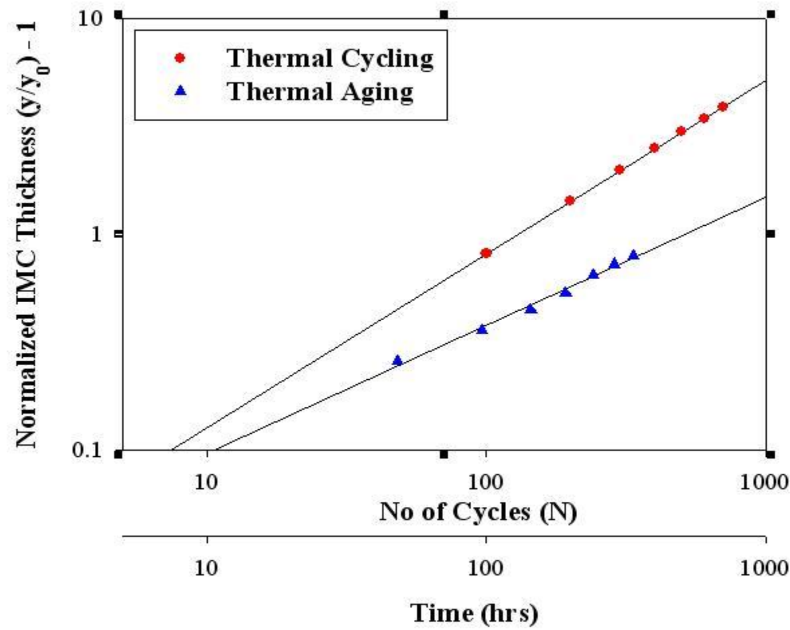

Figure 47: Combined plot Normalized IMC growth versus thermal aging time and thermal cycling

As the concept of damage equivalency holds true for this damage proxy as well same amount of IMC thickness can be achieved by either thermal cycling or thermal aging. Therefore if we equate $\left[\frac{y}{y_0}-1\right] = 0.0199(N)^{0.81}$ (32) and $\left[\frac{y}{y_0}-1\right] = 0.044(t)^{0.5}$ **(34)** we get a relationship between number of cycles and aging time ($N = 2.675(t)^{0.62}$ (**39**) using normalized IMC thickness as the damage proxy.

$$0.0199(N)^{0.81} = 0.044(t)^{0.5} \quad (38)$$

$$N = 2.675(t)^{0.62} \quad (39)$$

One of the vital observations that can be made from the combined plots of both the damage proxies vs. thermal cycling and thermal aging (Figure 46 and Figure 47) is the difference in the slopes for thermal cycling and thermal aging. It is evident from the combined plots that the damage accumulation and progression in thermal cyclic environment is faster than isothermal aging environment for both the damage proxies. This is because in thermal cycling the temperature ramps-up and down continuously which causes shearing of the solder joints due to CTE mismatch. Although creep which is a thermally activated phenomenon governs the plastic deformation in viscoplastic materials such as solders thermo-mechanical deformations due to low cycle thermal fatigue are dominant in thermal cyclic environments as compared to steady state isothermal aging environment. As the micro-structural evolution is directly proportional to these thermo-mechanical deformations both the damage proxies evolve relatively faster in thermal cyclic environments than in steady state thermal aging.

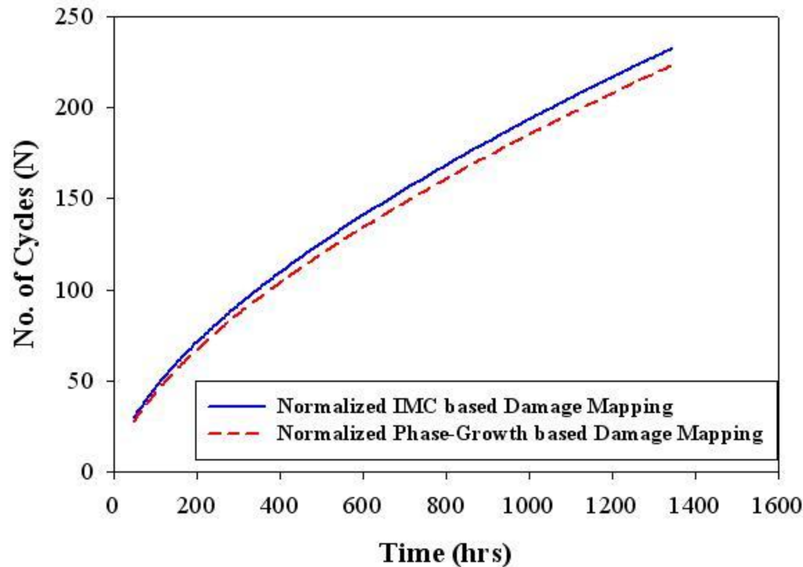

Figure 48: Combine plot of No of Cycles (N) versus Time in hrs, due to damage mapping from Phase growth and IMC thickness.

$N = 2.40(t)^{0.63}$ (**37**and $N = 2.675(t)^{0.62}$

(**39** are plotted are in Figure 48. It is a plot of number of cycles vs. aging time using normalized IMC growth and normalized phase-growth. Both the curves marked by blue and red line follow similar exponential trend which help us conclude that the damage mapping is correct and can be used to computer life expended due to storage. It shows the influence of dormant storage on thermal cyclic life. Table 6 summarizes the cyclic life consumed in -55°C to 125°C thermal cycle due to isothermal aging 125°C for different aging time intervals using both the leading indicators of failure. Last row in the table indicates that the cyclic life reduces by 100 cycles when the electronics is stored for 336 hours i.e. 14 days. This is a considerable amount of reduction in life due to storage which can not be neglected and have to be taken into account in the life prediction models for such complex environments.

Table 6: Damage Mapping from Leading Indicators of Failure

Time in Hrs	**Reduction in life from Normalized Phase Growth**	**Reduction in life from Normalized IMC thickness growth**
48	28	29
96	43	45
144	55	58
192	67	69
240	77	80
288	86	89
336	93	98

4.6.2 Prognostication of Life under Overlapping Stresses

Condition monitoring cell CM #3 (Table 5) was created consisting of multiple PBGA 676 test vehicles and was subjected to two different combinations of thermal

aging and thermal cycling viz. 48 hours in isothermal aging at 125°C followed by 100 cycles in -55°C to 125°C thermal cycle and 192 hours in isothermal aging at 125°C followed by 100 cycles in -55°C to 125°C. Prognostication of life for two combinations of aging + cyclic exposure has been presented to demonstrate the viability and prove the robustness of the proposed prognostic model.

The life in the sequential stress environment has been prognosticated in two ways to show the significance of dormant storage and its effect on the cyclic life. Life has been prognosticated at the end of storage as shown in Figure 49 and also after overlapping exposure as shown in Figure 50. Life in terms of number of hours in aging i.e. after storage has been computed using normalized IMC growth as the leading indicator of failure while total life consumed in overlapping environment has been computed using normalized phase-growth as the leading indicator of failure.

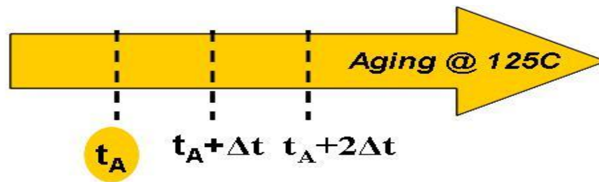

Figure 49: Prognostication of Life Consumed Due to Aging in number of hours.

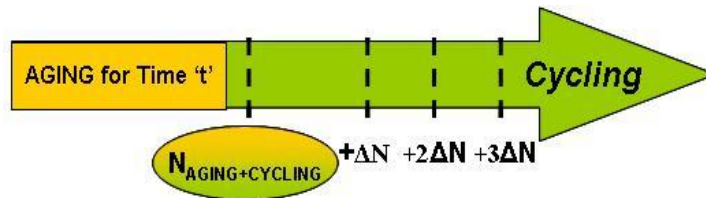

Figure 50: Prognostication of Life in Overlapping Environment

Normalized equation relating IMC growth with aging time is shown in Equation. 3 equations are needed to solve 3 unknown's y_0, k_{Nt} and t. Thus to get 3 equations packages have been subjected to known additional hours of aging (t+Δt and t+2Δt) at

125°C as depicted in Figure 49 followed by IMC growth analysis at each time interval (y_t, $y_{t+\Delta t}$ and $y_{t+2\Delta t}$). Levenberg-Marquardt algorithm explained in Chapter 3 has been used to solve the set of non-linear equations below ($\left[\frac{y_t}{y_0}-1\right] = k_{Nt}\sqrt{t}$ (**40**, $\left[\frac{y_{t+\Delta t}}{y_0}-1\right] = k_{Nt}\sqrt{t+\Delta t}$ (**41**and $\left[\frac{y_{t+2\Delta t}}{y_0}-1\right] = k_{Nt}\sqrt{t+2\Delta t}$ (**42**).

$$\left[\frac{y_t}{y_0}-1\right] = k_{Nt}\sqrt{t} \qquad (40)$$

$$\left[\frac{y_{t+\Delta t}}{y_0}-1\right] = k_{Nt}\sqrt{t+\Delta t} \qquad (41)$$

$$\left[\frac{y_{t+2\Delta t}}{y_0}-1\right] = k_{Nt}\sqrt{t+2\Delta t} \qquad (42)$$

Similarly normalized phase-growth parameter has been used as the leading indicator of failure to prognosticate total life in the overlapping stress environment i.e. aging followed by cycling. Levenberg-Marquardt algorithm explained in Chapter 3.5 has been used for the life prediction using normalized phase-growth as the leading indicator of failure. LM algorithm has been modified to take the phase-growth equations. As discussed earlier (Chapter 4.3) the generalized equation relating phase growth of the solder interconnect with number of cycles it has been subjected to is given by,

$$g^4 - g_0{}^4 = a(N)^b \qquad (43)$$

Where, 'g' is the grain size measured after N number of thermal cycles, 'g_0' is the grain size measured after reflow, 'N' is the number of cycles the system is exposed to in a thermal cycling environment, and 'a' and 'b' are the constant and exponent respectively which take into account material and temperature reliant factors. The damage incurred after each cycle is reflected in the grain size of the solder which can be measured by cross-sectioning the sample and analyzing it using the image processing software. Thus in real time, without the knowledge of prior stress histories one can only find g in the above equation while rest of the variables g_0, a, N and b are unknowns.

The prognostic model predicts the number of cycles 'N' the system has been exposed to in a thermal cycling environment based on the real time grain size measurement 'g'. In order to compute number of cycles, the non-linear normalized phase growth equation has to be solved for the 4 unknowns viz. N, a, b and g_0. To get 4 equations to solve 4 unknowns the system has to be subjected to known additional number of cycling ($N+\Delta N$, $N+2\Delta N$ and $N+3\Delta N$) depicted in Figure 50, followed by grain size measurement $g_{N+\Delta N}$, $g_{N+2\Delta N}$ and $g_{N+3\Delta N}$ after each additional cycling respectively. 4 normalized equations solved using LM algorithm to compute N, g_0, $a_{N\Delta T}$ and $b_{N\Delta T}$ are shown below.

$$\left[\left(\frac{g_N}{g_0}\right)^4 - 1\right] = a_{N\Delta T}(N)^{b_{N\Delta T}} \quad (44)$$

$$\left[\left(\frac{g_{N+\Delta N}}{g_0}\right)^4 - 1\right] = a_{N\Delta T}(N+\Delta N)^{b_{N\Delta T}} \quad (45)$$

$$\left[\left(\frac{g_{N+2\Delta N}}{g_0}\right)^4 - 1\right] = a_{N\Delta T}(N+2\Delta N)^{b_{N\Delta T}} \quad (46)$$

$$\left[\left(\frac{g_{N+3\Delta N}}{g_0}\right)^4 - 1\right] = a_{N\Delta T}(N+3\Delta N)^{b_{N\Delta T}} \quad (47)$$

The LM algorithm equation that iteratively minimizes the error in a multi-dimensional solution space is given by,

$$\left(J^T J + \mu I\right) h = -J^T E \quad (48)$$

Thus the Jacobian matrix J (

$$J = \begin{matrix} \frac{\partial g_1}{\partial g_0} & \frac{\partial g_1}{\partial a} & \frac{\partial g_1}{\partial N} & \frac{\partial g_1}{\partial b} \\ \frac{\partial g_2}{\partial g_0} & \frac{\partial g_2}{\partial a} & \frac{\partial g_2}{\partial N} & \frac{\partial g_2}{\partial b} \\ \frac{\partial g_3}{\partial g_0} & \frac{\partial g_3}{\partial a} & \frac{\partial g_3}{\partial N} & \frac{\partial g_3}{\partial b} \\ \frac{\partial g_4}{\partial g_0} & \frac{\partial g_4}{\partial a} & \frac{\partial g_4}{\partial N} & \frac{\partial g_4}{\partial b} \end{matrix}$$

(**53**) for phase-growth as the leading indicator will be a (4X4) matrix as there are 4 unknowns. As Jacobian is a partial derivative of the

governing equation with respect to each unknown sample individual components of the Jacobian matrix J are evaluated below.

$$\frac{\partial g}{\partial g_0} = \frac{g_0^{\,3}}{\left(g_0^{\,4} + a(N)^b\right)^{\frac{3}{4}}} \qquad (49)$$

$$\frac{\partial g}{\partial a} = \frac{N^b}{4\left(g_0^{\,4} + a(N)^b\right)^{\frac{3}{4}}} \qquad (50)$$

$$\frac{\partial g}{\partial N} = \frac{ab(N)^b}{4N\left(g_0^{\,4} + a(N)^b\right)^{\frac{3}{4}}} \qquad (51)$$

$$\frac{\partial g}{\partial b} = \frac{a\log(N)(N)^b}{4\left(g_0^{\,4} + a(N)^b\right)^{\frac{3}{4}}} \qquad (52)$$

$$J = \begin{bmatrix} \frac{\partial g_1}{\partial g_0} & \frac{\partial g_1}{\partial a} & \frac{\partial g_1}{\partial N} & \frac{\partial g_1}{\partial b} \\ \frac{\partial g_2}{\partial g_0} & \frac{\partial g_2}{\partial a} & \frac{\partial g_2}{\partial N} & \frac{\partial g_2}{\partial b} \\ \frac{\partial g_3}{\partial g_0} & \frac{\partial g_3}{\partial a} & \frac{\partial g_3}{\partial N} & \frac{\partial g_3}{\partial b} \\ \frac{\partial g_4}{\partial g_0} & \frac{\partial g_4}{\partial a} & \frac{\partial g_4}{\partial N} & \frac{\partial g_4}{\partial b} \end{bmatrix} \qquad (53)$$

Prognostication Results and Validation

Two combinations of sequential aging and cycling have been presented and prognosticated to demonstrate the influence of aging time on the cyclic life. The first combination is 48 hours in isothermal aging followed by 100 cycles in thermal cycling as shown in. Here the storage time or aging time is prognosticated using normalized IMC

growth as the leading indicator of failure. For this some of the packages from CM #3 after storage were subjected to known additional hours of aging to get 3 equations to solve 3 unknowns as shown in Figure 51. The IMC growth was extracted and analyzed after each additional aging interval respectively.

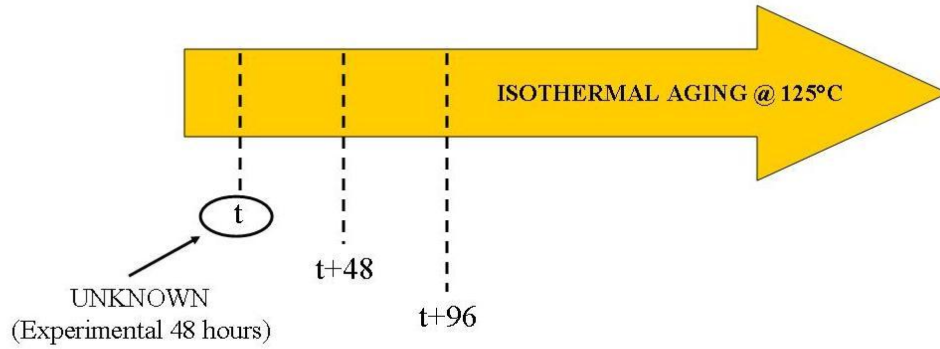

Figure 51: Schematic for Prognostication of Storage Time (for 48 hours Experimental Exposure)

Following three normalized IMC growth equations were solved using Levenberg-Marquardt algorithm to compute t, k_{Nt} and y_0.

$$\left[\frac{y_t}{y_0} - 1\right] = k_{Nt}\sqrt{t} \qquad (54)$$

$$\left[\frac{y_{t+48}}{y_0} - 1\right] = k_{Nt}\sqrt{t+48} \qquad (55)$$

$$\left[\frac{y_{t+96}}{y_0} - 1\right] = k_{Nt}\sqrt{t+96} \qquad (56)$$

Figure 52 shows the prognostication output for the life consumed due to storage. It is a 3D plot of number of hours in aging i.e. t, normalized IMC y/y0 and error. The 3D plot has been graphed to present how the error varies with respect to the two unknowns.

It can be seen that Levenberg-Marquardt algorithm iteratively minimizes the error in the solution space. Each and every blue dot is a solution to the non-linear set of equations but only the solution corresponding to the minimum error marked by red dotted line is selected as the final answers. Thus for experimental value of 48 hours in isothermal aging, prognostic model predicted 46 hours in storage.

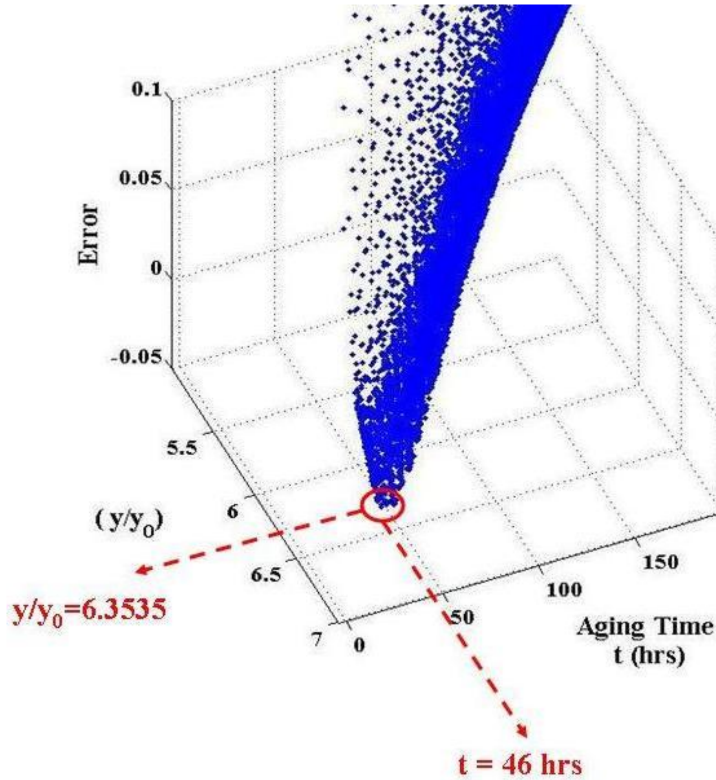

Figure 52: 3D plot of error versus aging time in hours for 676 PBGA 96.5Sn3.0Ag0.5Cu solder interconnects for experimental exposure of 48 hours in isothermal aging at 125°C.

Total life in sequential stress environment of 48 hours in thermal aging followed by 100 cycles in thermal cycling has been prognosticated using normalized phase-growth as the leading indicator of failure. As Levenberg-Marquardt algorithm has to solve 4 unknowns for phase-growth as the damage proxy some of the packages from CM #3 after were subjected to known additional number of cycles as shown in Figure 53 to get 4 equations.

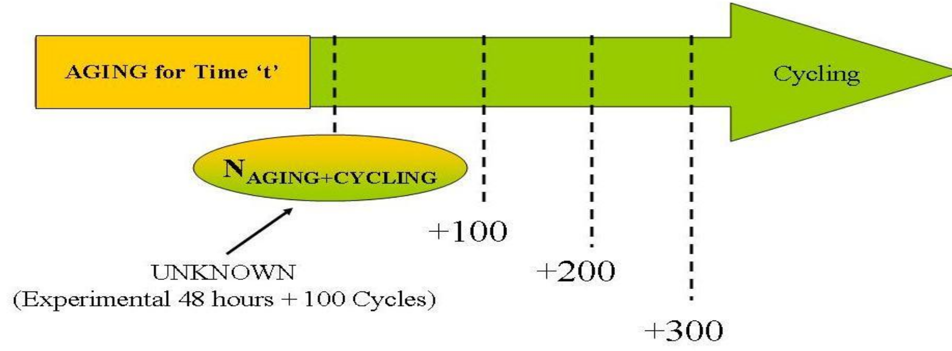

Figure 53: Schematic for Prognostication of Total Life in Sequential Stress Environment (for 48 hours+100 Cycles Experimental Exposure)

The set of normalized phase-growth equations solved to compute N, $a_{N\Delta T}$, $b_{N\Delta T}$ and g_0 are shown below,

$$\left[\left(\frac{g_N}{g_0}\right)^4 - 1\right] = a_{N\Delta T}(N)^{b_{N\Delta T}} \tag{57}$$

$$\left[\left(\frac{g_{N+100}}{g_0}\right)^4 - 1\right] = a_{N\Delta T}(N+100)^{b_{N\Delta T}} \tag{58}$$

$$\left[\left(\frac{g_{N+200}}{g_0}\right)^4 - 1\right] = a_{N\Delta T}(N+200)^{b_{N\Delta T}} \tag{59}$$

$$\left[\left(\frac{g_{N+300}}{g_0}\right)^4 - 1\right] = a_{N\Delta T}(N+300)^{b_{N\Delta T}} \tag{60}$$

Figure 54 shows the prognostication output for total life consumed in the sequential stress environment. It is a 3D plot of number of cycles N, normalized phase-growth g/g0 and error. Similar to previous output the 3D plot helps to comprehend the iterative minimization of error scheme adopted by LM algorithm for two unknowns. Thus in the sequential stress environment prognostic model predicted 143 cycles when

experimentally packages were subjected to a combination of 48 hours in storage + 100 cycles in operation.

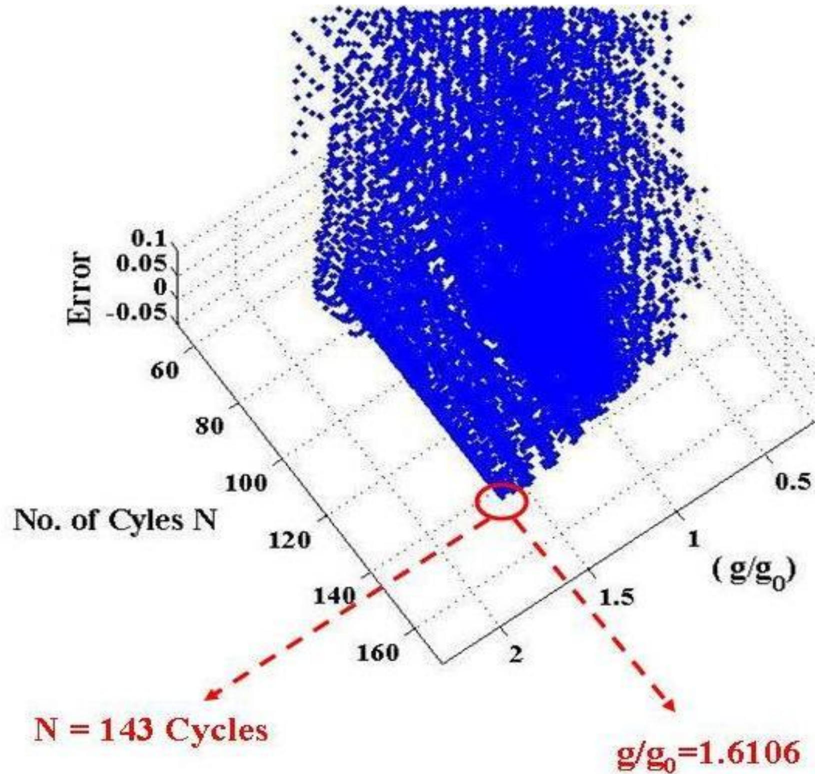

Figure 54: 3D plot of error versus number of cycles for 676 PBGA 96.5Sn3.0Ag0.5Cu solder interconnects for experimental exposure of 48 hours in isothermal aging at 125°C followed by 100 cycles in -55°C to 125°C.

Similar prognostication was carried out for packages subjected to 192 hours in isothermal aging followed by 100 cycles in cyclic thermal environment. The prognostication schematics for the life consumed due to storage and total life computation has been shown in Figure 55 and Figure 57. It should be noted that the prognostication equations solved to compute life in storage are similar to

$$\left[\frac{y_t}{y_0}-1\right] = k_{Nt}\sqrt{t}$$

(54

$$\left[\frac{y_{t+48}}{y_0}-1\right] = k_{Nt}\sqrt{t+48}$$

(55 $$\left[\frac{y_{t+96}}{y_0}-1\right]=k_{Nt}\sqrt{t+96}$$ (56 while prognostication equations solved to compute total cyclic life are similar to $$\left[\left(\frac{g_N}{g_0}\right)^4-1\right]=a_{N\Delta T}(N)^{b_{N\Delta T}}$$

(57, $$\left[\left(\frac{g_{N+100}}{g_0}\right)^4-1\right]=a_{N\Delta T}(N+100)^{b_{N\Delta T}}$$

(58, $$\left[\left(\frac{g_{N+200}}{g_0}\right)^4-1\right]=a_{N\Delta T}(N+200)^{b_{N\Delta T}}$$

(59 $$\left[\left(\frac{g_{N+300}}{g_0}\right)^4-1\right]=a_{N\Delta T}(N+300)^{b_{N\Delta T}}$$ (60. Prognostication outputs for life consumed due to storage and total life after sequential stress environments are shown in Figure 56 and Figure 58 respectively.

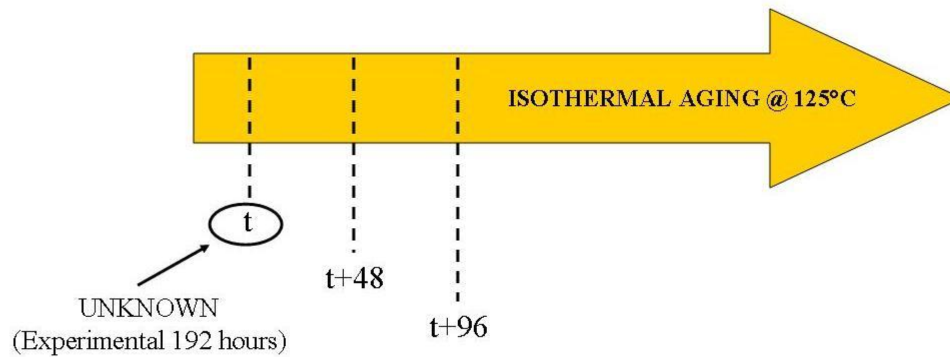

Figure 55: Schematic for Prognostication of Storage Time (for 192 hours Experimental Exposure)

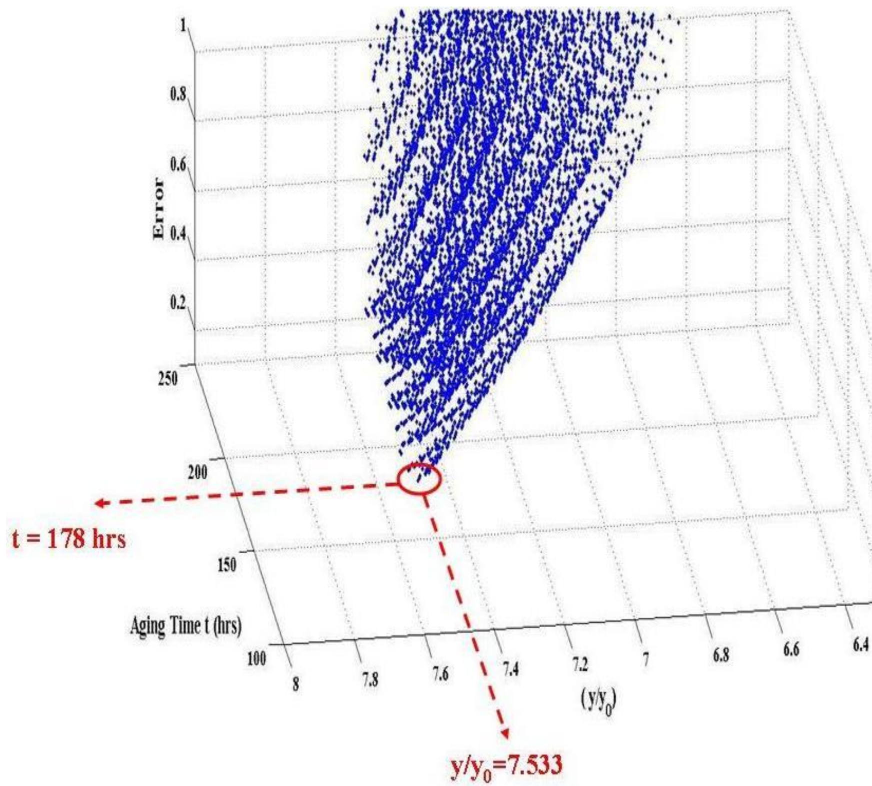

Figure 56: 3D plot of error versus aging time in hours for 676 PBGA 96.5Sn3.0Ag0.5Cu solder interconnects for experimental exposure of 192 hours in isothermal aging at 125°C.

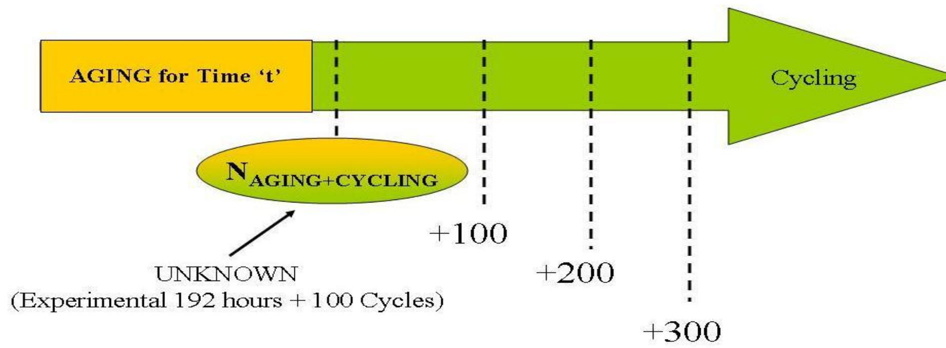

Figure 57: Schematic for Prognostication of Total Life in Sequential Stress Environment (for 192 hours+100 Cycles Experimental Exposure)

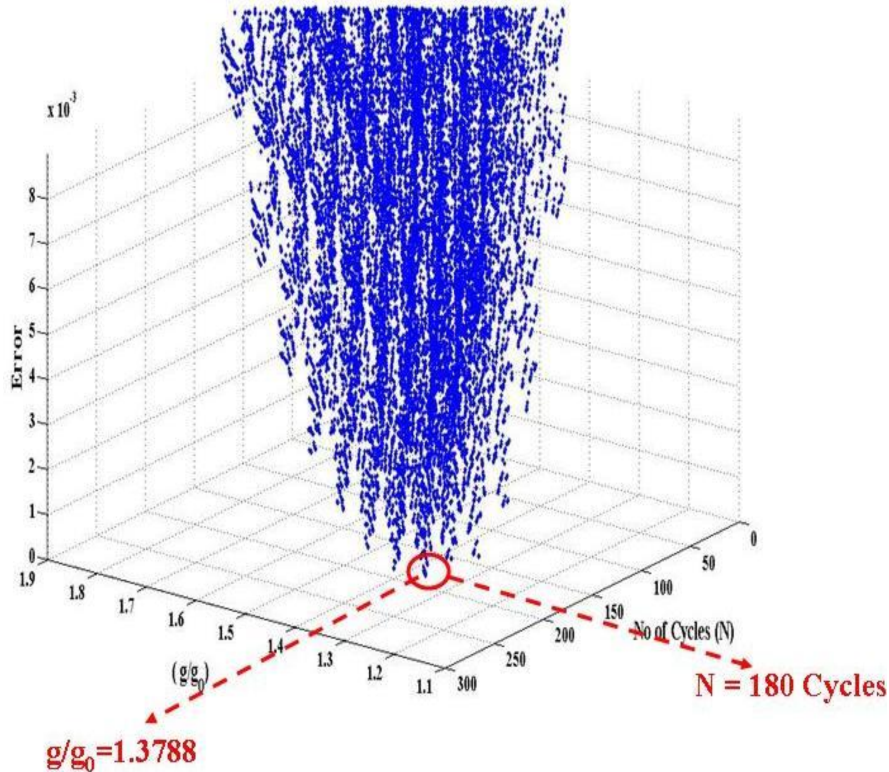

Figure 58: 3D plot of error versus number of cycles for 676 PBGA 96.5Sn3.0Ag0.5Cu solder interconnects for experimental exposure of 192 hours in isothermal aging at 125°C followed by 100 cycles in -55°C to 125°C.

Life computed at each stage i.e. after storage and after sequential stresses have been validated with the experimental values to study the errors associated with the prognostic model. Model predictions after storage for both the aging times have been validated in Table 7. Error is the in the range of 4 % to 7 % which is very good from a life prediction stand point. Error associated with the prognosticated reduction in cyclic life due to storage and experimental reduction in cyclic life due to storage has been tabulated in Table 8. Here the error ranges from 3 % to 5 % which is acceptable. From both these tables it can be concluded that the proposed prognostic model performs well for the life computation after storage as the model predictions correlate really well with the experimental values.

Table 7: Error Estimation in Prognostication of Thermal Aging (Storage)

Storage Time (Isothermal Aging Time)		
Experimental	**Model**	**% Error**
48 hours	46 hours	4.2
192 hours	178 hours	7.3

Table 8: Error Estimation in Reduction in Cyclic Life Due to Thermal Aging (Storage)

Experimental Aging Time (hrs)	**Equivalent Reduction in Cyclic Life** $N = 2.40(t)^{0.63}$ **(37) (A)**	**Prognosticated Aging Time (hrs)**	**Equivalent Reduction in Cyclic Life** $N = 2.40(t)^{0.63}$ **(37) (B)**	**% Error, (A) and (B)**
48	28	46	27	3.6
192	66	178	63	4.5

Prognosticated total life in overlapping environment of thermal aging and thermal cycling has been correlated with the experimental values in Table 9. For prognostication of total life error envelope is in the range of 8 % to 12 % which is quite good from a life prediction perspective. The total life has also been systematically split into aging time, reduction in cyclic time due to aging and only cyclic life for experimental as well as

prognosticated results for better understanding of life consumption in such complex sequential or overlapping thermal environments of thermal aging and thermal cycling.

Table 9: Error Estimation in Prognostication of Overlapping Damage

Stress History	Experimental			Prognostication			% Error (V+W) and (X)
	Cyclic Life Reduction due to Aging (Cycles), Column (A), Table 6 (V)	Imposed Thermal Cycles (W)	Total Cyclic Life (V+W)	Total Cyclic Life (X)	Cyclic Life Reduction Due to Aging (Cycles) Column (B),Table 6 (Y)	Cyclic Life Alone Cycles, (X-Y)	
48 Hours + 100 Cycles	28	100	128	143	27	116	-11.7
192 Hours + 100 Cycles	66	100	166	180	63	117	-8.4

4.7 Prognostic Performance Metrics

Prognostics is an emerging concept in condition based maintenance (CBM) of critical systems, where it is desired to predict residual life left in the system before any catastrophic failure takes place and so it is extremely important to check the validation of such prediction algorithms. Since these prognostics concepts are relatively new they lack standard definitions and there is an inconsistency in their interpretations. The lack of standards is in part due to the wide variety of end user requirements for different application, wide range of time scales involved, available domain information, domain dynamics etc. So there is actually very little means of comparing different prognostics approaches based on a common ground. Further in order to evaluate prognostics

approach in real world condition a rigorous testing of variety of parameters is required before they can be used in any critical system. So to serve this purpose performance metrics were established. Performance metrics help establish design requirements that must be met for comparison. In the absence of standardized metrics it has been difficult to quantify acceptable performance limits and specify crisp and unambiguous requirements to the designers. These metrics allows comparing different algorithms and also yields constructive feedback to further improve these algorithms. There are various performance metrics which have been used in domains like Aerospace, Electronics, medicine, Finance, Weather prediction, Nuclear and Automotive [Saxena 2008].

In this chapter two separate prognostication models based on two leading indicators of failure viz. normalized phase-growth and normalized inter-metallic compound (IMC) growth of second level solder interconnects have been proposed and implemented for the life prediction of electronics. The sole purpose of evaluating various performance metrics was to relatively compare the two models and see which leading indicator of failure accurately predicts life. For this seven different performance metrics viz. α-λ curve, accuracy, precision, Mean Squared Error (MSE), and Mean Absolute Percentage Error (MAPE), relative accuracy (RA) and cumulative relative accuracy (CRA) have been computed to compare the two models.

Terms and Notations:

- UUT is unit under test
- $\Delta^l(i)$ is the error between the predicted and the true RUL at time index *i* for UUT *l*.
- EOP (End-of-Prediction) is the earliest time index, *i*, after prediction crosses the failure threshold.

- EOL represents End-of-Life, the time index for actual end of life defined by the failure threshold.
- P is the time index at which the first prediction is made by the prognostic system.
- $r^{l}(i)$ is the RUL estimate for the lth UUT at time t_i as determined from measurement and analysis.
- $r_*^{l}(i)$ is the true RUL at time t_i given that data is available up to time t_i for the lth UUT.
- ℓ is the cardinality of the set of all time indices at which the predictions are made, i.e. $\ell = (i \mid P \leq i \leq EOP)$.
- Error $\Delta^{l}(i) = r_*^{l}(i) - r^{l}(i)$

Average Bias:

Average bias method averages the error in predictions made at all subsequent times after prediction starts for the lth UUT. The metric can be extended to average bias over all UUTs to establish overall bias.

$$B_l = \frac{\sum_{i=P}^{EOP} \left(\Delta^{l}(i) \right)}{\left(EOP - P + 1 \right)} \qquad (61)$$

Sample Standard Deviation (S):

Sample standard deviation measures the dispersion/speed of the error with respect to the sample mean of the error. This metric is restricted to the assumption of normal distribution of the error. It is, therefore, recommended to carry out a visual inspection of error plots.

$$S(i) = \sqrt{\frac{\sum_{l=1}^{n} \left(\Delta^{l}(i) - M\right)^{2}}{n-1}} \qquad (62)$$

Where M is sample mean of the error

Mean squared error (MSE):

Mean squared error averages the square prediction error for multiple UUTs at the same prediction horizon. A derivative of MSE is root mean square error (RMSE).

$$MSE(i) = \frac{1}{L} \sum_{i=1}^{L} \Delta^{l}(i)^{2} \qquad (63)$$

Mean absolute percentage error (MAPE):

MAPE averages the absolute error in the predictions of multiple UUTs at the same prediction horizon. Instead of the mean, median can be used to compute Median absolute percentage error (MdAPE) in similar fashion.

$$MAPE(i) = \frac{1}{L} \sum_{l=1}^{L} \left| \frac{100\Delta^{l}(i)}{r_{*}^{l}(i)} \right| \qquad (64)$$

α-λ accuracy:

Conventionally the primary purpose of plotting α-λ curve for any prognostic health management (PHM) model is to find the prognostic horizon point. The detailed technical definitions and discussion can be found in [Saxena 2008]. However it also helps visually understand the model performance at different intervals of time. In this paper the α-λ curve has been plotted for both the models as shown in Figure 59 and Figure 60. It is a normalized plot of Remaining Useful Life (RUL) Vs Life which is compared against the ground truth and the error bounds. In this case the ground truth is the experimental

data obtained from accelerated testing shown by blue line in the plots and ± 10% error bounds are imposed shown by dotted lines. It should be noted that the selection of error bounds is application specific and typically tighter bounds are imposed as the criticality of the system increases.

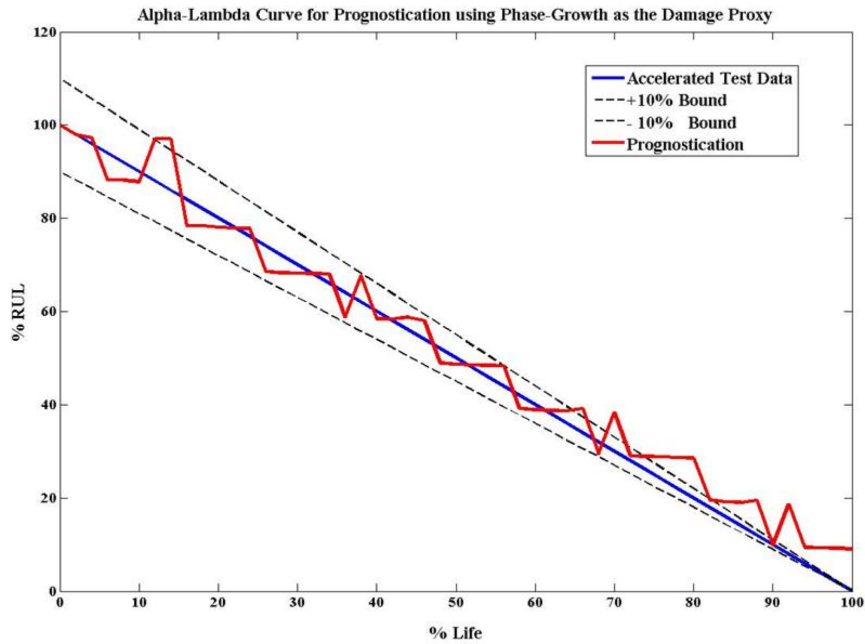

Figure 59: α-λ curve for Prognostication using normalized phase-growth as the leading indicator of failure

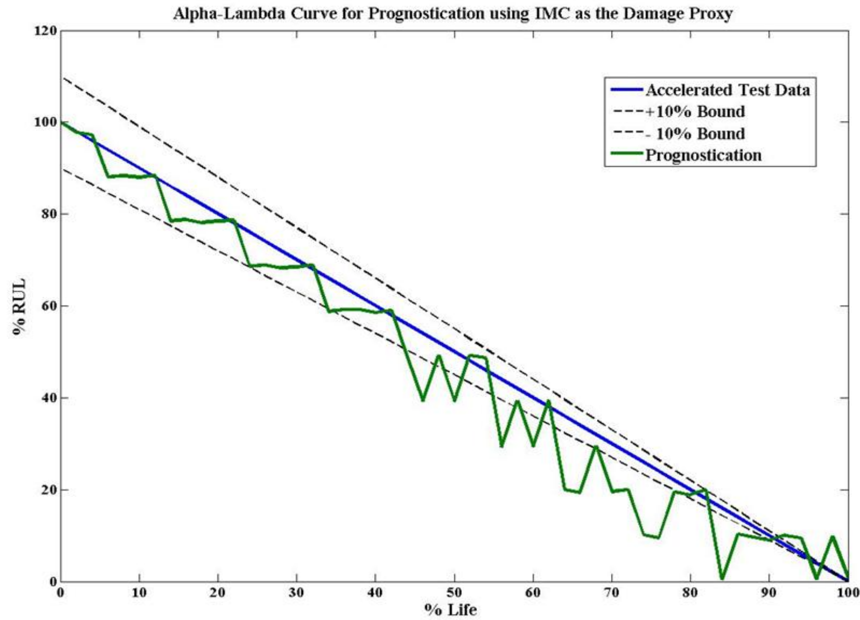

Figure 60: α-λ curve for Prognostication using normalized IMC growth as the leading indicator of failure

In this chapter the main idea to plot α-λ curves for the two models was not to find the prognostic horizon point but to compare the relative performance of the models visually. It is clear from the plots that although the red curve in Figure 59 diverges and goes outside error bounds at the end but still relatively it remains close to the blue line compared to the green curve in Figure 60. It helps conclude that the prognostication model developed using phase-growth parameter as the leading indicator of failure performs better than the prognostication model developed using IMC for the current field conditions.

Also α-λ curve does not provide absolute value based comparison but it provides useful information about the model at different intervals. For example visually it is evident from both the plots that the IMC model works better than the phase growth model until 50% of the life and then the IMC model diverges more than the Phase-growth

model. Thus this information can be used to modify the model by tweaking certain critical parameters and also check the factors affecting the variability.

Relative accuracy (RA):

Relative prediction accuracy is a notion similar to α-λ *accuracy* where, instead of finding out whether the predictions fall within a given accuracy levels at a given time instant, we measure the accuracy level. The time instant is again described as a fraction of actual remaining useful life from the point when the first prediction is made. An algorithm with higher relative accuracy is desirable.

$$RA = 1 - \frac{\left| r_*(t_\lambda) - r^l(t_\lambda) \right|}{r_*(t_\lambda)} \qquad (65)$$

Where $t_\lambda = P + \lambda\,(EOP - P)$

***Cumulative Relative Accuracy (CRA)*:**

Relative accuracy can be evaluated at multiple time instances. To aggregate these accuracy levels, we define Cumulative Relative Accuracy as a normalized weighted sum of relative prediction accuracies at specific time instances.

$$CRA = \frac{1}{EOP - P + 1} \sum_{l=P}^{EOL} RA \qquad (66)$$

Where *w* is a weight factor as a function of RUL at all time indices. In most cases it is desirable to weigh the relative accuracies higher closer to the EOL.

Table 10 summarizes all the prognostic metrics discussed above for both the PHM models viz. using normalized phase-growth and normalized IMC-growth respectively. From these metric values it can be concluded that both the damage proxies perform well and can be used as leading indicator of failures in the PHM models.

Table 10: Prognostic Metric Comparison

Prognostic Metrics	PHM Model for Phase-Growth	PHM Model for IMC Growth
Average Bias	-0.82316	2.225578
Sample Standard Deviation (S)	220.6121	292.8947
MSE	54181.35	130216.3
MAPE	0.065839	0.177259
RA (λ=0.5)	0.9732	0.7836
CRA	0.007713	0.0074246

4.8 Conclusion

State-of-art prognostic health management (PHM) model for electronics exposed to a combination of dormant storage and field application was proposed and implemented on commercial test vehicle. Dormant storage was simulated by isothermal aging environment while cyclic field application was replicated by thermal cyclic environment. Custom test vehicle was designed to accommodate 4 daisy chain patterns as against conventional 1 daisy chain for effective fault detection and isolation. Mathematical relationship between storage time and corresponding reduction in cyclic life was successfully established based on two physics-of-failure based damage proxies viz. phase-growth and inter-metallic compound (IMC) growth of second level solder interconnects. Life after storage and sequential stress application was prognosticated to show the influence of dormant storage on the cyclic life. Prognostication results were carefully studied to see if it captures the life expended during storage in thermal cyclic environment. It is clear from the prognostication results and damage equivalency

relationship that the effect of dormant storage can not be neglected as it considerably reduces the cyclic life and its effect has to be taken into account for accurate life predictions.

The viability of the proposed prognostic model was demonstrated for multiple combinations of overlapping stress environments to prove the robustness of the model. Correlation between the prognosticated damage and the actual accrued damage displays that the proposed PHM model can be used to assess damage accrued under overlapping thermo-mechanical stresses of thermal aging and thermal cycling. In addition, prognostics metrics have been used to quantitatively evaluate the performance of the prognostic algorithms using both the leading indicators. Results demonstrate that both damage proxies work well in estimating accrued damage and estimating residual life.

CHAPTER 5

SUMMARY AND FUTURE WORK

Electronics from a reliability perspective can be thought of as a function of three primary variables viz. materials, process, and application. There is a ton of literature available on reliability enhancement techniques specifically addressing materials and compliant processes. However even after employing all the reliability enhancement schemes it is well known that the deployed parts are observed to have erratic failure behavior and characteristics in the field even after rigorous qualification tests. Conventional life prediction models used for measuring electronics reliability are based on fear of failure whose decisions are based on pristine state and lack insight about the ongoing reliability of the system. The work presented in this thesis is an effort to address the growing need to develop techniques that can monitor in-field system state during the service life and make life predictions based on interrogation of system state. Although this technique requires condition monitoring it still eliminates the need for continuous monitoring of the system state to make life predictions which considerable saves the overhead associated with data acquisition systems. Two prognostic health management (PHM) models were presented for single and multiple thermal environments respectively.

5.1 PHM Model for Single Thermo-Mechanical Environment

Novel prognostic health management (PHM) model was developed for electronics exposed to steady-state temperature profiles. The proposed model was implemented on commercially relevant test vehicle to demonstrate its applicability in real field deployed electronics. The PHM model allowed life estimation of electronics subjected to single isothermal aging environments. The proposed methodology enabled spot assessment of life consumed due to isothermal aging environments in the pre-failure space, without any knowledge of prior stress histories. The prognostic model was based on physics-of-failure of lead-free second level solder interconnects commonly found in today's high I/O packaging architectures. It has been shown that the physics-of-failure based damage proxy identified as inter-metallic compound (IMC) growth, formed between the second level solder interconnect and copper pad at the board side interface can be used as a leading indicator of failure. Higher learning algorithm theory like Levenberg-Marquardt algorithm was used a non-linear least square (NLLSQ) method and was employed for the first time in evaluating electronics reliability.

The prognostic model proposed in Chapter 3 finds its application in a real world setting where one has to find the remaining useful life of the electronic system in the same isothermal environment well before the actual failure occurs i.e. in the pre-failure space without any knowledge of prior stress histories. In such scenario the proposed prognostic model can be implemented using condition monitoring devices which would be used to interrogate the damage progression in the form of IMC growth data. This data can be fed to the Levenberg-Marquardt algorithm developed for this model for accurate life predictions.

5.2 PHM Model for Sequential Thermal Environments of Thermal Aging and Thermal Cycling

In Chapter 4 a PHM model was developed for prognostication of accrued prior damage in electronics subjected to overlapping sequential environments of thermal aging and thermal cycling. Mathematical relationship between storage time and corresponding reduction in cyclic life was successfully established based on two physics-of-failure based damage proxies viz. phase-growth and inter-metallic compound (IMC) growth of second level solder interconnects. Life after storage and sequential stress application was prognosticated to show the influence of dormant storage on the cyclic life. Prognostication results were carefully studied to see if it captures the life expended during storage in thermal cyclic environment. It is clear from the prognostication results and damage equivalency relationship that the effect of dormant storage can not be neglected as it considerably reduces the cyclic life and its effect has to be taken into account for accurate life predictions.

The viability of the proposed prognostic model was demonstrated for multiple combinations of overlapping stress environments to prove the robustness of the model. Correlation between the prognosticated damage and the actual accrued damage displays that the proposed PHM model can be used to assess damage accrued under overlapping thermo-mechanical stresses of thermal aging and thermal cycling. In addition, prognostics metrics have been used to quantitatively evaluate the performance of the prognostic algorithms using both the leading indicators. Results demonstrate that both damage proxies work well in estimating accrued damage and estimating residual life.

5.3 Scope for Future Work

Prognostic model performance has been evaluated using standard prognostic metrics available in the literature. It would be interesting to relate these metrics for the model enhancement in the future. For example α-λ curve for both the leading indicator based models indicate that the models diverge at the end of life where it is critical to get tighter results. It would be worth to study various model parameters and check the sensitivity of each individual parameter with respect to the model outputs. The studied sensitivities can be incorporated in the models for accurate life predictions in the future.

Prognostic models in this thesis are based on non-linear least square (NLLSQ) method called Levenberg-Marquardt algorithm. It will also be interesting to apply other higher order learning algorithms to solve the set non-linear physic-of-failure based equations for life computation. Various models can then be compared using prognostic metrics and ranked for specific application.

In future prognostic models can be developed for more complex environments such as multiple combinations of thermal aging and thermal cycling. Also sequential low cycle thermal fatigue and transient drop event can be studied for prognosis. It would be valuable to study the effect of thermal aging and thermal cycling on the drop reliability of electronics. Complex overlapping environment such as thermal fatigue and high strain rate drop testing can be studied to extract damage proxies which can be incorporated as leading indicators of failure in future prognostic models.

BIBLIOGRAPHY

Abdulhamid, M., Basaran, C., “Influence of thermomigration on lead-free solder joint mechanical properties”, Journal of Electronic Packaging 131 (2009), p. 011002.

Allen, D., “Probabilities Associated with a Built-in-Test System, Focus on False Alarms”, Proceedings of AUTOTESTCON, IEEE Systems Readiness Technology Conference, pp. 643-645, September 22-25, 2003.

Al-Qutayri, M., Shepherd, P., “Go/No-Go Testing of Analogue Macros”, IEE Proc. On Circuits, Devices and Systems-Part G, Vol.139, pp.534-540, August 1992.

Amagai, M., “Chip Scale Package (CSP) Solder Joint Reliability and Modeling”, IEEE INTERNATIONAL RELIABILITY PHYSICS PROCEEDINGS 1998, ISSUE 36, pages 260-268.

Anand, L., “Constitutive Equation for the Rate-dependent Deformation of Metals at Elevated Temperatures,” Transactions of ASME, Journal of Engineering Materials and Tech., Vol. 104, No. 1, pp.12-17, 1985.

Baldwin, C., J. Kiddy, T. Salter, P. Chen, and J. Niemczuk, “Fiber Optic Structural Health Monitoring System: Rough Sea Trials Testing of the RV Triton,” MTS/IEEE Oceans 2002, Volume 3, pp. 1807-1814, October 2002.

Barke, D., Chiu, W., K., “Structural Health Monitoring in the Railway Industry: A Review”, Structural Health Monitoring, Vol. 4, No. 1, pp. 81-93, 2005.

Bellini, A., Filippetti, F., Tassoni, C., Capolino, G., “Advances in Diagnostic Techniques for Induction Machines”, IEEE TRANSACTIONS ON INDUSTRIAL ELECTRONICS, VOL. 55, NO. 12, DECEMBER 2008.

Bradely, E., Banerki, K., Effect of PCB Finish on the Reliability and Wettability of Ball Grid Array Packages. IEEE Transaction on Component Packaging and Manufcaturing Technology Part B-Advanced Packaging Vol.19, pp.320-330, 1996.

Brown, D., Kalgren, P., Byington, C., Roemer M., "Electronic prognostics – A case study using global positioning system (GPS)", Microelectronics Reliability, Volume 47, Issue 12, December 2007, Pages 1874-1881.

Chandramouli, R., Pateras, S., "Testing Systems on a Chip", IEEE Spectrum, Vol. 33, No. 11, pp. 42-47, Nov. 1996.
Chang, P. C. Flatau, A. Liu, S. C., "Review Paper: Health Monitoring of Civil Infrastructure", STRUCTURAL HEALTH MONITORING -SAGE- 2003, VOL 2; NUMB 3, pages 257-267.

Charles, H.K., Clatterbaugh, G.V., "Solder Joint Reliability — Design Implications From Finite Element Modeling and Experimental Testing", Journal of Electronic. Packaging, June 1990, Volume 112, Issue 2, 135.

Chiang, K. N. Lin, Y. T. Cheng, H. C. "On Enhancing Eutectic Solder Joint Reliability Using a Second-Reflow-Process Approach", IEEE TRANSACTIONS ON ADVANCED PACKAGING 2000, VOL 23; PART 1, pages 9-14.

Chiu, S. H. Shao, T. L. Chen, C. Yao, D. J. Hsu, C. Y., "Infrared microscopy of hot spots induced by Joule heating in flip-chip SnAg solder joints under accelerated electromigration", APPLIED PHYSICS LETTERS 2006, VOL 88; NUMB 2, pages 022110.

Choi, W. J. Yeh, E. C. C. Tu, K. N., "Mean-time-to-failure study of flip chip solder joints on Cu/Ni(V)/Al thin-film under-bump-metallization", JOURNAL OF APPLIED PHYSICS 2003, VOL 94; PART 9, pages 5665-5671.

Clech, Jean-Paul. Acceleration Factors and Thermal Cycling Test Efficiency For Lead Free Sn-Ag-Cu Assemblies. SMTA International, Chicago IL. Sept. 25-29, 2005.

Coffin, L. F., "A Study of the Effects of Cyclic Thermal Stresses on a Ductile Metal", Transactions of ASME, Vol. 76, pp. 931-950, 1954.

Darveaux, R. and Banerji, K., Constitutive Relations for Tin-Based Solder Joints, IEEE Trans-CPMT-A, Vol. 15, No.6, pp. 1013-1024, 1992.

Darveaux, R., Effect of Simulation Methodology on Solder Joint Crack Growth Correlation, Proceedings of the 2000 Electronic Components and Technology Conference, pp. 1048-1058, May 2000.

DeWolf, J., Lauzon, R., Culmo, R., "Monitoring Bridge Performance", Structural Health Monitoring, Vol. 1, No. 2, 129-138 (2002).

Drees, R., and Young, N., "Role of BIT in Support System Maintenance and Availability", IEEE A&E Systems Magazine, pp. 3-7, August 2004.

Dussault,P., Byington, C., Kalgren, P., “Field Data Evaluation and Continuous Health Assessment of Critical Avionics Subsystem Degradation”, Aerospace Conference, 2006 IEEE.

Dutta, I., “Impression Creep Testing and Microstructually Adaptive Creep Modeling of Lead-Free Solder Interconnects”, TRC, October 25-27 2004.

Engelmaier, W., “Effects of Power Cycling on Leadless Chip Carrier Mounting Reliability and Technology”, presented at Proceedings of International Electronic Packaging, San Diego, California, November 1982.

Engelmaier, W., “Functional Cycles and Surface Mounting Attachment Reliability”, ISHM Technical Monograph Series, pp. 87-114, 1984.

Fernando, G. F. Hameed, A. Winter, D. Tetlow, J. Leng, J. Barnes, R. Mays, G. Kister, G., “Structural Integrity Monitoring of Concrete Structures via Optical Fiber Sensors: Sensor Protection Systems”, STRUCTURAL HEALTH MONITORING -SAGE- 2003, VOL 2; NUMB 2, pages 123-136.

Frear, D. R. Burchett, S. N. Neilsen, M. K. Stephens, J. J., “Microstructurally Based Finite Element Simulation of Solder Joint Behaviour”, SOLDERING AND SURFACE MOUNT TECHNOLOGY 1997, ISSUE 25, pages 39-42.

Friswell, M., Penny, J., “Crack Modeling for Structural Health Monitoring”, Structural Health Monitoring, Vol. 1, No. 2, 139-148 (2002).

Gao, R. X., Suryavanshi, A., “BIT for Intelligent System Design and Condition Monitoring”, IEEE Transactions on Instrumentation and Measurement, Vol. 51, Issue: 5, pp. 1061-1067, October 2002.

Goldmann, L.S., “Geometric Optimization of Controlled Collapse Interconnections”, IBM Journal of Research Development, Vol. 13, pp. 251-265, 1969.

Hassan, A., Agarwal, V. K., Nadeau-Dostie, B., Rajski, J., “BIST of PCB Interconnects Using Boundary- Scan Architecture”, IEEE Transactions on Computer-Aided Design, Vol. 11, No. 10, pp. 1278-1288, October 1992.

Hecht, H., “Why prognostics in avionics?” IEEE Proceedings of Aerospace Conference, March 2006.

Henderson, D.W., “The Microstructure of Sn in Near Eutectic Sn-Ag-Cu Alloy Solder Joints and Its Role In Thermo-mechanical Fatigue”, Materials Research Society, Vol.19, No.6, June 2004.

Hess KR, Zhang W, Baggerly KA, Stivers DN, Coombes KR: Microarrays: handling the deluge of data and extracting reliable information *Trends Biotechnol* 2001, 19:463-468.

Jarrell, D., Sisk, D., Bond, L., “Prognostics and Condition Based Maintenance (CBM) A Scientific Crystal Ball”, Pacific Northwest National Laboratory, Richland, WA, International Congress on Advanced Nuclear Power Plants (ICAPP), paper #194 June 2002.

Kok, R., Furlong, C., “Development and Characterization of MEMS Inertial System for Health Monitoring of Structures”, Experimental Techniques, Vol. 29, No. 6, pp. 46-53, November-December 2005.

Kolarik, V., Lubaszewski, M., Courtois, B., “Towards Self-Checking Mixed-Signal Integrated Circuits”, Proceedings of European Solid State Circuits Conference, Seville pp.202-205, 1993.

Lala, P. K., “Fault Tolerant and Fault Testable Hardware Design”, Prentice Hall, 1985.

Lall, P. Islam, N., Evans, J., Suhling, J., Damage Mechanics of Electronics on Metal-Backed Substrates in Harsh Environments. Proceedings of the 2004 Electronic Components and Technology Conference, pp. 704-711, 2004.

Lall, P., Bhat, C., Hande, M., More, V., Vaidya, R., Suhling, J., “Interrogation of System State for Damage Assessment in Lead-Free Electronics Subjected to Thermo-Mechanical Loads”, 58th ECTC, Orlando, FL, pp. 918-929, May 27-30, 2008[a].

Lall, P., Bhat, C., Hande, M., More, V., Vaidya, R., Suhling, J., “Algorithms for Prognostication of Prior Damage and Residual Life in Lead-Free Electronics Subjected to Thermo-Mechanical Loads”, ITHERM 2008, Orlando, FL, May 28-31,2008[b].

Lall, P., Hande, M., Bhat, C., Islam, M., Suhling, J.C., Lee, J., “Prognostics Health Monitoring (PHM) for Prior-Damage Assessment in Electronics Equipment under Thermo-Mechanical Loads”, Electronic Components and Technology Conference, Reno, Nevada, pp. 1097-1111, 2007[a].

Lall, P., Hande, M., Bhat, C., Islam, M., Suhling, J.C., Lee, J., “Feature Extraction and Damage-Precursors for Prognostication of Lead-Free Electronics”, Microelectronics Reliability Journal, Volume 47, pp. 1907–1920, December 2007[b].

Lall, P., Hande, M., Bhat, C., Islam, M., Suhling, J.C., Lee, J., “Feature Extraction and Damage-Precursors for Prognostication of Lead-Free Electronics”, Electronic Components and Technology Conference, San Diego, California, pp. 718-727, 2006[a].

Lall, P., Islam, N., Rahim, K., Suhling, J. C., “Prognostics and Health management of Electronic Packaging”, IEEE Transactions on Components and Packaging Technologies, Vol. 29, No. 3, pp. 666-677, September 2006[b].

Lall, P., Islam, N., Suhling, J., “Prognostication and Health Monitoring of Leaded and Lead Free Electronic and MEMS Packages in Harsh Environments”, Proceedings of the 55th IEEE Electronic Components and Technology Conference, Orlando, FL, pp. 1305-1313, June 1-3, 2005.

Lau, J. H. Pan, S. H. Chang, C., “A New Thermal-Fatigue Life Prediction Model for Wafer Level Chip Scale Package (WLCSP) Solder Joints”, TRANSACTIONS-AMERICAN SOCIETY OF MECHANICAL ENGINEERS JOURNAL OF ELECTRONIC PACKAGING 2002, VOL 124; PART 3, pages 212-220.

Lau, J. H., Ball Grid Array Technology, McGraw-Hill, New York, 1995.

Liu C., Huang Z., Conway P., Thomson R., “Materials Behavior and Intermetallics Characteristics in Reaction between SnAgCu and Sn-Pb Solder Alloys”, 54th Proceeding of Electronic Components and Technology Conference, 2004.

Lopez, L., “Advanced electronic prognostics through system telemetry and pattern recognition methods”, Microelectronics Reliability, Volume 47, Issue 12, December 2007, Pages 1865-1873.

Lung Lin., Chi Liu P., Ming Song L., “Wetting Interaction between Pb-Free Sn-Zn Solders and Cu, Ag Substrates”, 54th Proceeding of Electronic Components and Technology Conference, 2004.

Maalej, M. Ahmed, S. F. U. Kuang, K. S. C. Paramasivam, P., “Fiber Optic Sensing for Monitoring Corrosion-Induced Damage”, STRUCTURAL HEALTH MONITORING -SAGE- 2004, VOL 3; NUMB 2, pages 165-176.

Manson, S.S. and Hirschberg, M.H., Fatigue: An Interdisciplinary Approach, Syracuse University Press, Syracuse, NY, pp. 133, 1964.

Morris, J. W., et al, “Creep Properties of Sn-rich Solder Joints”, 53rd ECTC 2003, pp. 54-57.

Munns, T. E., R. M. Kent, “Structural Health Monitoring: Degradation Mechanism and System Requirements”, Digital Avionics Systems Conferences, pp. 6C2/1-6C2/8, Vol. 2, 2000.

Norris, K.C., Landzberg, A.H, “Reliability of Controlled Collapse Interconnections”, IBM Journal of Research Development, Vol. 13, pp. 266-271, 1969.

Orsagh, R., Brown, D., Roemer, M., Dabney, T., Hess, A., “Prognostic Health Management for Avionics System Power Supplies,” Proceedings of the IEEE Aerospace Conference, Big Sky, MT, March 2005.

Oza, N., Tumer, K., Tumer, I., & Huff, E. Classification of Aircraft Maneuvers for Fault Detection. Lecture Notes in Computer Science, Volume 2709, 2003, pp. 375 – 384.

Park, H. G., Mackey, R., James, M., Zak, M., Kynard, M., Greene, W., Sebghati, J., "Analysis of Space Shuttle Main Engine Data Using Beacon-based Exception Analysis for Multi-Missions," IEEE Aerospace Conference, Big Sky, Montana, March 2002.

Popelar, S., "A Parametric Study of Flip Chip Reliability Based on Solder Fatigue Modeling", *1997 International Electronics Manufacturing Technology Symposium* October 13-15, 1997.

Rosenthal, D., and Wadell, B., "Predicting and Eliminating Built-in Test False Alarms", IEEE Transactions on Reliability, Vol. 39, No 4, pp. 500-505, October 1990.

Saxena, A., Celaya, J., Balaban, E., Goebel, K., Saha, B., Saha, S., Schwabacher, M., "Metrics for Evaluating Performance of Prognostic Techniques", International Conference on Prognostics and Health Management, 2008.

Schubert et al., Fatigue Life Models for SnAgCu and SnPb Solder Joints Evaluated by Experiments and Simulation. Proceedings of the 2003 Electronic Components and Technology Conference, pp. 603-610, 2003.

Schubert, A., et al, "Fatigue Life Models of SnAgCu and SnPb Solder Joints Evaluated by Experiements and Simulations," 53rd ECTC 2003, pp. 603-610.

Schwabacher, M. Machine Learning for Rocket Propulsion Health Monitoring. Proceedings of the SAE World Aerospace Congress, Dallas, TX, 2005.

Seeling, K., "A Study of Lead Free Solder Alloys", AIM INC, Cranston 2003.

Sekhar, A. S., "Identification of a Crack in a Rotor System Using a Model-based Wavelet Approach", STRUCTURAL HEALTH MONITORING -SAGE- 2003, VOL 2; NUMB 4, pages 293-308.

Shetty, S. Reinikainen, T., "Three- and Four-Point Bend Testing for Electronic Packages", TRANSACTIONS- AMERICAN SOCIETY OF MECHANICAL ENGINEERS JOURNAL OF ELECTRONIC PACKAGING 2003, VOL 125; PART 4, pages 556-561.

Shi, X.Q. Pang, H.L.J. Zhou, W. Wang, Z.P., "A modified energy-based low cycle fatigue model for eutectic solder alloy", SCRIPTA MATERIALIA 1999, VOL 41; NUMBER 3, pages 289-296.

Shimizu, K. Nakanishi, T. Karasawa, K. Hashimoto, K., "Solder Joint Reliability of Indium-Alloy Interconnection", JOURNAL OF ELECTRONIC MATERIALS 1995, VOL 24; NUMBER 1, pages 39.

Sleszynski, W., Nieznanski, J., Cichowski, A., “Open-Transistor Fault Diagnostics in Voltage-Source Inverters by Analyzing the Load Currents”, IEEE TRANSACTIONS ON INDUSTRIAL ELECTRONICS, VOL. 56, NO. 11, NOVEMBER 2009.

Solomon, H., “Fatigue of 60/40 Solder”, IEEE Transactions on Components, Hybrids and Manufacturing Technology 1986, ISSN: 0148-6411 Vol. 9, Issue 4, Pages: 423 – 432.

Suhling, et al. “Reliability of Small Ball Grid Arrays in the Automotive Environment”. Proceedings of IMAPS 2002 International Symposium on Microelectronics, pp. 524-532, Denver, Co, September 4-6, 2002.

Syed, A., R., Thermal Fatigue Reliability Enhancement of Plastic Ball Grid Array (PBGA) Packages, Proceedings of the 1996 Electronic Components and Technology Conference, pp.1211-1216, Orlando, FL. May 28-31, 1996.

Syed, Ahmer., Accumulated Creep Strain and Energy Density Based Thermal Fatigue Life Prediction Models for SnAgCu Solder Joints. Proceedings of the 2004 Electronic Components and Technology Conference, pp. 737-746. 2004.

Syed, Ahmer., Reliability of Lead-Free Solder Connections for Area-Array Packages. IPC SMEMA Council APEX. Amkor Technology, Inc. Chandler, AZ 2001.

Tee, T., Ng, H., Lim, C., Pek, E., Zhong, Z., “Impact life prediction modeling of TFBGA packages under board level drop test”, *Microelectronic Reliability* 44 (2004) (7), pp. 1131–1142.

Tee, T.Y., Zhong, Z.W., “Board level solder joint reliability analysis and optimization of pyramidal stacked die BGA packages”, *Microelectronics Reliability* 44 (2004) (12), pp. 1957–1965.

Tsai I., Tai J., Yen S.F., Chuang T.H., Lo Robert, Ku T., Wu E., “Identification of Mechanical Properties of Intermetallic Compounds on Lead-Free Solders”, 55th Proceeding of Electronic Components and Technology Conference, 2005.

Vandevelde, B., et al., Thermal Cycling Reliability of SAC and SnPb Solder Joints: Comparison of Several IC-Packages. 5th international conference of EuroSimE 2004. pp.565-570.

Vianco, P. T. Burchett, S. N. Neilsen, M. K. Rejent, J. A. Frear, D. R., “Coarsening of the Sn-Pb Solder Microstructure in Constitutive Model-Based Predictions of Solder Joint Thermal Mechanical Fatigue”, JOURNAL OF ELECTRONIC MATERIALS, 1999, VOL 28; NUMBER 11, pages 1290-1298.

Wang, G. Z. Cheng, Z. N. Becker, K. Wilde, J., “Applying Anand Model to Represent the Viscoplastic Deformation Behavior of Solder Alloys”, TRANSACTIONS-

AMERICAN SOCIETY OF MECHANICAL ENGINEERS JOURNAL OF ELECTRONIC PACKAGING 2001, VOL 123; PART 3, pages 247-253.

Wiese, S., et al, "Microstructural Dependendence of Constitutive Properties of Eutectic SnAg and SnAgCu Solders," 53rd ECTC 2003, pp. 197-206.

Williams, T. W., Parker, K. P., "Design for Testability-A Survey", Proceedings of the IEEE, January 1983.

Wong, B., Helling, D., "A Mechanistic Model for Solder Joint Failure Prediction Under Thermal Cycling", Journal of electronic packaging 1990, ISSN: 1043-7398, Vol. 112, Issue 2, Page 104.

Wong, B., Helling, D., Clark, R., W., "A Creep-Rupture Model for Two-Phase Eutectic Solders", IEEE Transactions of Components, Hybrids, and Manufacturing Technology, Vol. 11, No.3, pp 284 – 290, September 1988.

Wood, S. M., Goodman, D. L., "Return-on-investment (ROI) for Electronic Prognostics in High Reliability Telecom Applications," *Proceedings of the International Telecommunications Energy Conference*, pp. 229-231, Providence, RI, September 2006.

Woodgate Ralph. "Solder Joint Inspection Criteria", Printed Circuit Assembly, February 1987,pp-6-10.

Xiong, Y., Cheng, X., Shen, Z., Mi, C., Wu, H., Garg, V., "Prognostic and Warning System for Power-Electronic Modules in Electric, Hybrid Electric and Fuel-Cell Vehicles", IEEE TRANSACTIONS ON INDUSTRIAL ELECTRONICS, VOL. 55, NO. 6, JUNE 2008.

Yamada, S., E., "A Fracture Mechanics Approach to Soldered Joint Cracking", IEEE Transactions on Components, Hybrids, and Manufacturing Technology, Vol. 12, No.1, pp. 99 – 104, March 1989.

Ye, H. Basaran, C. Hopkins, D. C., "Experimental Damage Mechanics of Micro/Power Electronics Solder Joints under Electric Current Stresses", INTERNATIONAL JOURNAL OF DAMAGE MECHANICS 2006, VOL 15; NUMB 1, pages 41-68.

Ye, H. Basaran, C. Hopkins, D., "Thermomigration in Pb-Sn solder joints under joule heating during electric current stressing", APPLIED PHYSICS LETTERS 2003, VOL 82; PART 7, pages 1045-1047.

Zhan, B., Solder Joint Fatigue Life Model Methodology for 63Sn37Pb and 95.5Sn4Ag0.5Cu Materials. Proceedings of the Electronic Components and Technology Conference. New Orlenas, LA, pp. 83-94, 2003.

Zhang, Q., & Dasgupta, A., Constitutive Properties and Durability of Lead-Free Solders, Lead-Free Electronics, S. Ganesan & M. Pecht, eds., CALCE EPSC Press, Maryland, pp. 65-137, 2003.

Zhang, Q., et al, "Viscoplastic Constitutive Properties and Energy-Partioning Model of Lead-Free Sn3.9Ag0.6Cu Solder Alloy," 53rd ECTC 2003, pp. 1862-1868.

Zhang, X. Lee, S.-W. R. Pao, Y.-H., "A Damage Evolution Model for Thermal Fatigue Analysis of Solder Joints", TRANSACTIONS- AMERICAN SOCIETY OF MECHANICAL ENGINEERS JOURNAL OF ELECTRONIC PACKAGING 2000, VOL 122; PART 3, pages 200-206.

Zhang, Y., Cai, Z., Suhling, J., Lall, P., Bozack M., "The Effects of SAC Alloy Composition on Aging Resistance and Reliability", 59th Electronic Component and Technology Conference, San Diego, CA, May 26-May 29 2009.

Zhang, Y., Cai, Z., Suhling, J., Lall, P., Bozack M., "The Effects of Aging Temperature on SAC Solder Joint Material Behavior and Reliability", 58th Electronic Component and Technology Conference, Orlando, FL,May 27-May 30 2008.

Zhong, C.H., Sung, Y., "Solder joint reliability of plastic ball grid array packages", SOLDERING AND SURFACE MOUNT TECHNOLOGY 1999, VOL 11; NUMBER 1, pages 44-55.